2073

ARL 64-41
MARCH 1964

111-p $2.50

Aerospace Research Laboratories

ANALYSIS OF THE OPTIMUM PERFORMANCE OF BUFFERED SHOCK TUBES

BRUCE H. FETZ
CORNELL AERONAUTICAL LABORATORY, INC.
BUFFALO, NEW YORK

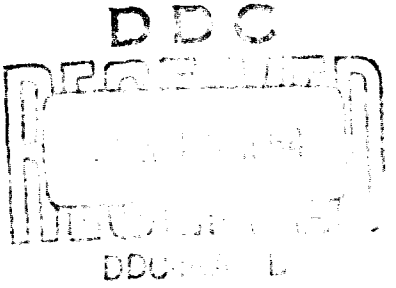

OFFICE OF AEROSPACE RESEARCH

United States Air Force

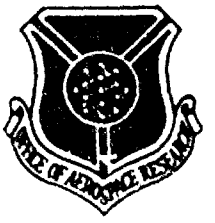

NOTICES

When Government drawings, specifications, or other data are used for any purpose other than in connection with a definitely related Government procurement operation, the United States Government thereby incurs no responsibility nor any obligation whatsoever, and the fact that the Government may have formulated, furnished, or in any way supplied the said drawings, specifications, or other data, is not to be regarded by implication or otherwise as in any manner licensing the holder or any other person or corporation, or conveying any rights or permission to manufacture, use, or sell any patented invention that may in any way be related thereto.

- - - - - - - - - -

Qualified requesters may obtain copies of this report from the Defense Documentation Center, (DDC), Cameron Station, Alexandria, Virginia.

- - - - - - - - - -

This report has been released to the Office of Technical Services, U. S. Department of Commerce, Washington 25, D. C. for sale to the general public.

- - - - - - - - - -

Copies of ARL Technical Documentary Reports should not be returned to Aerospace Research Laboratories unless return is required by security considerations, contractual obligations or notices on a specified document.

300 - May 1964 - 162-39-777

ARL 64-41

ANALYSIS OF THE OPTIMUM PERFORMANCE OF BUFFERED SHOCK TUBES

BRUCE H. FETZ

CORNELL AERONAUTICAL LABORATORY, INC.
BUFFALO, NEW YORK

MARCH 1964

Contract AF 33(657)-8860
Project 7065
Task 7065-01

AEROSPACE RESEARCH LABORATORIES
OFFICE OF AEROSPACE RESEARCH
UNITED STATES AIR FORCE
WRIGHT-PATTERSON AIR FORCE BASE, OHIO

FOREWORD

This interim technical report was prepared by the Aerodynamic Research Department of Cornell Aeronautical Laboratory, Inc., Buffalo, New York, on contract AF 33(657)-8860 for the Aerospace Research Laboratories, Office of Aerospace Research, United States Air Force. The research reported herein was accomplished during the period from May 1962 to July 1963 on Task 7065-01, "Fluid Dynamics Facilities Research" of Project 7065, "Aerospace Simulation Techniques Research" under the technical cognizance of Mr. Robert G. Dunn of the Fluid Dynamics Facilities Research Laboratory of ARL.

ABSTRACT

This report presents a general investigation of buffered shock tubes. For the case of strong shocks the number of variables needed for the analysis of buffered shock tubes is reduced to three. An expression is obtained from which the buffer conditions necessary for the production of the maximum shock Mach number are determined. The strong shock analysis is extended to include shock tubes with many buffers and buffered shock tubes with area changes at either or both diaphragms. The concept of using a detonable mixture as a buffer gas is explored and its limitations are indicated. Also, a study is included of different shock tube geometrical configurations to indicate means of achieving the maximum testing time.

The strong shock assumption implies that for given over-all conditions the final shock strength depends only upon the upstream density ratio. This simplification permits the study of the buffered tube throughout its entire range of operating conditions. A number of general conclusions can be drawn from this study. For given over-all conditions a buffered shock tube will produce stronger shocks than a simple shock tube provided that the optimum buffer conditions are used. The performance of a shock tube improves as the number of buffers increases, but the final shock strength soon approaches an asymptotic value. The performance of a buffered tube is improved by using an over-all area contraction; the most efficient distribution involves equal area changes at each diaphragm. The gain in performance obtained with a detonation buffer is limited when the final shocks are very strong. For fixed driver conditions and final shock strength, increasing the diameter of the driven section does not significantly increase the testing time.

TABLE OF CONTENTS

LIST OF ILLUSTRATIONS

LIST OF SYMBOLS

a	sound speed
A	area
B, C, D, E	functions of specific heat ratios, defined in text
C	Chapman-Jouguet point
c_p	specific heat per unit mass at constant pressure
c_v	specific heat per unit mass at constant volume
d	diameter
e	internal energy per unit mass
f	function of Mach number, defined in text
F	functions expressing the dependence of the π's upon the other variables, defined in text - Fahrenheit degree
g	equivalence factor for an area change near the first diaphragm
G	equivalence factor for an area change near the second diaphragm
H_2	hydrogen
He	helium
Hg	mercury
K	$\left(\frac{\rho_{41}}{P_{41}}\right)^{1/2}$ - Kelvin degree
M	$\frac{u}{a}$, flow Mach number
M_s	shock Mach number, speed of shock relative to gas ahead of it divided by speed of sound ahead of it
n	numbers of buffers - number used to denote a certain region of flow in a shock tube
p	pressure
P	Riemann invariant $\frac{2}{\gamma-1} a + u$ or the associated wave with slope $u + a$

Q	Riemann invariant $\frac{2a}{\gamma-1} - u$ or the associated wave with slope $u-a$
s	entropy per unit mass
t	time
T	temperature - similarity parameter for testing time
u	velocity of flow in laboratory coordinates
U_D	velocity of detonation wave
u_p	piston velocity
U_s	velocity of shock
v	volume per unit mass
V	velocity of gas relative to shock front
x	distance - points to indicate exact calculations on Fig. 20
X	similarity parameter used in testing time analysis
X, Y	functions of the Z's , defined in text
Z	shock strength parameter
Z'	shock strength parameter for shock tubes with area changes
$\bar{Z}$	compressibility
β	parameter used in defining displacement thickness at the contact surface
γ	ratio of specific heats
Γ	a density ratio
ΔE_c	heat of reaction per unit mass at constant temperature and pressure
μ	molecular weight - dynamic viscosity - microns
ρ	density
σ	Prandtl number
τ	delay time - testing time

φ	dimensionless heat of reaction

Subscripts

1, 2, 3a, 5′, etc.	denote regions of quasi-steady flow in shock tubes - used to distinguish various shock waves, expansion waves, contact surfaces, variables, and functions from one another
∞	implies infinite area contraction
av.	average value
i	ideal
max.	maximum
s_j	refers to shock wave numbered j
s_r	refers to reflected shock wave
s.t.p.	room temperature and one atmosphere pressure
*	conditions at the minimum area

Special Symbols

A_{ij}	$\frac{a_i}{a_j}$, sound speed ratio
A_{ij}'	effective sound speed ratio for a simple shock tube with an area change
P_{ij}	$\frac{p_i}{p_j}$ pressure ratio
P_{ij}'	effective pressure ratio for a simple shock tube with an area change
T_{ij}	$\frac{T_i}{T_j}$, temperature ratio
Γ_{ij}	$\frac{\rho_i}{\rho_j}$, density ratio
Γ_{ij}'	effective density ratio for a shock tube with an area change
μ_{ij}	$\frac{\mu_i}{\mu_j}$, molecular weight ratio
$\vec{C}$	contact surface moving to the right

$\vec{S}, \vec{R}$	forward-facing (P -type) shock waves and rarefaction waves, respectively
$\overleftarrow{S}, \overleftarrow{R}$	backward-facing (Q -type) shock waves and rarefaction waves, respectively
$\vec{W}$	forward-facing wave of unknown type

1. INTRODUCTION

The shock tube has become a common laboratory tool for the study of aerodynamics, chemical kinetics, combustion processes, and high temperature gas physics. The literature on shock tubes is very extensive, compilations of published works can be found, for example, in Refs. 1 and 2. In recent years the shock tube has been extensively used as a driver for shock tunnels in which Mach numbers and stagnation enthalpies of hypersonic flight can be simulated (Ref. 3 has a large bibliography on the subject). Among the driver gases which have been used for these devices are the following: cold hydrogen, cold helium, hydrogen-oxygen mixtures with and without diluent, heated hydrogen, and arc-heated helium. The present desire to simulate flight at escape velocity (36,000 ft/sec) and higher has stimulated interest in extending driver capabilities.[4,5]

The purpose of this report is to study a particular method for increasing the shock Mach number in a shock tube with any given driver. This method is the use of the buffered (or multiple-diaphragm) shock tube. The use of buffering has been considered by many authors during the past ten years.[1, 6-18] However, because of the complexity of the problem, the previous studies have dealt with specific examples only, and, therefore, do not reveal in a general form the maximum gains to be obtained. The present report utilizes an assumption of strong shocks to simplify the analysis of optimum performance. With this simplification the optimum buffer conditions are predicted over the entire range of over-all (i.e. driver to driven) conditions. Analytical expressions are derived for the maximum final shock strength obtainable with the optimum buffer conditions.

Manuscript released by the author January, 1964 for publication as an ARL Technical Documentary Report.

It may be noted that a number of buffered tubes have been built,[13-18] and, in general, the experimental results support the theory. However, the actual performance of these tubes is below that predicted by ideal theory due to such effects as shock wave attenuation, wave reflections, contact zone mixing, and real gas effects.

The convenience of using strong shock assumptions to simplify the present analysis of buffered shock tubes was pointed out in the work of Hall and Russo.[19] They present a useful simplification to the simple shock tube equation for shock Mach numbers exceeding about three. For a given driver gas specific heat ratio, shock tube performance can be explicitly expressed for all initial conditions (including area change) in terms of two variables. They note that the performance of buffered tubes (with strong shocks) can be expressed in terms of corresponding variables with only the upstream density ratio as an additional variable. They further state that previous results of Russo and Hertzberg[10] showing the effects of varying buffer gas pressure and molecular weight can be correlated in terms of this density ratio.

In Section 2.1 a survey of previous studies of buffered shock tubes is presented. The theoretical studies all bear out the fact that the performance of any shock tube can be improved by the inclusion of a buffer section. Calculations of the performance of a buffered shock tube for any given initial conditions in the driver and driven sections are quite lengthy because of the number of variables involved: buffer gas specific heat ratio, molecular weight, temperature, and pressure. For a given buffer gas at a fixed initial temperature the final shock Mach number varies only with the buffer pressure. There exists a certain buffer gas pressure (which shall be called the optimum

pressure) for which the final shock strength is a maximum. The determination of this optimum pressure is complicated by the fact that the calculation of the driven section shock Mach number involves two iterations for each set of initial conditions.

In Section 2.2 the equations are simplified with the assumption of strong shock waves so that analytical expressions for the optimum buffer conditions are obtained. When the optimum conditions have been determined, analytical expressions are obtained for the maximum final shock strength for any given over-all conditions. The strong shock analysis is extended with similar results to the study of shock tubes with many buffers and to buffered tubes with area changes at either or both diaphragms.

The use of a detonable mixture as a buffer gas[12] is considered in Section 2.3. This device has most of the characteristics of a buffered shock tube with the added advantage that chemical energy is released to the flow in the buffer section. When the strong shock assumption is applied to the detonation buffer equations (assuming ideal gases), the optimum performance conditions can be determined. If the tube is operated so that the detonation in the buffer is close to a Chapman-Jouguet detonation, a substantial increase in final shock Mach number is possible. However, if the detonation is strongly over-driven, the detonation buffer offers only moderate gains over the inert-gas buffer.

In Section 3 studies are made to determine the geometrical configuration which yields the greatest testing time for a given final shock strength and specified driver conditions. It has been pointed out that there is a severe decrease in flow duration for shock tubes operating at low pressures due to the

effects of the boundary layer behind the shock waves.[20-23] The testing time as limited by boundary layer growth has been shown to be directly proportional to the pressure and to the area of the driven section. This fact has stimulated interest in shock tubes with larger driven sections than driver sections. For most cases of interest the benefit of the larger diameter is found to be offset by the need for a lower initial pressure to maintain the same shock Mach number.

2. OPTIMUM PERFORMANCE OF BUFFERED SHOCK TUBES

2.1 REVIEW OF PREVIOUS ANALYSES

The use of the double-diaphragm shock tube (i.e. the buffered shock tube) has been considered by a number of authors.[1,6-18] In the following analyses it will be assumed that the flow is one-dimensional and inviscid with no heat conduction and no mixing at the interfaces. For the most part the gases will be assumed to be ideal gases with constant specific heats.

The basic arrangement is illustrated in Figure 1 for the "unsteady-expansion" type of buffered shock tube. The initial flow phenomena are represented on a distance vs. time (x-t) plot which is commonly known as a wave diagram. The high pressure in the driver (region 4) causes the initial diaphragm to rupture. A shock wave $\vec{S}_1$ propagates into the buffer gas, while a rarefaction (or expansion) wave $\overleftarrow{R}_1$ propagates into the high pressure driver gas. The driver gas and the buffer gas remain separated by a contact surface $\vec{C}_1$ across which the pressure and velocity are equal, but the density, temperature, and entropy are, in general, different.

Assuming that the second diaphragm bursts instantaneously upon the impact of the initial shock, the wave diagram is represented by Figure 1. The

flow from region 2 to region 8 resembles that of a simple shock tube except that the "driver" has an initial velocity u_2 and has been heated by the shock to a temperature T_2 . However, the pressure p_2 is less than the initial driver pressure p_4 . Therefore, the double-diaphragm shock tube can be considered as a device which effectively sacrifices pressure ratio in favor of an increased speed-of-sound (or temperature) ratio.

A second possibility, termed the reflected-shock type of buffered shock tube, is illustrated in Figure 2.[1,9] With this configuration the initial shock is allowed to undergo complete reflection from the second diaphragm leaving the gas in region 5 at rest. After a predetermined delay τ the second diaphragm is ruptured mechanically; the ensuing flow is shown in Figure 2. While this configuration offers a slight improvement over the unsteady-expansion type, the mechanical difficulties involved in breaking the second diaphragm will preclude its further consideration. The reflected-shock type buffered tube should not be confused with the shock tube with an area contraction at the second diaphragm. This tube also produces a reflected shock, but the ensuing flow is fundamentally different from that of the reflected-shock type of tube.

Consider some of the characteristics of the unsteady-expansion buffered shock tube. Before the shock strikes the second diaphragm the flow is identical to that which is found in a simple shock tube. Therefore, the well-known simple shock tube equation is valid (see Appendix I).

$$P_{41} = \frac{2\gamma_1 M_{s_1}^2 - (\gamma_1 - 1)}{\gamma_1 + 1} \left[1 - \frac{\gamma_4 - 1}{\gamma_1 +} \cdot \frac{\left(M_{s_1}^2 - 1\right)}{A_{41} M_{s_1}} \right]^{-\frac{2\gamma_4}{\gamma_4 - 1}} \qquad (1)$$

where

$M_{s_1} = U_{s_1}/a_1$	initial shock Mach number
U_{s_1}	speed of the shock relative to the tube
a	speed of sound
$P_{41} = p_4/p_1$	initial diaphragm pressure ratio
$A_{41} = a_4/a_1$	initial diaphragm speed-of-sound ratio
$\gamma = c_p/c_v$	ratio of specific heats

Referring to Figure 1 and applying the usual equations of one-dimensional unsteady flow, the basic equation for the constant-area buffered shock tube is obtained (see Appendix I).

$$P_{48} = \frac{2\gamma_8 M_{s_8}^2 - (\gamma_8 - 1)}{\gamma_8 + 1} \left[1 - \frac{\gamma_4 - 1}{\gamma_1 + 1} \left(\frac{\gamma_1}{\gamma_4}\right)^{1/2} \left(\frac{\Gamma_{41}}{P_{41}}\right)^{1/2} \frac{M_{s_1}^2 - 1}{M_{s_1}} \right]^{-\frac{2\gamma_4}{\gamma_4 - 1}}$$

$$\left\{ 1 - \frac{(\gamma_1 - 1) M_{s_1}}{\left[2\gamma_1 M_{s_1}^2 - (\gamma_1 - 1)\right]^{1/2} \left[(\gamma_1 - 1) M_{s_1}^2 + 2\right]^{1/2}} \left[\frac{\gamma_1 + 1}{\gamma_8 + 1} \left(\frac{\gamma_8}{\gamma_1}\right)^{1/2} \left(\frac{\Gamma_{48}}{P_{48}}\right)^{1/2} \right. \right. \tag{2}$$

$$\left. \left. \left(\frac{P_{41}}{\Gamma_{41}}\right)^{1/2} \left(M_{s_8} - \frac{1}{M_{s_8}}\right) - \left(M_{s_1} - \frac{1}{M_{s_1}}\right) \right] \right\}^{-\frac{2\gamma_1}{\gamma_1 - 1}}$$

where

M_{s_8}	final shock Mach number
$\Gamma_{41} = \rho_4/\rho_1$	density ratio

The final shock strength M_{s_8} is a function of the following eight variables: γ_1, γ_4, γ_8, P_{48}, Γ_{48}, P_{41}, M_{s_1}, and Γ_{41}. However, these are not all independent, and one can be eliminated by the use of the simple shock tube equation (Eq. (1)). As in the case of the simple shock tube, M_{s_8} is increased if P_{48} is made large and Γ_{48} is made small (i.e. making A_{48} large). Also, as with the simple shock tube, the best performance is obtained when γ_4 is small which suggests a diatomic driver gas. The effect of

varying γ_8 is found to be negligible; a monatomic driven gas is found to be only slightly better than a diatomic gas.

When conditions in the driver and the driven sections (4 and 8) have been specified, M_{s_8} depends upon the three variables γ_1, P_{41}, and Γ_{41}. Russo and Hertzberg[10] have shown that the performance of a buffered shock tube improves with increasing buffer specific heat ratio γ_1. Also, the use of monatomic buffer gases will minimize real gas effects which tend to reduce performance.

Henshall[9] presents results for a buffered tube in which the same diatomic gas at the same initial temperature is used throughout. In this case $\gamma_1 = \gamma_4 = \gamma_8 = 7/5$, $P_{41} = \Gamma_{41}$, $P_{48} = \Gamma_{48}$ and $\mu_1 = \mu_4 = \mu_8$ where μ is the molecular weight. The final shock Mach number depends only upon the over-all pressure ratio and the upstream pressure ratio. Figure 3 shows M_{s_8} as a function of the downstream pressure ratio P_{18} with P_{48} as a parameter. It will be noted that the maximum value of M_{s_8} occurs when P_{18} is approximately $(P_{48})^{1/2}$. A similar result can be seen from Figure 4 which shows the performance of a tube in which the same monatomic gas at the same initial temperature is used throughout. Of course, in a more general case, the geometric mean may not be the optimum buffer pressure. The shock Mach numbers obtained from simple shock tubes with the same over-all conditions are included in Figures 3 and 4 for comparison.

Hydrogen is a widely used driver gas since it has the smallest molecular weight, and therefore, the smallest density at a given temperature and pressure. Figure 5 shows the performance of a tube with hydrogen driver, monatomic buffer, and air as the driven gas at an over-all pressure ratio of 10^4. The

temperature is assumed constant throughout so that

$$\Gamma_{48} = P_{48}\mu_{48} \qquad \text{and} \qquad \Gamma_{41} = P_{41}\mu_{41} \tag{3}$$

where $\mu_{48}=\mu_4/\mu_8$ the ratio of molecular weights. Therefore, M_{s_8} is a function only of μ_{41} and P_{41}.

A study of Figure 5 reveals the following interesting feature. While the optimum downstream pressure ratio P_{18} varies with the buffer gas molecular weight, the maximum value of M_{s_8} is relatively unaffected. This seems to indicate that certain simplifications of the basic equations are possible which reduce the number of independent variables. It will be shown presently that this is indeed the case and that the simplified buffer equation may be used to determine the optimum buffer conditions.

2.2 INERT-GAS-BUFFERED SHOCK TUBES

2.2.1 Simple Constant-Area Buffered Tubes

Recently Hall and Russo[19] have shown that the analysis of a simple shock tube with an area change near the diaphragm can be greatly simplified by assuming that the shock Mach number is greater than about three. This theory is reviewed in Appendix II where it is shown that for given γ_1 and γ_4 the basic equation involves only two variables: $Z_1' = \frac{M_{s_1}}{\gamma_g P_{41}}$ and $\Gamma_{41}' = g^{1/\gamma_4}\Gamma_{41}$ where g is the equivalence factor of Resler, Lin, and Kantrowitz.[6] A plot of the basic relation is given in Figure 6 for various values of γ_4 : the variation in performance with γ_1 is found to be negligible. The plot can be interpreted as representing the performance of a simple shock tube merely by setting g equal to one.

Now apply the strong shock assumptions to the constant-area buffered

tube. Assuming that both M_{s_1} and M_{s_8} are greater than about three, Eq. (2) can be simplified to the relation

$$\bar{z}_8^2 = \frac{\gamma_8+1}{2\gamma_8}\left[1-B\,\Gamma_{41}^{1/2}\bar{z}_1\right]^{\frac{2\gamma_4}{\gamma_4-1}}\left\{1-\frac{(\gamma_1-1)M_{s_1}}{(2\gamma_1)^{1/2}\left[(\gamma_1-1)M_{s_1}^2+2\right]^{1/2}}\times\right. \tag{4}$$

$$\left.\left[\frac{\gamma_1+1}{\gamma_8+1}\left(\frac{\gamma_8}{\gamma_1}\right)^{1/2}\left(\frac{\Gamma_{48}}{\Gamma_{41}}\right)^{1/2}\frac{\bar{z}_8}{\bar{z}_1}-1\right]\right\}^{\frac{2\gamma_1}{\gamma_1-1}}$$

where

$$B=\frac{\gamma_4-1}{\gamma_1+1}\left(\frac{\gamma_1}{\gamma_4}\right)^{1/2}$$

$$\bar{z}_1=\frac{M_{s_1}}{\sqrt{\gamma P_{41}}} \qquad \text{and} \qquad \bar{z}_8=\frac{M_{s_8}}{\sqrt{\gamma P_{48}}}$$

This equation can be further simplified by the use of the simple shock tube equation, which in this case becomes

$$\bar{z}_1^2=\frac{\gamma_1+1}{2\gamma_1}\left[1-B\,\Gamma_{41}^{1/2}\bar{z}_1\right]^{\frac{2\gamma_4}{\gamma_4-1}} \tag{5}$$

Equation (5) is easily solved for Γ_{41} yielding

$$\Gamma_{41}=\frac{\left[1-\left(\frac{2\gamma_1}{\gamma_1+1}\bar{z}_1^2\right)^{\frac{\gamma_4-1}{2\gamma_4}}\right]^2}{B^2\bar{z}_1^2} \tag{6}$$

When Eqs. (5) and (6) are used in Eq. (4),

$$\bar{z}_8^2=C_1\bar{z}_1^2\left\{1-\frac{(\gamma_1-1)M_{s_1}}{(2\gamma_1)^{1/2}\left[(\gamma_1-1)M_{s_1}^2+2\right]^{1/2}}\times\right.$$

$$\left.\left[\frac{\gamma_4-1}{\gamma_8+1}\left(\frac{\gamma_8}{\gamma_4}\right)^{1/2}\frac{\Gamma_{48}^{1/2}\bar{z}_8}{\left[1-\left(\frac{2\gamma_1}{\gamma_1+1}\bar{z}_1^2\right)^{\frac{\gamma_4-1}{2\gamma_4}}\right]}-1\right]\right\}^{\frac{2\gamma_1}{\gamma_1-1}} \tag{7}$$

where

$$C_1 = \frac{\gamma_8 + 1}{\gamma_1 + 1} \frac{\gamma_1}{\gamma_8}$$

For given specific heat ratios and fixed over-all density ratio Γ_{48}, Z_8 depends upon M_{s_1} and Z_1. It is possible to maximize Z_8 with respect to these two variables and obtain the conditions for optimum performance. The details of this calculation are presented in Appendix III. The important point is that, once the maximizing is done, the final shock strength Z_8 is a function only of the over-all density ratio Γ_{48}

Upon now making the additional assumption that $M_{s_1}^2$ is large compared to $\frac{2}{\gamma_1 - 1}$, Eq. (7) reduces to a particularly simple form.

$$Z_8^2 = C_1 Z_1^2 \left\{ D_1 - \frac{B E_1 \Gamma_{48}^{1/2} Z_8}{1 - \left(\frac{2\gamma_1}{\gamma_1 + 1} Z_1^2 \right)^{\frac{\gamma_4 - 1}{2\gamma_4}}} \right\}^{\frac{2\gamma_1}{\gamma_1 - 1}} \tag{8}$$

where

$$D_1 = 1 + \left(\frac{\gamma_1 - 1}{2\gamma_1} \right)^{1/2}$$

and

$$E_1 = \left(\frac{\gamma_1 - 1}{2\gamma_1} \right)^{1/2} \left(\frac{\gamma_8}{\gamma_1} \right)^{1/2} \frac{\gamma_1 + 1}{\gamma_8 + 1}$$

Equation (8) can be written symbolically as

$$Z_8 = F_1 \left(\gamma_1, \gamma_4, \gamma_8, Z_1, \Gamma_{48} \right) \tag{9}$$

When the over-all density ratio and the specific heat ratios of all gases are specified, the final shock strength depends only upon Z_1. Alternatively, Eq. (6) may be used to eliminate the explicit dependence of Z_8 upon Z_1. Then, for specified over-all density ratio and specific heat ratios, Z_8 would depend only upon the upstream density ratio Γ_{41}. This result was previously

noted in Ref. 19. The value of $\bar{z}_1$ needed to yield a maximum $\bar{z}_8$ should be a solution to the equation

$$\frac{\partial F_1}{\partial \bar{z}_1} = 0 \tag{10}$$

The details of this calculation are shown in Appendix III where it is found that

$$\Gamma_{48} = \frac{\left[1-\left(\frac{2\gamma_1}{\gamma_1+1}\bar{z}_1^2\right)^{\frac{\gamma_4-1}{2\gamma_4}}\right]^2 \left(\frac{1+X_1}{X_1}\right)^{\frac{2\gamma_1}{\gamma_1-1}}}{B^2 E_1^2 D_1^{2/\gamma_1-1} C_1 (1+X_1)^2 \bar{z}_1^2} \tag{11}$$

and

$$\bar{z}_8 = \left(\frac{D_1 X_1}{1+X_1}\right)^{\frac{\gamma_1}{\gamma_1-1}} C_1^{1/2} \bar{z}_1 \tag{12}$$

where

$$X_1 = \frac{\frac{\gamma_1}{\gamma_4}\frac{\gamma_4-1}{\gamma_1-1}\left(\frac{2\gamma_1}{\gamma_1+1}\bar{z}_1^2\right)^{\frac{\gamma_4-1}{2\gamma_4}}}{1-\left(\frac{2\gamma_1}{\gamma_1+1}\bar{z}_1^2\right)^{\frac{\gamma_4-1}{2\gamma_4}}} \tag{13}$$

Equations (11) and (12) may be used to determine $\bar{z}_8$ -maximum as a function of Γ_{48} by means of the parametric dependence of these two quantities upon $\bar{z}_1$. Thus, for any given Γ_{48} , $\bar{z}_1$ (optimum) can be calculated from (11), the required upstream density ratio Γ_{41} can be found from (6), and the maximum final shock strength can be obtained from (12). Figure 7 is a plot of Eq. (11) for the special case in which $\gamma_4 = \gamma_8 = 7/5$ and $\gamma_1 = 5/3$, while Fig. 8 of $\bar{z}_8$ vs. Γ_{48} is obtained from Eqs. (11) and (12). Also, on Fig. 8, for comparison, is a plot of $\bar{z}_1$ vs. Γ_{41} for a simple shock tube with $\gamma_4 = \gamma_1 = 7/5$ (Eq. (6)).

As an example of the calculational procedure, consider a tube with a hydrogen driver, a monatomic buffer, and driven air all initially at the same temperature. Then

$$\Gamma_{48} = .0696\ P_{48}$$

In order to compare this with the results of Fig. 5 let $P_{48} = 10^4$, $\Gamma_{48} = 696$. Then from Fig. 7 $\mathcal{Z}_1 = .189$, from Fig. 8 $\mathcal{Z}_8 = .117$, and from Fig. 6 $\Gamma_{41} = 130$. Now since $P_{48} = 10^4$, $M_{s_8} = 11.7$ which is in good agreement with Fig. 5. If we assume that the buffer gas is argon ($\mu_1 = 39.9$) then $P_{41} = \Gamma_{41}/\mu_{41} = 2580$ or $P_{18} = 3.88$ which is again in excellent agreement with Fig. 5.

Some idea of the validity of the assumptions can be obtained from Fig. 9 which shows a comparison of the exact solution (Eq. (2)), approximation 1 (Eq. (7)), and approximation 2 (Eq. (8)) for two different monatomic buffer gases ($\mu_1 = 4$ and $\mu_1 = 80$). The plots for other values of the molecular weight are similar. Approximation 2 becomes noticably worse as P_{18} becomes large; this is to be expected since M_{s_1} will be small for large P_{18} . Since the maximum M_{s_8} for the $\mu_1 = 80$ gas occurs at small P_{18} , approximation 2 reliably predicts the maximum while the approximation for the $\mu_1 = 4$ case is less accurate. This and other calculations indicate that approximation 2 always yields values of M_{s_8} lower than the exact solution, so that it can be considered as a lower bound. The curves of M_{s_8} vs. P_{18} for approximation 2 are all exactly similar (no matter what the buffer gas molecular weight), while the curves for approximation 1 show a slight dependence of $\mathcal{Z}_8$ max. upon molecular weight (just as the exact curves do).

Figure 10 presents another comparison of the approximations, this time

for the case where $\gamma_1 = \gamma_4 = \gamma_8 = 7/5$, $\mu_1 = \mu_4 = \mu_8$, $T_1 = T_4 = T_8$ and $P_{48} = 10^5$. In this case approximation 2 gives a value of M_{s_8} which is in error by about 15% near the optimum. This error is due to the low values of M_{s_1} (around 3) which occur near the optimum conditions. When the production of strong shocks is a primary concern, however, the values of M_{s_1} which are needed are usually such as to make approximation 2 reasonably good.

In Appendix III the problem of determining the optimum conditions from approximation 1 is given detailed consideration. No analytical expression was found from which the optimum conditions for any Γ_{48} could be determined. Solutions to the problem were obtained for fixed values of Γ_{48} and K where

$$K^2 \equiv \frac{\Gamma_{41}}{P_{41}} = \frac{\mu_{41}}{T_{41}}$$

and

$$T_{41} = \frac{T_4}{T_1}$$

but the calculations are quite lengthy. However, the following important fact can be noted: for fixed Γ_{48} the value of $\bar{z}_8$ —maximum increases as the value of K increases. This result is illustrated in Fig. 9 which shows that $\bar{z}_8$ —maximum is greater for $\mu_1 = 4$ ($K^2 = .5$) than for $\mu_1 = 80$ ($K^2 = .025$). It is interesting to note that as K increases, the value of M_{s_1} at $\bar{z}_8$ —maximum decreases, and, therefore, the strong shock assumption is becoming increasingly invalid.

The difficulties involved in determining the optimum conditions with the use of approximation 1 are comparable to those involved with the use of the exact equation. The calculations of the optimum conditions with approximation 2, on the other hand, are relatively straightforward. Even in cases where the

second approximation is not very accurate, approximate values for the optimum conditions can be obtained for use as initial guesses for exact calculations.

2.2.2 The Many-Buffered Tube

A shock tube with more than one buffer section should produce a stronger final shock than a simple buffered tube. Henshall[9] considers the special case of all diatomic gases with the same molecular weight and initial temperatures. He assumes that the optimum pressure ratio distribution will be equal pressure ratios across each diaphragm. Under these assumptions the final shock strength increases with the number of diaphragms but the relative gain decreases as the number of diaphragms increases. As the number of diaphragms becomes very large, the final shock Mach number approaches an asymptotic value.

The calculation of the optimum conditions for a many-buffered tube is very difficult because the final shock strength depends upon the density and the pressure in every section of the tube. It is therefore very desirable that a method be developed to determine quickly these optimum conditions. The basic equation for the many-buffered tube is developed in Appendix I and is based upon an idealized wave diagram such as that shown in Fig. 11.

The wave diagram in Fig. 11 indicates the numbering system that will be used when discussing the many-buffered shock tube. The system used for numbering the flow regions in simple shock tubes (driver-4, driven-1) is almost universally accepted. The numbering system for the buffered shock tube which is most widely used is that which labels the driven section 8 and the region behind the reflected shock (if any) 5. Figure 11 represents the extension of this system to a double-buffered tube. Regions 5 and 9 are omitted because there

are no reflected shocks.

For simplicity, begin by considering a double-buffered shock tube. The basic equations are (A-23), the simple bufer Eq. (2), and the simple shock tube Eq. (1). Assuming that $M_{s_1}^2 \gg 1$, $M_{s_8}^2 \gg 1$, and $M_{s_{12}}^2 \gg 1$, an initial approximation is obtained, but the equations are still so complex that no attempt will be made to maximize them. When the rather restrictive assumptions that $M_{s_1}^2 \gg \frac{2}{\gamma_1 - 1}$ and $M_{s_8}^2 \gg \frac{2}{\gamma_8 - 1}$ are made, it is found that Eq. (1) reduces to Eq. (5), Eq. (2) reduces to Eq. (8), and Eq. (A-23) reduces to

$$\frac{P_4}{P_{12}} = \frac{2\gamma_{12} M_{s_{12}}^2}{\gamma_{12}+1} \left[1 - B\Gamma_{41}^{1/2} Z_1\right]^{-\frac{2\gamma_4}{\gamma_4-1}} \cdot \quad x$$

$$\left\{D_1 - \frac{BE_1\Gamma_{48}^{1/2} Z_8}{1-\left(\frac{2\gamma_1}{\gamma_1+1} Z_1^2\right)^{\frac{\gamma_4-1}{2\gamma_4}}}\right\}^{-\frac{2\gamma_1}{\gamma_1-1}} \left\{D_8 - E_8\left(\frac{\Gamma_{4,12}}{\Gamma_{48}}\right)^{1/2} \frac{Z_{12}}{Z_8}\right\}^{-\frac{2\gamma_8}{\gamma_8-1}} \tag{14}$$

where $$Z_{12} = \frac{M_{s_{12}}}{\sqrt{P_4/P_{12}}}$$

$$D_8 = 1 + \left(\frac{\gamma_8 - 1}{2\gamma_8}\right)^{1/2}$$

and $$E_8 = \left(\frac{\gamma_8 - 1}{2\gamma_8}\right)^{1/2} \left(\frac{\gamma_{12}}{\gamma_8}\right)^{1/2} \frac{\gamma_8 + 1}{\gamma_{12}+1}$$

Now Eq. (8) can be solved for Γ_{48} yielding

$$\Gamma_{48}^{1/2} = \left[D_1 - \left(\frac{1}{C_1} \frac{Z_8^2}{Z_1^2}\right)^{\frac{\gamma_1-1}{2\gamma_1}}\right] \frac{\left[1 - \left(\frac{2\gamma_1}{\gamma_1+1} Z_1^2\right)^{\frac{\gamma_4-1}{2\gamma_4}}\right]}{BE_1 Z_8} \tag{15}$$

So that Eq. (14) becomes

$$Z_{12}^2 = C_8 Z_8^2 \left\{ D_8 - \frac{B E_1 E_8 Z_{12} \Gamma_{4,12}^{1/2}}{\left[D_1 - \left(\frac{1}{C_1} \frac{Z_8^2}{Z_1^2} \right)^{\frac{\gamma_1 - 1}{2\gamma_1}} \right] \left[1 - \left(\frac{2\gamma_1}{\gamma_1 + 1} Z_1^2 \right)^{\frac{\gamma_4 - 1}{2\gamma_4}} \right]} \right\}^{\frac{2\gamma_8}{\gamma_8 - 1}} \tag{16}$$

where $$C_8 = \frac{\gamma_{12} + 1}{\gamma_8 + 1} \frac{\gamma_8}{\gamma_{12}}$$

Equation (16) can be represented symbolically as

$$Z_{12} = F_2 \left(\gamma_1, \gamma_4, \gamma_8, \gamma_{12}, Z_1, Z_8, \Gamma_{4,12} \right) \tag{17}$$

So, for given specific heat ratios and over-all density ratio, the conditions for maximum Z_{12} are

$$\frac{\partial F_2}{\partial Z_1} = 0 \qquad \text{and} \qquad \frac{\partial F_2}{\partial Z_8} = 0 \tag{18}$$

The calculations are quite lengthly, but fortunately the results can be expressed as equations involving only the single independent variable Z_1 .

$$\Gamma_{4,12} = \frac{\left[1 - \left(\frac{2\gamma_1}{\gamma_1 + 1} Z_1^2 \right)^{\frac{\gamma_4 - 1}{2\gamma_4}} \right]^2 \left(\frac{1 + X_1}{X_1} \right)^{\frac{2\gamma_1}{\gamma_1 - 1}}}{B^2 D_1^{2/\gamma_1 - 1} D_8^{2/\gamma_8 - 1} E_1^2 E_8^2 (1 + X_1)^2 (1 + X_8)^2} \times \frac{\left(\frac{1 + X_8}{X_8} \right)^{\frac{2\gamma_8}{\gamma_8 - 1}}}{Z_1^2 C_1 C_8} \tag{19}$$

where

$$X_8 = \frac{\gamma_1 - 1}{\gamma_8 - 1} \frac{\gamma_8}{\gamma_1} X_1$$

$$\mathcal{Z}_{12} = D_1^{\frac{\gamma_1}{\gamma_1-1}} \; D_8^{\frac{\gamma_8}{\gamma_8-1}} \; C_1^{1/2} \, C_8^{1/2} \left(\frac{X_1}{1+X_1}\right)^{\frac{\gamma_1}{\gamma_1-1}} \left(\frac{X_8}{1+X_8}\right)^{\frac{\gamma_8}{\gamma_8-1}} \mathcal{Z}_1 \tag{20}$$

and

$$\mathcal{Z}_8 = D_1^{\frac{\gamma_1}{\gamma_1-1}} \; C_1^{1/2} \left(\frac{X_1}{1+X_1}\right)^{\frac{\gamma_1}{\gamma_1-1}} \mathcal{Z}_1 \tag{21}$$

Figure 12 shows $\mathcal{Z}_{12}$ vs. $\Gamma_{4,12}$ calculated from Eqs. (19) and (20), for the special case in which $\gamma_1 = \gamma_4 = \gamma_8 = \gamma_{12} = 5/3$. This result is shown compared with the results from the simple shock tube equation and the simple buffered tube equation. The double-buffered tube curve lies above the other curves, the relative improvement increasing near the two limits $\Gamma_{4,12} \to 0 \left(\frac{a_4}{a_{12}} \to \infty\right)$ and $\Gamma_{4,12} \to \infty \left(P_{4,12} \to \infty\right)$. It is interesting to note that in one region ($\Gamma \approx 11.5$, $\mathcal{Z} \approx .36$) no improvement is obtained by using buffers. This point was checked by several exact calculations and found to be quite accurate, so that in this range a simple shock tube is just as efficient as a buffered one. It will also be noticed that the relative gain of the double-buffered tube over the simple buffered tube is always less than the relative gain of the simple buffered tube over the simple shock tube. Similar results are indicated in Figs. 13 and 14 for different gas combinations.

Evaluating the triple-buffered-tube equations (assuming strong shocks), it is found that

$$\mathcal{Z}_{16} = F_3\left(\gamma_1, \gamma_4, \gamma_8, \gamma_{12}, \gamma_{16}, \Gamma_{4,16}, \mathcal{Z}_1, \mathcal{Z}_8, \mathcal{Z}_{12}\right) \tag{22}$$

so that the following conditions must be satisfied to determine the maximum final shock strength:

$$\frac{\partial F_8}{\partial z_1} = 0 \quad , \quad \frac{\partial F_3}{\partial z_8} = 0 \quad , \quad \text{and} \quad \frac{\partial F_3}{\partial z_{12}} = 0 \tag{23}$$

The final results are quite similar to Eqs. (19), (20) and (21). In fact, the resulting equations indicate a general trend, so that it is possible immediately to generalize to a many-buffered tube of any number of sections. For example, if the driven section is called number ($n + 4$) (based on the general numbering system indicated in Fig. 11), then

$$\Gamma_{4,n+4} = \frac{\Gamma_{4n} \left(\frac{1+X_n}{X_n} \right)^{\frac{2\gamma_n}{\gamma_n - 1}}}{D_n^{2/\gamma_n - 1} E_n^2 C_n (1+X_n)^2} \tag{24}$$

and

$$z_{n+4} = D_n^{\frac{\gamma_n}{\gamma_n - 1}} C_n^{1/2} \left(\frac{X_n}{1+X_n} \right)^{\frac{\gamma_n}{\gamma_n - 1}} z_n \tag{25}$$

where

$$X_n = \frac{\gamma_{n-4} - 1}{\gamma_n - 1} \frac{\gamma_n}{\gamma_{n-4}} X_{n-4}$$

$$D_n = 1 + \left(\frac{\gamma_n - 1}{2\gamma_n} \right)^{1/2}$$

$$E_n = \left(\frac{\gamma_n - 1}{2\gamma_n} \right)^{1/2} \left(\frac{\gamma_{n+4}}{\gamma_n} \right)^{1/2} \frac{\gamma_n + 1}{\gamma_{n+4} + 1}$$

and

$$C_n = \frac{\gamma_{n+4} + 1}{\gamma_n + 1} \frac{\gamma_n}{\gamma_{n+4}}$$

These equations are valid only under the assumption that all the intermediate shock Mach numbers are greater than about seven. Of course, as the number of sections becomes large, these assumptions will generally be violated.

The results obtained from (24) and (25) are then only qualitative indications of performance, but as such they indicate an important trend. The final shock strength rapidly approaches some asymptotic value as the number of diaphragms increases, and this value depends only upon the over-all density ratio. In actual practice the performance of a many-buffered tube will depend critically upon the lengths chosen for each section. Wave interactions will generate new waves which travel in the same direction as the final shock and tend to limit testing time.

2.2.3 Effects of Area Contractions

A method for improving the performance of a simple shock tube is to employ a monotonic area contraction near the diaphragm (see Appendix II). The performance of such a shock tube is the same as that of a simple shock tube with a pressure ratio of φP_{41} and a speed of sound ratio of $\varphi^{\frac{\gamma_4-1}{2\gamma_4}} A_{41}$ where φ is the equivalence factor. Obviously, the performance of a buffered shock tube could be improved by the use of an area contraction, but here a contraction may be put at the first or second diaphragm or both.

Consider a contraction at the first diaphragm (see Fig. 15). The initial flow from region 4 to region 1 is just the same as that in a simple shock tube with an area change at the diaphragm (Eq. (A-34)), while the flow from region 2 to region 8 is the same as that in a constant-area buffered tube. Therefore, the basic equation for this configuration is

$$P_{48} = \frac{2\gamma_8 M_{s_8}^2 - (\gamma_8 - 1)}{\gamma_8 + 1} \frac{1}{g}\left[1 - \frac{\gamma_4 - 1}{\gamma_1 + 1}\left(\frac{\gamma_1}{\gamma_4}\right)^{1/2} \frac{\Gamma_{41}^{1/2}}{g^{\frac{\gamma_4 - 1}{2\gamma_4}} P_{41}^{1/2}} \times \left(M_{s_1} - \frac{1}{M_{s_1}}\right)\right]^{-\frac{2\gamma_4}{\gamma_4 - 1}} \left\{1 - \frac{(\gamma_1 - 1) M_{s_1}}{\left[2\gamma_1 M_{s_1}^2 - (\gamma_1 - 1)\right]^{1/2}\left[(\gamma_1 - 1) M_{s_1}^2 + 2\right]^{1/2}} \times \left[\frac{\gamma_1 + 1}{\gamma_8 + 1}\left(\frac{\gamma_8}{\gamma_1}\right)^{1/2}\left(\frac{\Gamma_{48}}{P_{48}}\right)^{1/2}\left(\frac{P_{41}}{\Gamma_{41}}\right)^{1/2}\left(M_{s_8} - \frac{1}{M_{s_8}}\right) - \left(M_{s_1} - \frac{1}{M_{s_1}}\right)\right]\right\}^{-\frac{2\gamma_1}{\gamma_1 - 1}} \quad (26)$$

The analysis of the buffered tube with the area contraction at the second diaphragm is a much more difficult problem. The general theory is developed in Appendix IV where it is shown that there are three possible wave diagrams when $M_2 > 1$ (see Fig. 16). The case of most practical interest is the one for which the area contraction will be great enough to produce a reflected shock (Fig. 16-c). Under these conditions the flow is adequately represented by Eqs. (A-72) and (A-76). Unfortunately, (A-76) is a fourth order algebraic equation for M_{s_r} the reflected shock Mach number, and it is usually solved by iteration.

If the shock tube has area changes at both diaphragms, the problem can be analyzed by a combination of the above two methods. Figure 17 shows the performance of a H_2-He-air shock tube operating at constant initial temperature and with an over-all pressure ratio of 10^4. When the over-all contraction ratio is nine, Fig. 17 shows the effect of different distributions of contraction ratios. The best performance is obtained with equal area ratios at each diaphragm. If, however, it is desired to have all of the contraction at one diaphragm, the better performance is obtained with the area change at the second diaphragm.

Strong shock approximations can be applied to the two cases of interest (area change at 1st or 2nd diaphragms). Consider Eq. (26) under the assumptions that $M_{s_8}^2 \gg 1$ and $M_{s_1}^2 \gg \frac{2}{\gamma_1 - 1}$; it becomes

$$Z_8^2 = C_1 Z_1^2 \left\{ D_1 - \frac{B E_1 \Gamma_{48}^{1/2} Z_8}{g^{\frac{\gamma_4 - 1}{2\gamma_4}} - \left(\frac{2\gamma_1}{\gamma_1 + 1} Z_1^2\right)^{\frac{\gamma_4 - 1}{2\gamma_4}}} \right\}^{\frac{2\gamma_1}{\gamma_1 - 1}} \tag{27}$$

After Z_8 is maximized with respect to Z_1 ,

$$\Gamma_{48} = \frac{\left[g^{\frac{\gamma_4 - 1}{2\gamma_4}} - \left(\frac{2\gamma_1}{\gamma_1 + 1} Z_1^2\right)^{\frac{\gamma_4 - 1}{2\gamma_4}} \right]^2 \left(\frac{1 + Y_1}{Y_1}\right)^{\frac{2\gamma_1}{\gamma_1 - 1}}}{B^2 E_1^2 C_1 D_1^{2/\gamma_1 - 1} (1 + Y_1)^2 Z_1^2} \tag{28}$$

and

$$Z_8 = C_1^{1/2} \left(\frac{D_1 Y_1}{1 + Y_1}\right)^{\frac{\gamma_1}{\gamma_1 - 1}} Z_1 \tag{29}$$

where

$$Y_1 = \frac{\frac{\gamma_4 - 1}{\gamma_1 - 1} \frac{\gamma_1}{\gamma_4} \left(\frac{2\gamma_1}{\gamma_1 + 1} Z_1^2\right)^{\frac{\gamma_4 - 1}{2\gamma_4}}}{g^{\frac{\gamma_4 - 1}{2\gamma_4}} - \left(\frac{2\gamma_1}{\gamma_1 + 1} Z_1^2\right)^{\frac{\gamma_4 - 1}{2\gamma_4}}} \tag{30}$$

When the area change is all at the second diaphragm, an analytical solution to the optimization problem can be obtained only if the contraction is infinite. Fortunately, for area ratios of ten or greater, the area change may be considered essentially infinite. In this case

$$M_{s_r}^2 = \frac{2\gamma_1 M_{s_1}^2 - (\gamma_1 - 1)}{(\gamma_1 - 1) M_{s_1}^2 + 2} \tag{31}$$

and the basic Eq. (A-72) is greatly simplified (see (A-78)). When the assumption that $M_{s_8}^2 \gg 1$ and $M_{s_1}^2 \gg \frac{2}{\gamma_1 - 1}$ is made,

$$Z_8'^2 = \frac{3\gamma_1 + 1}{\gamma_1 - 1} C_1 Z_1^2 \left\{ 1 - \frac{\frac{\gamma_4 - 1}{\gamma_8 + 1}\left(\frac{\gamma_8}{\gamma_4}\right)^{1/2}\left[\frac{\gamma_1 - 1}{2(3\gamma_1 - 1)}\right]^{1/2} Z_8' \Gamma_{48}'^{1/2}}{1 - \left(\frac{2\gamma_1}{\gamma_1 + 1} Z_1^2\right)^{\frac{\gamma_4 - 1}{2\gamma_4}}} \right\}^{\frac{2\gamma_1}{\gamma_1 - 1}} \tag{32}$$

where

$$Z_8' = \frac{M_{s_8}}{\sqrt{G_\infty P_{48}}} \qquad \Gamma_{48}' = G_\infty^{1/\gamma_1} \Gamma_{48}$$

and

$$G_\infty = \left(\frac{\gamma_1 + 1}{2}\right)^{\frac{\gamma_1}{\gamma_1 - 1}}$$

G_∞ is the equivalence factor for an infinite area contraction at the second diaphragm. Obviously Z_8 can be maximized with respect to Z_1 in exactly the same way as for a constant-area buffered tube. The results are as follows:

$$\Gamma_{48}' = \frac{2\left[1 - \left(\frac{2\gamma_1}{\gamma_1 + 1} Z_1^2\right)^{\frac{\gamma_4 - 1}{2\gamma_4}}\right]^2 \left(\frac{1 + X_1}{X_1}\right)^{\frac{2\gamma_1}{\gamma_1 - 1}}}{(1 + X_1)^2 Z_1^2 B^2 \frac{\gamma_1 + 1}{\gamma_8 + 1}} \tag{33}$$

and

$$Z_8' = C_1^{1/2} \left(\frac{3\gamma_1 - 1}{\gamma_1 - 1}\right)^{1/2} \left(\frac{X_1}{1 + X_1}\right)^{\frac{\gamma_1}{\gamma_1 - 1}} Z_1 \tag{34}$$

In Fig. 18 a comparison is shown between the exact Eq. (A-78) and the strong shock Eq. (32) for the case of cold hydrogen driver, monatomic buffer, and driven air. The agreement is excellent at large values of buffer gas molecular weight and reasonably good even for a helium buffer. Figure 18 is entirely analogous to Fig. 9 except for the area change, and the discussion of Fig. 9

applies equally well here.

Figure 19 can be constructed from Eqs. (33) and (34). The graph again points up the fact that some improvement may be obtained by using gases with small values of γ_4, but the performance is quite insensitive to changes in γ_a.

2.3 DETONATION BUFFERS

One method of improving shock tube performance is the use of some combustion process in the driver to raise the pressure and temperature.[1,6,11,12,24] The most widely used of these techniques is constant-volume combustion in which the gas is ignited and the diaphragm ruptures just as the peak pressure is reached. Performance calculations for this type of shock tube can be made by using the simple shock tube equation and effective values of p_4, γ_4, and a_4 corresponding to conditions after combustion. Therefore, the previous methods of analysis are applicable to any shock tube with a constant-volume combustion driver.

Two other combustion processes which have been used for driver gas heating are constant-pressure combustion[24] and detonation. Both of these methods suffer because the initial shocks are closely followed by rarefaction waves which limit steady flow and cause shock wave attenuation. Also, there is a lack of uniformity of diaphragm ruptures with constant-pressure combustion.

The fundamental equations of detonation wave theory are reviewed in Appendix V where it is shown that a pure detonation is always followed by an expansion wave that lowers the pressure and velocity. If a piston were maintained in motion behind the detonation with a velocity equal to that of the flow immediately behind the detonation front, no expansion could exist. If the piston where maintained at a higher velocity, the detonation wave would be propagated

at a faster speed, that is, it would be overdriven.

Consider a constant-area buffered tube with a detonable mixture in the buffer. Such a device will be called a detonation buffer. If the conditions in the driver section are such that p_2 and u_2 are equal to or greater than the Chapman-Jouguet values, the detonation in the buffer will be followed by a region of quasi-steady flow. The wave diagram will then be similar to that shown in Fig. 1, but the calculations will not be so straightforward. In particular, the flow through the unsteady expansion between regions 2 and 6 must be calculated by integrating the characteristic equation

$$du = -\frac{a}{\rho}\, d\rho \tag{35}$$

along an isentrope.[25]

Some exact calculations were performed for a shock tube with a hydrogen driver gas, air driven gas, and a stoichiometric hydrogen-oxygen buffer gas (with an without helium diluent). Equation (35) was integrated with the help of Mollier charts constructed from data obtained from Dr. Sanford Gordon at Lewis Research Center, NASA. Conditions behind the over-driven detonation were found by using the equilibrium normal shock IBM 704 program developed by Dr. Russell E. Duff of Los Alamos Scientific Laboratories. Throughout the calculations the hydrogen driver was considered as an ideal gas, and the air was treated as being in equilibrium.[26,27] The exact calculations are very time consuming, and, consequently, only a few of them were made. Some typical results are shown in Fig. 20 as a comparison to the approximate theory that is developed below.

The addition of helium diluent to stoichiometric hydrogen-oxygen has some interesting effects.[28] As helium is added, the detonation velocity

increases and the molecular weight of the burnt gas decreases. The pressure and temperature behind the detonation drop, but the speed of sound increases. As a net result, the final shock strength does not vary much with the addition of helium. Of course, the detonation buffer does offer an improvement in performance over the inert gas buffer, but the gain is not outstanding.

In order to compare the detonation buffer with the constant-area inert-gas-buffered tubes over the full range of operating conditions, it is desirable to maximize the final shock strength and present a general Γ_{48} vs. $\bar{z}_8$ curve for the detonation buffer. To facilitate such an analysis a number of assumptions will have to be made. Suppose that the detonable mixture may be treated as an ideal gas before detonation and as a different ideal gas after detonation. Further assume that the unsteady-expansion flow can be calculated in terms of an average specific heat ratio γ_{av}. Then the basic equation for the shock tube becomes

$$P_{48} = P_{78} \left\{ 1 - \frac{\gamma_4 - 1}{2} \frac{u_2}{a_1} \frac{a_1}{a_4} \right\}^{-\frac{2\gamma_4}{\gamma_4 - 1}} \left\{ 1 - \frac{\gamma_{av} - 1}{2a_2} (u_7 - u_2) \right\}^{-\frac{2\gamma_{av}}{\gamma_{av} - 1}} \tag{36}$$

where

$$\frac{u_2}{a_1} = \left(\frac{P_{21} - 1}{\gamma_1} \right)^{1/2} \left\{ \frac{\frac{2}{\gamma_2 - 1} P_{21} - \frac{2}{\gamma_1 - 1} - \frac{2\gamma_1}{\gamma_1 - 1} \varphi}{1 + \frac{\gamma_2 + 1}{\gamma_2 - 1} P_{21}} \right\}^{1/2} \tag{37}$$

and

$$\varphi = \frac{\Delta E_c}{c_{p_1} T_1}$$

ΔE_c is the heat released per unit mass by the chemical reaction at constant temperature and pressure (see Appendix V).

The resulting equations will be simplified by using P_{21} and P_{78} to

represent shock strengths rather than M_{s_1} and M_{s_8}. When the normal shock relations are applied, it is found that

$$\frac{u_7}{a_8} = \left(\frac{2}{\gamma_8}\right)^{1/2} \frac{P_{78}-1}{\left[(\gamma_8+1)P_{78}+(\gamma_8-1)\right]^{1/2}} \tag{38}$$

and

$$\frac{a_2}{a_1} = \left(\frac{\gamma_2 P_{21}}{\gamma_1}\right)^{1/2} \left\{\frac{P_{21}+\frac{\gamma_1+1}{\gamma_1-1}+\frac{2\gamma_1}{\gamma_1-1}\varphi}{\frac{\gamma_2+1}{\gamma_2-1}P_{21}+1}\right\}^{1/2} \tag{39}$$

If Eqs. (38) and (39) are used in Eq. (36),

$$P_{48} = P_{78}\left\{1-\frac{\gamma_4-1}{2\sqrt{\gamma_4}}\left(\frac{\Gamma_{41}}{P_{41}}\right)^{1/2}\left(P_{21}-1\right)^{1/2} \times \right.$$

$$\left.\left[\frac{\frac{2}{\gamma_2-1}P_{21}-\frac{2}{\gamma_1-1}-\frac{2\gamma_1}{\gamma_1-1}\varphi}{1+\frac{\gamma_2+1}{\gamma_2-1}P_{21}}\right]^{1/2}\right\}^{-\frac{2\gamma_4}{\gamma_4-1}} \left\{1-\frac{(\gamma_{av}-1)\left[\frac{\gamma_2+1}{\gamma_2-1}P_{21}+1\right]^{1/2}}{2(\gamma_2 P_{21})^{1/2}\left[P_{21}+\frac{\gamma_1+1}{\gamma_1-1}+\frac{2\gamma_1}{\gamma_1-1}\varphi\right]^{1/2}} \times \right. \tag{40}$$

$$\left.\left[\frac{\sqrt{2}\,(P_{78}-1)}{\left[(\gamma_8+1)P_{78}+(\gamma_8-1)\right]^{1/2}}\left(\frac{\Gamma_{48}}{P_{48}}\right)^{1/2}\left(\frac{P_{41}}{\Gamma_{41}}\right)^{1/2}-\left(P_{21}-1\right)^{1/2}\left[\frac{\frac{2}{\gamma_2-1}P_{21}-\frac{2}{\gamma_1-1}-\frac{2\gamma_1}{\gamma_1-1}\varphi}{1+\frac{\gamma_2+1}{\gamma_2-1}P_{21}}\right]^{1/2}\right]\right\}^{-\frac{2\gamma_{av}}{\gamma_{av}-1}}$$

Now apply a strong shock approximation $P_{21} >> 1$ and $P_{78} >> 1$ This is essentially the same as assuming $M_{s_1}^2 >> 1$ and $M_{s_6}^2 >> 1$. Then

$$\frac{P_{78}}{P_{48}} = \left\{1 - \frac{\gamma_4 - 1}{2\sqrt{\gamma_4}} \left(\frac{\Gamma_{41}}{P_{41}}\right)^{1/2} \frac{\left[\frac{2}{\gamma_2 - 1} P_{21} - \frac{2\gamma_1}{\gamma_1 - 1} \varphi\right]^{1/2}}{\left(\frac{\gamma_2 + 1}{\gamma_2 - 1}\right)^{1/2}}\right\}^{+\frac{2\gamma_4}{\gamma_4 - 1}} \times$$

$$\left\{1 - \frac{(\gamma_{av} - 1)\left(\frac{\gamma_2 + 1}{\gamma_2 - 1}\right)^{1/2}}{2\sqrt{\gamma_2}\left[P_{21} + \frac{\gamma_1 + 1}{\gamma_1 - 1} + \frac{2\gamma_1}{\gamma_1 - 1}\varphi\right]^{1/2}} \left[\sqrt{2}\left(\frac{P_{78}}{P_{48}}\right)^{1/2}\left(\frac{\Gamma_{48}}{\gamma_8 + 1}\right)^{1/2}\left(\frac{P_{41}}{\Gamma_{41}}\right)^{1/2}\right.\right. \tag{41}$$

$$\left.\left. - \left(\frac{\gamma_2 - 1}{\gamma_2 + 1}\right)^{1/2}\left[\frac{2}{\gamma_2 - 1} P_{21} - \frac{2\gamma_1}{\gamma_1 - 1}\varphi\right]^{1/2}\right]\right\}^{+\frac{2\gamma_{av}}{\gamma_{av} - 1}}$$

or

$$\frac{P_{78}}{P_{48}} = F_4\left(\gamma_1, \gamma_2, \gamma_4, \gamma_8, \gamma_{av}, P_{21}, \varphi, \Gamma_{41}/P_{41}, \Gamma_{48}\right) \tag{42}$$

By the use of the relation

$$P_{41} = P_{21}\left\{1 - \frac{\gamma_4 - 1}{2\sqrt{\gamma_4}}\left(\frac{\gamma_2 - 1}{\gamma_2 + 1}\right)^{1/2}\left[\frac{2}{\gamma_2 - 1} P_{21} - \frac{2\gamma_1}{\gamma_1 - 1}\varphi\right]^{1/2}\left(\frac{\Gamma_{41}}{P_{41}}\right)^{1/2}\right\}^{-\frac{2\gamma_4}{\gamma_4 - 1}} \tag{43}$$

the dependence of F_4 upon $\frac{\Gamma_{41}}{P_{41}}$ could be replaced by a dependence upon P_{41} only. It is interesting to note that Eq. (41) can't be appreciably simplified by making more stringent assumptions about the initial shock strength. Of course, it is true that for $P_{21} \gg \frac{2\gamma_1\varphi}{\gamma_1 - 1}$ the equations are no longer dependent on φ, but this is the trivial case corresponding to no appreciable chemical energy. Suppose that the initial specific heat ratios γ_1, γ_4, γ_8 and the over-all density ratio Γ_{48} are fixed. It is found that P_{78}/P_{48} is still

a function of the five variables γ_2 , γ_{av}, φ , P_{41} , and P_{21} .

To make this problem tractable assume that γ_2 , γ_{av} , and φ are known beforehand. Reasonable estimates of these quantities can be obtained if the buffer gas and its initial temperature are known. If the temperature and molecular weight of the driver gas are known, then

$$\frac{\Gamma_{41}}{P_{41}} = \frac{\mu_{41}}{T_{41}} = K^2 \qquad \text{a constant} \qquad (44)$$

and P_{78}/P_{48} depends only upon P_{21} . The maximizing procedure is then straightforward and a plot of P_{78}/P_{48} vs. Γ_{48} can be obtained. Of course, a different plot will be obtained for every value of the set of variables K , γ_2 , γ_{av} , and φ . This procedure is the same as that used to predict the first approximation curves for an inert-gas-buffered tube (Appendix III). By analogy with the inert-gas tube, it is reasonable to assume that the variation of the performance curves with K will be small.

Maximizing (41) for fixed values of γ_2 , γ_{av}, φ , and K is straightforward but tedious. The results of the computation for two different values of K are shown in Fig. 20. Both curves show the performance of a tube with a hydrogen driver, stoichiometric hydrogen-oxygen buffer, and air as the driven gas. The values of the various constants used are as follows:

$\gamma_2 = 1.15$ $\qquad$ $\gamma_{av} = 1.23$

$\Delta E_c = 57$ kcal./mole $\qquad$ $\varphi = 23.0$

for $T_4 = 1000°K$ $\qquad$ $K = .22$

for $T_4 = 300°K$ $\qquad$ $K = .41$

The X's represent typical points from the "exact" calculation with $K = .22$. The agreement with the approximate solution curve indicates that the assump-

tions used in the approximation are reasonable. The lower curve ($K = .22$) corresponds to a heated hydrogen driver and large values of P_{21} for a given Γ_{48} . The values of P_{21} corresponding to this curve are considerably above the Chapman-Jouguet value so that the detonation is strongly overdriven. This performance curve is almost identical to that of a tube with an inert buffer gas.

The curve which corresponds to a cold hydrogen driver ($K = .41$) is somewhat higher than might be expected. However, in this case the optimum P_{21} is the Chapman-Jouguet value up to about $\Gamma_{48} = 3 \cdot 10^3$. This should give the maximum gain over the inert-gas tube since the ratio of the chemical energy to the total energy is the greatest in this case. Above $\Gamma_{48} = 3 \cdot 10^3$ the detonation is overdriven and the relative gain of this device should decrease. At very large values of Γ_{48} the chemical energy released by the detonation is insignificant compared to the total energy, and the performance of the tube is essentially that of an inert-gas-buffered tube.

3. TESTING TIME

Testing time is defined as the interval of time between the arrival of the shock and the arrival of the contact surface at some point in the test section of the shock tube. By considering the equation of continuity we can arrive at a simple expression for the ideal testing time.[21]

$$\tau_i = \frac{X}{a_1 M_{s_1}(\Gamma_{21} - 1)} \tag{45}$$

where X is the distance from the diaphragm. Ideally the testing time could be increased to any value merely by building the driven section long enough. Of course, for a simple shock tube with a driver section of finite length, the

expansion wave $\overleftarrow{R}_1$ will reflect off the end of the driver and overtake the contact surface (see Fig. 21). So, for a fixed driver length, there is an optimum length of the driven section which will yield the maximum test time.[29]

The wave diagram analysis for the buffered shock tube becomes much more complex (Fig. 22). Many different wave interactions must be considered: for example, the interaction of $\vec{R}_3$ and $\vec{C}_1$, the interaction of $\vec{C}_1$ and $\overleftarrow{R}_2$, the interaction of $\vec{R}_3$ and $\overleftarrow{R}_2$, etc. Figure 22 represents one possible length distribution that will lead to relatively long testing times in the driven section. If area changes are present in the shock tube, the wave diagram is further complicated by more reflected waves.

Unfortunately, the actual testing time is not accurately determined by the idealized wave diagram technique. In the first place, if the driven section is very long, shock wave attenuation will be important. The testing times calculated for ideal gases will be lowered somewhat by considering real gas effects. However, Eq. (45) does not require that the driven gas be ideal, so that real gas calculations can be used with it. In practice the contact surface will not be a discontinuity but will be turbulent and diffuse. This reduces the test time considerably; a good rule of thumb is to multiply the ideal test time by a factor of one-half.

At pressures below about five millimeters of mercury the testing time is found to be much lower than that predicted even with the above corrections. Roshko showed that this could be largely explained in terms of the loss of mass across the contact surface due to the laminar boundary layer behind the shock.[21] He solves the problem in terms of two similarity parameters X and T.

$$X = 16 \left(\frac{P\mu}{\rho a}\right)_{s.t.p.} \beta^2 \frac{\bar{Z}_2}{M_{s_1}} \frac{T_2}{T_1} \frac{(\Gamma_{21}-1)}{\Gamma_{21}} \frac{x}{p_1 d^2} \tag{46}$$

$$T = X (\Gamma_{21}-1) \frac{a_1 \tau M_{s_1}}{x} \tag{47}$$

where s.t.p. implies room temperature and atmospheric pressure

β parameter depending on Γ_{21} , γ_1 , and σ

σ Prandtl number

τ actual testing time

$\bar{Z}_2$ compressibility of shocked gas

d diameter of driven section

μ dynamic viscosity coefficient

Roshko found the relation between the two parameters to be

$$X = -2 \left[\ln\left(1 - T^{1/2}\right) + T^{1/2}\right] \tag{48}$$

for which $T \longrightarrow 1$ as $X \longrightarrow \infty$. Hooker expanded Roshko's theory to account for boundary layer mass accumulation between the shock wave and the contact surface.[22] Hooker's equation for $X(T)$ is more complicated than Eq. (47), but the improvement is relatively minor.

Recently Mirels has analyzed this problem and removed some inconsistencies which appeared in the previous analyses.[23] In particular, by considering the variations in free stream conditions between the shock and the contact surface he was able to find improved values of the parameter β . The improvement provides much better correlation with experimental data for low shock Mach numbers; for large Mach numbers the analysis basically agrees

with that of Roshko and Hooker and with the experimental data.

The fact that τ approaches a limit indicates that the actual testing time does not continue to increase as the length of the driven section is increased. After a certain time the contact surface moves at the same speed as the shock, and the testing time is at a constant value that shall be denoted by τ_{max} . Roshko shows that

$$\tau_{max} = \frac{1}{16\beta^2}\left(\frac{\rho}{\mu P}\right)_{s.t.p.} \frac{T_1}{\bar{z}_2 T_2}\left(\frac{\Gamma_{21}}{(\Gamma_{21}-1)^2}\right) p_1 d^2 \qquad (49)$$

Throughout the analyses of Roshko, Hooker, and Mirels it is assumed that the boundary layer is thin (relative to the tube hydraulic radius) and laminar between the shock and the contact surface. Mirels has evaluated both the Reynolds number and the boundary layer thickness at the contact surface (when it is at the maximum distance from the shock) and found these assumptions to be good for strong shocks and low initial pressures. For relatively weak shocks (under Mach three, say) and low initial pressure such as those used by Duff,[20] the boundary layer becomes rather thick at the contact surface.

For a fixed value of shock Mach number the maximum testing time as determined by boundary layer development depends directly upon the initial pressure and on the diameter squared. This fact has aroused interest in shock tubes with large diameter driven sections for improving testing time. The size of the shock tube driver is usually limited by structural and economic considerations. Therefore, shock tubes with larger diameter driven sections than driver sections have been studied.

A simple shock tube with an increase in area at the diaphragm admits to one of four possible flow patterns (see Appendix II and Fig. 23). Generally,

for strong shocks the flow will be of type (a), but for very large area changes the other types are possible. Figure 24 illustrates the performance of such a tube with varying values of driven pressure and diameter. With fixed driver conditions (hydrogen, T_4 = 750°F, p_4 = 15,000 psia, d_4 = 3.5") and the shock Mach number held at 20, the pressure in the driven section must be lowered for operation at larger diameters. These calculations were performed assuming that hydrogen is an ideal gas with γ = 7/5 and using the properties of equilibrium air. From Fig. 24 it can be seen that testing time is being lost by going to larger diameter driven sections since the quantity $p_8 d_8^2$ decreases. The maximum testing time is obtained with a constant-area buffered tube.

The analysis of buffered tubes with larger driven sections than driver sections is more complex. For example, if all the area change is at the second diaphragm, a typical wave diagram is shown in Fig. 25. The upstream-facing wave $\overleftarrow{W}$ is either a shock wave or a rarefaction fan depending upon the final shock strength and the area ratio. The flow from region 2 to region 5 is a steady expansion and is completely determined by conditions in region 2 and the area change. The most efficient operation of this type of shock tube occurs when the buffer pressure is so chosen that $\overleftarrow{W}$ reduces to a sound wave. Of course, if the area change is small, it may not be possible to reduce it to a sound wave. Figure 24 compares the performance of the shock tube configuration of Fig. 25 at the optimum buffer pressure with that of a simple shock tube with an area change and the same driver conditions. The comparison certainly indicates the importance of using a buffer with this type of a shock tube.

Using the values of p_8, d_8, and M_{s_8} from Fig. 24, calculations of τ_{max} were made from Roshko's theory. The testing time drops with

increasing diameter, though not as severely as for the simple shock tube. For certain arc-heated facilities the testing time is found to actually increase with increasing diameter and fixed Mach number.[5] With an arc-heated helium driver the speed-of-sound ratio from the driver gas to the driven gas may be as high as thirteen. In this range the gain in shock Mach number with increasing pressure ratio is greater than in the more conventional range of speed-of-sound ratios. Nevertheless, the gain in testing time is quite small. There appears to be no strong reason for using large diameter driven sections when operating at high Mach numbers.

Now consider a buffered tube similar to that of Fig. 25 but with a converging-diverging area change at the second diaphragm. A typical wave diagram for this configuration is shown in Fig. 26. Again $\overleftarrow{W}$ may be a shock or an expansion, and this must be determined in each particular problem. Figure 27 compares the performance of such a configuration with that of a tube with just a monotonic divergence at the second diaphragm. Notice that there is always a loss in performance by using the converging-diverging section. This result is analogous to the result obtained for the case of an area change at the first diaphragm[32] (see Appendix II). It is apparently true that the most efficient way to accomplish an area change at a diaphragm is monotonically.

Finally, examine the effect of distributing a total area expansion between the two diaphragm stations. Figure 28 presents results for given over-all conditions and varying buffer diameter and pressure. The maximum final shock Mach number increases as the buffer diameter is increased from the driver size to the driven section size. Although the performance continues to improve as the buffer diameter is further increased, the improvement is

rather limited and by the time that $A_1 = 2A_8$ the performance curve is again below the curve for $A_1 = A_8$. So, for practical purposes, the most efficient geometrical configuration is one for which all the area expansion occurs at the first diaphragm.

4. CONCLUDING REMARKS

A method has been presented for quickly determining the optimum operating conditions of buffered shock tubes and the final shock strength obtainable at these optimum conditions. While the resulting equations are based on a strong shock assumption, these equations are quite accurate for most of the cases of interest. Even in problems to which the assumptions do not wholly apply, the analysis indicates the range of conditions to consider for making exact calculations.

Most of the report is concerned with applying the strong shock analysis to different buffered shock tube configurations. Although much has been written about buffered shock tubes, it seems worthwhile to summarize our present knowledge about these devices.

1. For given over-all conditions a buffered shock tube will produce stronger final shocks than a simple shock tube provided that the optimum buffer conditions are used. However, if the over-all density ratio is of order ten, the improvement is negligible. The relative improvement increases as the over-all density ratio approaches its two limits $(\Gamma_{48} \to 0\,,\ \Gamma_{48} \to \infty)$.

2. Within the framework of the strong shock approximation, the final shock strength $\bar{z}_8$ depends only upon the upstream density ratio Γ_{41} when the specific heat ratios and the over-all density ratio are specified. After optimizing, $\bar{z}_8$ -maximum depends only upon Γ_{48} and the specific heat ratios.

3. Other factors being equal, the best driver gas is diatomic and the

best buffer gas is monatomic. The specific heat ratio of the driven gas is relatively unimportant.

4. If the strong shock assumption is relaxed somewhat, it is found that $\bar{z}_s$ -maximum depends not only upon Γ_{48} but also (to a lesser degree) upon $K = \left(\frac{\Gamma_{41}}{P_{41}}\right)^{1/2}$. For fixed Γ_{48} , $\bar{z}_s$ -maximum increases as K increases (M_{s_1} decreases).

5. The performance of a buffered shock tube improves as the number of buffers increases provided, of course, that the optimum conditions are used. However, as the number of buffers increases, the final shock strength approaches its asymptotic value, and the relative gain decreases.

6. A buffered tube with an area contraction at either or both diaphragms yields higher shock strengths than a constant-area tube. The optimum distribution of a given area contraction is in equal proportions between the two diaphragm stations. However, if all the area reduction is to be at one diaphragm station, it is better for the change to be at the second diaphragm.

7. A shock tube with a detonable gas in the buffer can produce stronger final shocks than inert-gas-buffered tubes. The maximum gain is obtained when the initial shock (detonation) is near the Chapman-Jouguet value. However, for the production of very strong final shocks, the detonation must be considerably overdriven. In these cases the gain in performance over the inert-gas tubes is not significant.

8. For fixed driver conditions, increasing the diameter of the driven section requires that the pressure in the driven section be lowered in order to maintain the same final shock Mach number. The net effect of the increased diameter but decreased pressure is to reduce the available testing time in

most cases of interest. When the speed-of-sound ratio across the diaphragm is very high, only a small increase in testing time may be obtained.

ACKNOWLEDGEMENT

The author wishes to acknowledge the assistance received from Dr. J. Gordon Hall throughout this research and during the preparation of this report. Also, grateful acknowledgement is given to Dr. Sanford Gordon of Lewis Research Center, NASA, for the data he furnished on the thermodynamic properties of hydrogen-oxygen mixtures (with and without helium diluent).

REFERENCES

1. Glass, I. I., and Hall, J. G., Handbook of Supersonic Aerodynamics, NAVORD Rept. 1488, Vol. 6, Sec. 18, "Shock Tubes". December, 1959.

2. Lin, S. C., A Survey of Shock Tube Research Related to the Aerophysics Problem of Hypersonic Flight. Avco Everett AMP 63, AFCRL 700, July, 1961.

3. Hertzberg, A., Wittliff, Charles E., and Hall, J. Gordon, Summary of Shock Tunnel Development and Application to Hypersonic Research. CAL Rept. AD-1052-A-12, AFOSR TR 60-139, July, 1961.

4. Warren, W. R., Rogers, D. A., and Harris, C. J., "The Development of an Electrically Heated Shock Driven Test Facility". Second Symposium on Hypervelocity Techniques, March 20-21, 1962.

5. Camm, John C., "Escape-Velocity Shock Tube with Arc-Heated Driver." Second Symposium on Hypervelocity Techniques, March 20-21, 1962.

6. Resler, E. L., Lin, Shao-Chi, and Kantrowitz, A., "The Production of High Temperature Gases in Shock Tubes". J. Appl. Physics, Vol. 23, No. 12, December, 1952.

7. Bernstein, H., "A Double-Diaphragm Shock Tube to Produce Transient High Mach Number Flows". J. Aeronaut. Sci., Vol. 20, November, 1953.

8. Glass, I. I., Martin, W. A., and Patterson, G. N., A Theoretical and Experimental Study of the Shock Tube. University of Toronto Institute of Aerophysics, Rept. No. 2, November, 1953.

9. Henshall, B. D., The Use of Multiple Diaphragms in Shock Tubes. Aeronautical Research Council Tech. Rept. 18062, December, 1955.

10. Russo, Anthony L., and Hertzberg, A., Modifications of the Basic Shock Tube to Improve its Performance. CAL Rept. AD-1052-A-7, AFOSR TN 58-716, August, 1958.

11. Slawsky, Z. I., and Seigel, A. E., A Two-Stage Driver for Shocktubes and Shock Tunnels. NAVORD Rept. 5669, Ballistics Research Report 1, June, 1960.

12. Gaydon, A. G., and Hurle, I. R., The Shock Tube in High-Temperature Chemical Physics. Chapman and Hall, Ltd., London, 1963.

13. Schexnayder, Charles J., Jr., "On the Performance of a Double-Diaphragm Shock Tube Using the Reflected-Shock Method and a Light-Gas Buffer". Jour. Aero/Space Sci., Vol. 25, No. 8, August, 1958.

14. Hey, J. S., Pinson, J. T., and Smith, P. G., "Radio Observations of Hypersonic Shock Waves". Nature, Vol. 182, November, 1958.

15. Chapin, S. G., and Heyman, R. J., Performance Characteristics of the High-Performance Shock Tube. Martin Research Rept., R-60-37, February, 1961.

16. Humphreys, R. P., and Chapin, S. G., Uniform Flow Duration in Shock Tubes. Martin Marietta Research Rept. R-61-46, December, 1961.

17. Hacker, D. S., and Wilson, L. N., "Shock Tube Results for Hypersonic Stagnation Heating at Very Low Reynolds Numbers." Symposium on Dynamics of Manned Lifting Planetary Entry. John Wiley and Sons, Inc., New York, 1963.

18. McDill, P. L., Brown, E. A., and Ross, P.A., The Performance of a Buffered Shock Tube with Area Reduction. Boeing Airplane Company, Document D2-12867, March, 1962.

19. Hall, J. Gordon, and Russo, Anthony, L., "Simplification of the Shock-Tube Equation". AIAA Journal, Vol. 1, No. 4, April, 1963.

20. Duff, Russell E., "Shock-Tube Performance at Low Initial Pressure". The Phys. of Fluids, Vol. 2, No. 2, March-April, 1959.

21. Roshko, Anatol, "On Flow Duration in Low-Pressure Shock Tubes". The Phys. of Fluids, Vol. 3, No. 6, November-December, 1960.

22. Hooker, William J., "Testing Time and Contact-Zone Phenomena in Shock-Tube Flows". The Phys. of Fluids, Vol. 4, No. 12, December, 1961.

23. Mirels, Harold, Test Time in Low Pressure Shock Tubes. Aerospace Corporation, Rept. No. TDR-169 (3230-12) TN-5, December, 1962.

24. Hertzberg, A. and Smith, W., "A Method for Generating Strong Shock Waves". J. of Appl. Phys., Vol. 25, January, 1954.

25. Courant, R., and Friedrichs, K. O., Supersonic Flow and Shock Waves. Interscience Publishers, Inc., New York, 1948.

26. Feldman, S., Hypersonic Gas Dynamic Charts for Equilibrium Air. Avco Research Laboratory., Everett Mass., January, 1957.

27. Ziemer, Richard W., Extended Hypervelocity Gas Dynamic Charts for Equilibrium Air. Space Technology Lab. Rept. STL TR-60-0000-09093, April, 1960.

28. Lewis, B., and von Elbe, G., Combustion, Flames and Explosions of Gases. Academic Press, Inc., New York and London, 1961.

29. Lobb, R. K., On the Length of a Shock Tube. Naval Ordnance Laboratory Memo 10494, July, 1950.

30. Rudinger, G., Wave Diagrams for Nonsteady Flow in Ducts. D. Van Nostrand Co., Inc., New York, 1955.

31. Lukasiewicz, J., Shock Tube Theory and Applications. National Aeronautical Establishment, Report 15, 1952.

32. Alpher, R. A., and White, D. R., Ideal Theory of Shock Tubes with Area Change Near Diaphragm. General Electric Research Laboratory Rept. No. 57-RL-1664, January, 1957.

33. Russell, D. A., A Study of Area Change Near the Diaphragm of a Shock Tube. GALCIT Hypersonic Research Project Memorandum No. 57, July, 1960.

34. Rudinger, George, "Passage of Shock Waves Through Ducts of Variable Cross Section". The Phys. of Fluids, Vol. 3, No. 3, May-June, 1960.

35. Brower, W. B., Jr., An Investigation of the Flow Due to Shock Impingement on a Constriction. Rensselaer Polytechnic Institute, Department of Aeronautical Engineering, TR AE 6107, August, 1961.

APPENDIX I

DERIVATION OF THE BASIC EQUATIONS FOR CONSTANT-AREA BUFFERED SHOCK TUBES

Many of the results derived in these appendices are well known and are presented in several places in the literature. They are included here for convenience and to introduce the notation.

Consider the constant-area buffered shock tube shown in Fig. 1. The wave diagram is drawn subject to the following assumptions: the flow is one-dimensional and inviscid with no heat conduction, the diaphragms are instantaneously removed, no mixing occurs at the contact surfaces, and there is no shock wave attenuation. Across the contact surfaces velocities and pressures are equal, while other thermodynamic variables may be discontinuous.

$$p_2 = p_3\,, \qquad u_2 = u_3\,, \qquad p_6 = p_7 \quad \text{and} \quad u_6 = u_7 \tag{A-1}$$

The ordinary Rankine-Hugoniot shock relations hold across the shock waves in coordinate systems at rest with respect to the shocks. For the initial shock

$$\rho_1 U_{s_1} = \rho_2 \left(U_{s_1} - u_2\right) \tag{A-2}$$

$$p_1 + \rho_1 U_{s_1}^2 = p_2 + \rho_2 \left(U_{s_1} - u_2\right)^2 \tag{A-3}$$

$$e_1 + \frac{p_1}{\rho_1} + \frac{1}{2} U_{s_1}^2 = e_2 + \frac{p_2}{\rho_2} + \frac{1}{2} \left(U_{s_1} - u_2\right)^2 \tag{A-4}$$

where e is the internal energy per unit mass. A similar set of equations holds for the final shock $\vec{S}_8$. Applying the method of characteristics to the one-dimensional unsteady motion in the upstream-facing expansion waves $\overleftarrow{R}_1$ and

$\overleftarrow{R}_2$ it is found that the P Riemann invariant $u + \int \frac{a}{\rho} d\rho$ is constant.[25] Given the initial conditions in regions 4, 1, and 8 and the thermal and caloric equations of state for the gases, the shock Mach numbers M_{s_1} and M_{s_8} can be uniquely determined. In what follows it will be assumed that the gases used in the shock tube are ideal and have constant specific heats. In this case, the Riemann invariant expression can be integrated to yield

$$u + \frac{2a}{\gamma - 1} = \text{const.} \tag{A-5}$$

across an upstream facing wave (Q-wave). Also, since the flow across any expansion is isentropic,

$$\frac{p_4}{p_3} = \left(\frac{a_4}{a_3}\right)^{\frac{2\gamma_4}{\gamma_4 - 1}} \tag{A-6}$$

The velocity u_4 is zero so that Eq (A-5) applied to $\overleftarrow{R}_1$ yields

$$a_4 = a_3 + \frac{\gamma_4 - 1}{2} u_3 \tag{A-7}$$

From Eqs. (A-1), (A-6), and (A-7)

$$p_4 = p_2 \left[1 - \frac{\gamma_4 - 1}{2} \frac{u_2}{a_4}\right]^{-\frac{2\gamma_4}{\gamma_4 - 1}} \tag{A-8}$$

The pressure ratio and the density ratio across the initial shock are

$$P_{21} = \frac{2\gamma_1 M_{s_1}^2 - (\gamma_1 - 1)}{\gamma_1 + 1} \tag{A-9}$$

$$\Gamma_{21} = \frac{(\gamma_1 + 1) M_{s_1}^2}{(\gamma_1 - 1) M_{s_1}^2 + 2} \tag{A-10}$$

CONT.

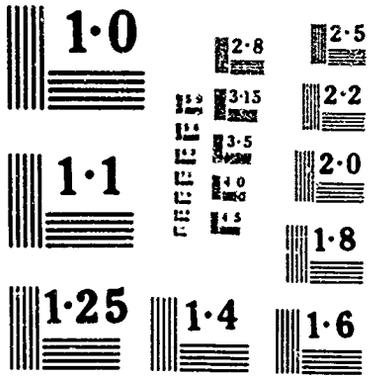
1·0
1·1
1·25
2·8
3·15
3·5
4·0
4·5
1·4
2·5
2·2
2·0
1·8
1·6

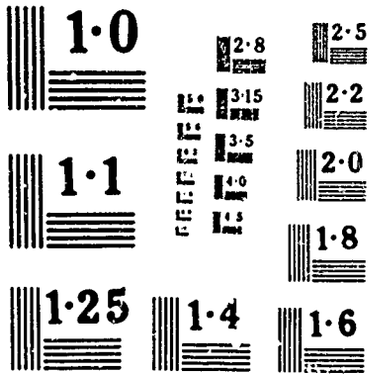
1·0
1·1
1·25
2·8
3·15
3·5
4·0
4·5
1·4
2·5
2·2
2·0
1·8
1·6

BLANK PAGE

Using Eq. (A-10) in (A-2), it is seen that

$$u_2 = \frac{2a_1}{\gamma_1+1}\,\frac{M_{s_1}^2-1}{M_{s_1}} \tag{A-11}$$

Finally, using (A-8), (A-9), and (A-11), the well-known simple shock tube equation is obtained.

$$P_{41} = \frac{2\gamma_1 M_{s_1}^2-(\gamma_1-1)}{\gamma_1+1}\left[1-\frac{\gamma_4-1}{\gamma_1+1}\,\frac{(M_{s_1}^2-1)}{A_{41}M_{s_1}}\right]^{-\frac{2\gamma_4}{\gamma_4-1}} \tag{A-12}$$

Across $\overleftarrow{R_2}$ the following fundamental relations hold:

$$a_2+\frac{\gamma_1-1}{2}\,u_2 = a_6+\frac{\gamma_1-1}{2}\,u_6 \tag{A-13}$$

and

$$P_{27} = \left(\frac{a_6}{a_2}\right)^{-\frac{2\gamma_1}{\gamma_1-1}} \tag{A-14}$$

Relations similar to (A-9) and (A-11) hold across the final shock $\overrightarrow{S_8}$.

$$P_{78} = \frac{2\gamma_8 M_{s_8}^2-(\gamma_8-1)}{\gamma_8+1} \tag{A-15}$$

$$u_7 = \frac{2a_8}{\gamma_8+1}\,\frac{M_{s_8}^2-1}{M_{s_8}} \tag{A-16}$$

Using (A-13), (A-11) and (A-16) in (A-14), one finds that

$$P_{27} = \left[1-\frac{\gamma_1-1}{a_2}\left(\frac{a_8}{\gamma_8+1}\,\frac{M_{s_8}^2-1}{M_{s_8}}-\frac{a_1}{\gamma_1+1}\,\frac{M_{s_1}^2-1}{M_{s_1}}\right)\right]^{-\frac{2\gamma_1}{\gamma_1-1}} \tag{A-17}$$

From (A-15), (A-17), (A-12) and (A-9) the fundamental equation for the constant-area buffered shock tube is obtained.

$$P_{48} = P_{78} P_{42} P_{27} = \frac{2\gamma_8 M_{s_8}^2 - (\gamma_8 - 1)}{\gamma_8 + 1} \quad \times$$

$$\left[1 - \frac{\gamma_4 - 1}{\gamma_1 + 1} \frac{M_{s_1}^2 - 1}{A_{41} M_{s_1}}\right]^{-\frac{2\gamma_4}{\gamma_4 - 1}} \left\{1 - \frac{\gamma_1 - 1}{a_2}\left[\frac{a_8}{\gamma_8 + 1}\left(M_{s_8} - \frac{1}{M_{s_8}}\right)\right.\right. \tag{A-18}$$

$$\left.\left. - \frac{a_1}{\gamma_1 + 1}\left(M_{s_1} - \frac{1}{M_{s_1}}\right)\right]\right\}^{-\frac{2\gamma_1}{\gamma_1 - 1}}$$

With the use of the normal shock relation

$$\frac{a_2}{a_1} = \frac{\left[2\gamma_1 M_{s_1}^2 - (\gamma_1 - 1)\right]^{1/2} \left[(\gamma_1 - 1) M_{s_1}^2 + 2\right]^{1/2}}{(\gamma_1 + 1) M_{s_1}} \tag{A-19}$$

and the ideal gas relation

$$\frac{a_4}{a_1} = \left(\frac{\gamma_4}{\gamma_1}\right)^{1/2} \left(\frac{P_{41}}{\Gamma_{41}}\right)^{1/2} \tag{A-20}$$

(A-18) can be written as follows:

$$P_{48} = \frac{2\gamma_8 M_{s_8}^2 - (\gamma_8 - 1)}{\gamma_8 + 1} \left[1 - \frac{\gamma_4 - 1}{\gamma_1 + 1}\left(\frac{\gamma_1}{\gamma_4}\right)^{1/2} \left(\frac{\Gamma_{41}}{P_{41}}\right)^{1/2} \quad \times\right.$$

$$\left.\left(M_{s_1} - \frac{1}{M_{s_1}}\right)\right]^{-\frac{2\gamma_4}{\gamma_4 - 1}} \left\{1 - \frac{(\gamma_1 - 1) M_{s_1}}{\left[2\gamma_1 M_{s_1}^2 - (\gamma_1 - 1)\right]^{1/2} \left[(\gamma_1 - 1) M_{s_1}^2 + 2\right]^{1/2}} \quad \times\right. \tag{A-21}$$

$$\left.\left[\frac{\gamma_1 + 1}{\gamma_8 + 1}\left(\frac{\gamma_8}{\gamma_1}\right)^{1/2} \left(\frac{\Gamma_{18}}{P_{48}}\right)^{1/2} \left(\frac{P_{41}}{\Gamma_{41}}\right)^{1/2} \left(M_{s_8} - \frac{1}{M_{s_8}}\right) - \left(M_{s_1} - \frac{1}{M_{s_1}}\right)\right]\right\}^{-\frac{2\gamma_1}{\gamma_1 - 1}}$$

Next consider a double-buffered tube (of the "unsteady-expansion" type) as shown in Fig. 11. The wave diagram represents only the initial flow phenomena in such a tube. Interactions between $\vec{C}_1$ and $\overleftarrow{R}_2$ or between $\vec{C}_2$ and $\overleftarrow{R}_3$ will generate waves that will limit the testing time (i.e., the time between the passage of $\vec{S}_{12}$ and the arrival of the contact surface $\vec{C}_3$).

The flow between regions 7 and 10 is completely similar to the flow between regions 2 and 6, so that, in analogy to Eq. (A-17),

$$\frac{p_7}{p_{10}} = \left[1 - \frac{\gamma_8 - 1}{a_7}\left[\frac{a_{12}}{\gamma_{12}+1}\,\frac{M_{s_{12}}^2 - 1}{M_{s_{12}}} - \frac{a_8}{\gamma_8+1}\,\frac{M_{s_8}^2 - 1}{M_{s_8}}\right]\right]^{-\frac{2\gamma_8}{\gamma_8 - 1}} \tag{A-22}$$

Also, the basic shock relations across $\vec{S}_{12}$ are similar to Eqs. (A-9), (A-11), and (A-19). Therefore, the basic equation for the double-buffered shock tube can be written down.

$$\frac{p_4}{p_{12}} = \frac{p_{11}}{p_{12}}\,\frac{p_4}{p_2}\,\frac{p_2}{p_7}\,\frac{p_7}{p_{11}} = \frac{2\gamma_{12} M_{s_{12}}^2 - (\gamma_{12} - 1)}{\gamma_{12}+1} \times$$

$$\left[1 - \frac{\gamma_4 - 1}{\gamma_1 + 1}\left(\frac{\gamma_1}{\gamma_4}\right)^{1/2}\left(\frac{\Gamma_{41}}{p_{41}}\right)^{1/2}\left(M_{s_1} - \frac{1}{M_{s_1}}\right)\right]^{-\frac{2\gamma_4}{\gamma_4 - 1}}\left\{1 - \frac{(\gamma_1 - 1) M_{s_1}}{\left[2\gamma_1 M_{s_1}^2 - (\gamma_1 - 1)\right]^{1/2}} \times\right.$$

$$\left.\frac{1}{\left[(\gamma_1 - 1) M_{s_1}^2 + 2\right]^{1/2}}\left[\frac{\gamma_1 + 1}{\gamma_8 + 1}\left(\frac{\gamma_8}{\gamma_1}\right)^{1/2}\left(\frac{\Gamma_{48}}{p_{48}}\right)^{1/2}\left(\frac{p_{41}}{\Gamma_{41}}\right)^{1/2}\left(M_{s_8} - \frac{1}{M_{s_8}}\right) - \left(M_{s_1} - \frac{1}{M_{s_1}}\right)\right]\right\}^{-\frac{2\gamma_1}{\gamma_1 - 1}} \times \tag{A-23}$$

$$\left\{1 - \frac{(\gamma_8 - 1) M_{s_8}}{\left[2\gamma_8 M_{s_8}^2 - (\gamma_8 - 1)\right]^{1/2}\left[(\gamma_8 - 1) M_{s_8}^2 + 2\right]^{1/2}}\left[\frac{\gamma_8 + 1}{\gamma_{12} + 1}\left(\frac{\gamma_{12}}{\gamma_8}\right)^{1/2}\left(\frac{\Gamma_{4,12}}{p_{4,12}}\right)^{1/2} \times\right.\right.$$

$$\left.\left.\left(\frac{p_{48}}{\Gamma_{48}}\right)^{1/2}\left(M_{s_{12}} - \frac{1}{M_{s_{12}}}\right) - \left(M_{s_8} - \frac{1}{M_{s_8}}\right)\right]\right\}^{-\frac{2\gamma_8}{\gamma_8 - 1}}$$

Of course, the simple shock tube Eq. (A-12) and the constant-area buffer Eq. (A-21) are also valid for this configuration, so that there are three equations to determine M_{s_1}, M_{s_8}, and $M_{s_{12}}$. The above procedure can be extended to a constant-area shock tube with a large number of buffer sections. If the final driven section is labeled $n+4$, the general equation (analogous to (A-23)) can be written down immediately.

$$P_{4,n+4} = \frac{2\gamma_{n+4}M_{s_{n+4}}^2 - (\gamma_{n+4}-1)}{(\gamma_{n+4}+1)} \left[1 - B\left(\frac{\Gamma_{41}}{P_{41}}\right)^{1/2}\left(M_{s_1} - \frac{1}{M_{s_1}}\right)\right]^{-\frac{2\gamma_4}{\gamma_4-1}}$$

$$\cdots \left\{1 - \frac{(\gamma_n - 1)\, M_{s_n}}{\left[2\gamma_n M_{s_n}^2 - (\gamma_n - 1)\right]^{1/2}\left[(\gamma_n - 1)M_{s_n}^2 + 2\right]^{1/2}}\left[\frac{\gamma_n + 1}{\gamma_{n+4}+1}\left(\frac{\gamma_{n+4}}{\gamma_n}\right)^{\frac{1}{2}}\left(\frac{\Gamma_{4,n+4}}{P_{4,n+4}}\right)\right.\right. \times \quad \text{(A-24)}$$

$$\left.\left.\left(\frac{P_{4n}}{\Gamma_{4n}}\right)\left(M_{s_{n+4}} - \frac{1}{M_{s_{n+4}}}\right) - \left(M_{s_n} - \frac{1}{M_{s_n}}\right)\right]\right\}^{-\frac{2\gamma_n}{\gamma_n - 1}}.$$

APPENDIX II

THE SIMPLE SHOCK TUBE WITH AREA CHANGE NEAR THE DIAPHRAGM

While the flow in a duct of varying cross-sectional area is not strictly one-dimensional, the simplification of quasi-one-dimensional flow in which the area A (x, t) appears as one of the variables in the fundamental equations is often made. Once A (x, t) is specified, the problem can be solved by the application of well-developed wave diagram techniques.[30] A further approximation which can often be made is to replace the gradual change in duct area by a discontinuous change. Such an approximation can only be used to evaluate the effect of the area change at a sufficient distance from the

change.[31-33] Since the changes in the flow variables are assumed to occur instantaneously, they may be computed by using the steady flow equations for an isentropic nozzle.

The possible wave patterns for a simple shock tube with an area change near the diaphragm that are compatible with the above assumptions are shown in Fig. 23. The wave diagrams always indicate a primary shock, an upstream-facing expansion wave, and a contact surface. In general, an upstream-facing secondary wave will be required to match conditions at the interface. The steady flow relations are assumed to hold from region 3a to 3b. In any particular case the flow pattern will be determined by the initial conditions and the area ratios.

Russell has done a detailed study of all four types of solutions for varying values of A_4/A_1 and A_*/A_1 .[33] He demonstrates that for any value of A_*/A_1, the shock strength increases with increasing A_4/A_1, and for any value of A_4/A_1 the maximum shock strength corresponds to the maximum A_*/A_1. Therefore, the best over-all performance is obtained with a monotonic area contraction at the diaphragm station. With this configuration only solutions of type (a) or type (d) are possible. For these solutions the steady expansion is subsonic and the second non-steady expansion (if any) is supersonic. The improved performance follows from the fact that a steady subsonic expansion is more efficient than an unsteady subsonic expansion for the conversion of thermal to kinetic energy.[31,32]

The following analysis is valid for any flow of either type (a) or type (d) whether $A_1 = A_*$ or not. For the steady flow from region 3a to 3b the following relations hold:

$$a_{3a}^2 \left[1 + \frac{\gamma_4 - 1}{2} M_{3a}^2\right] = a_{3b}^2 \left[1 + \frac{\gamma_4 - 1}{2} M_{3b}^2\right] \tag{A-25}$$

and

$$\frac{A_4}{A_1} = \frac{M_{3b}}{M_{3a}} \left[\frac{1 + \frac{\gamma_4 - 1}{2} M_{3a}^2}{1 + \frac{\gamma_4 - 1}{2} M_{3b}^2}\right]^{\frac{\gamma_4 + 1}{2(\gamma_4 - 1)}} \tag{A-26}$$

where

$$M_{3a} < 1$$

Across $\overleftarrow{R}_1$

$$a_4 = a_{3a} \left[1 + \frac{\gamma_4 - 1}{2} M_{3a}\right] \tag{A-27}$$

and across $\overleftarrow{R}_2$

$$a_{3b} \left[1 + \frac{\gamma_4 - 1}{2} M_{3b}\right] = a_3 + \frac{\gamma_4 - 1}{2} u_2 \tag{A-28}$$

Using these relations one finds that

$$\frac{a_3}{a_4} = \frac{a_3}{a_{3b}} \frac{a_{3b}}{a_{3a}} \frac{a_{3a}}{a_4} = \frac{\left[1 + \frac{\gamma_4 - 1}{2} M_{3b}\right]}{\left[1 + \frac{\gamma_4 - 1}{2} M_{3a}\right]} \times \tag{A-29}$$

$$\left[\frac{1 + \frac{\gamma_4 - 1}{2} M_{3a}^2}{1 + \frac{\gamma_4 - 1}{2} M_{3b}^2}\right]^{1/2} \cdot \frac{1}{1 + \frac{\gamma_4 - 1}{2} \frac{u_2}{a_3}}$$

Define

$$g \equiv \left[\frac{1 + \frac{\gamma_4 - 1}{2} M_{3a}^2}{1 + \frac{\gamma_4 - 1}{2} M_{3b}^2} \left(\frac{1 + \frac{\gamma_4 - 1}{2} M_{3b}}{1 + \frac{\gamma_4 - 1}{2} M_{3a}} \right)^2 \right]^{\frac{\gamma_4}{\gamma_4 - 1}} \tag{A-30}$$

then

$$\frac{a_3}{a_4} = \frac{g^{\frac{\gamma_4 - 1}{2\gamma_4}}}{1 + \frac{\gamma_4 - 1}{2} \frac{u_2}{a_3}} \tag{A-31}$$

Equation (A-31) can be written as

$$\frac{a_3}{a_4} = g^{\frac{\gamma_4 - 1}{2\gamma_4}} - \frac{\gamma_4 - 1}{2} \frac{u_2}{a_4} \tag{A-32}$$

Therefore,

$$P_{41} = P_{21} \left(\frac{a_3}{a_4} \right)^{-\frac{2\gamma_4}{\gamma_4 - 1}} = P_{21} \left[g^{\frac{\gamma_4 - 1}{2\gamma_4}} - \frac{\gamma_4 - 1}{2} \frac{u_2}{a_4} \right]^{\frac{2\gamma_4}{\gamma_4 - 1}} \tag{A-33}$$

Equations (A-9) and (A-11) may be used to obtain

$$P_{41} = \frac{1}{g} \frac{2\gamma_1 M_{s_1}^2 - (\gamma_1 - 1)}{\gamma_1 + 1} \left[1 - \frac{\gamma_4 - 1}{\gamma_1 + 1} \frac{M_{s_1}^2 - 1}{M_{s_1}} \frac{1}{A_{41} g^{\frac{\gamma_4 - 1}{2\gamma_4}}} \right]^{-\frac{2\gamma_4}{\gamma_4 - 1}} \tag{A-34}$$

Define new variables by

$$P'_{41} = g P_{41}$$

and

$$A'_{41} = g^{\frac{\gamma_4 - 1}{2\gamma_4}} A_{41}$$

Then Eq. (A-34) is merely the simple shock tube Eq. (A-12) for a shock tube with a pressure ratio P_{41}' and a speed of sound ratio A_{41}'.

The specific case of interest is the configuration for which $A_1 = A_*$. Then if $M_3 \geq 1$, $M_{3b} = 1$ and g can be calculated from (A-26) and (A-30). If, on the other hand, $M_3 < 1$, $M_{3b} = M_3$ and the problem must be solved by iteration.

Hall and Russo[19] have pointed out that for M_{s_1} exceeding about three, and for a given driver gas specific heat ratio, shock tube performance can be represented by a single curve for all initial conditions. If M_{s_1} is greater than about three, certain terms in Eq. (A-34) can be neglected. Then the equation can be simplified to

$$g P_{41} = \frac{2\gamma_1 M_{s_1}^2}{\gamma_1 + 1} \left\{ 1 - \frac{B\left(g^{1/\gamma_4}\, \Gamma_{41}\right)^{1/2} M_{s_1}}{\left(g P_{41}\right)^{1/2}} \right\}^{-\frac{2\gamma_4}{\gamma_4 - 1}} \tag{A-35}$$

Define two new variables by

$$Z_1' = \frac{M_{s_1}}{\sqrt{g P_{41}}} \quad \text{and} \quad \Gamma_{41}' = g^{1/\gamma_4}\, \Gamma_{41} \tag{A-36}$$

Then,

$$Z_1'^2 = \frac{\gamma_1 + 1}{2\gamma_1} \left\{ 1 - B\, \Gamma_{41}'^{1/2}\, Z_1' \right\}^{\frac{2\gamma_4}{\gamma_4 - 1}} \tag{A-37}$$

The basic equation has been reduced from a relation involving six variables M_{s_1}, P_{41}, g, Γ_{41}, γ_1, and γ_4 to a relation among four variables Z_1', Γ_{41}', γ_1, and γ_4. Figure 6 shows a plot of Z_1' vs. Γ_{41}' for various values of driver gas specific heat ratio. The use of different values for γ_1 does not noticeably

affect the curves of Fig. 6, so, the variation in performance with driven gas specific heat ratio can be neglected. Figure 6 indicates that for given Γ_{41}', $\bar{z}_1'$ increases as γ_4 decreases. By using numerical values it is found that for given Γ_{41}, $\bar{z}_1$ (the actual shock strength parameter) increases as γ_4 decreases.

APPENDIX III

CALCULATIONS OF THE OPTIMUM PERFORMANCE OF CONSTANT-AREA BUFFERED TUBES

The performance of a constant-area buffered tube can be calculated from the buffer Eq. (A-21) and the simple shock tube Eq. (A-12). In the main body of the text it is shown that when $M_{s_1}^2$ and $M_{s_8}^2$ are large compared to one, approximation 1 is obtained.

$$\bar{z}_8^2 = C_1 \bar{z}_1^2 \left\{ 1 - \frac{(\gamma_1 - 1) M_{s_1}}{(2\gamma_1)^{1/2} \left[(\gamma_1 - 1) M_{s_1}^2 + 2 \right]^{1/2}} \times \right.$$

$$\left. \left[\frac{\gamma_4 - 1}{\gamma_8 + 1} \left(\frac{\gamma_8}{\gamma_4} \right)^{1/2} \frac{\Gamma_{48}^{1/2} \bar{z}_8}{1 - \left(\frac{2\gamma_1 \bar{z}_1^2}{\gamma_1 + 1} \right)^{\frac{\gamma_4 - 1}{2\gamma_4}}} - 1 \right] \right\}^{\frac{2\gamma_1}{\gamma_1 - 1}} \qquad \text{(A-38)}$$

The additional assumption that $M_{s_1}^2 \gg \gamma_1 - 1$, simplifies (A-38) to approximation 2, which no longer explicitly depends upon M_{s_1}.

$$\bar{z}_8^2 = C_1 \bar{z}_1^2 \left\{ D_1 - \frac{B E_1 \Gamma_{48}^{1/2} \bar{z}_8}{1 - \left(\frac{2\gamma_1}{\gamma_1 + 1} \bar{z}_1^2 \right)^{\frac{\gamma_4 - 1}{2\gamma_4}}} \right\}^{\frac{2\gamma_1}{\gamma_1 - 1}} \qquad \text{(A-39)}$$

$\bar{z}_8$ can be maximized with respect to $\bar{z}_1$ by differentiating (A-39) with respect to $\bar{z}_1$ and setting $\frac{\partial \bar{z}_8}{\partial \bar{z}_1}$ equal to zero. Upon differentiation, Eq. (A-39)

becomes

$$0 = 2C_1 Z_1 \left\{ D_1 - \frac{BE_1 \Gamma_{48}^{1/2} Z_8}{1 - \left(\frac{2\gamma_1}{\gamma_1 + 1} Z_1^2 \right)^{\frac{\gamma_4 - 1}{2\gamma_4}}} \right\}^{\frac{2\gamma_1}{\gamma_1 - 1}}$$

$$+ \frac{(-2C_1 Z_1) BE_1 \Gamma_{48}^{1/2} Z_8 \frac{\gamma_4 - 1}{\gamma_1 - 1} \frac{\gamma_1}{\gamma_4} \left(\frac{2\gamma_1}{\gamma_1 + 1} Z_1^2 \right)^{\frac{\gamma_4 - 1}{2\gamma_4}}}{\left[1 - \left(\frac{2\gamma_1}{\gamma_1 + 1} Z_1^2 \right)^{\frac{\gamma_4 - 1}{2\gamma_4}} \right]^2} \left\{ D_1 - \frac{BE_1 \Gamma_{48}^{1/2} Z_8}{1 - \left(\frac{2\gamma_1}{\gamma_1 + 1} Z_1^2 \right)^{\frac{\gamma_4 - 1}{2\gamma_4}}} \right\}^{\frac{\gamma_1 + 1}{\gamma_1 - 1}} \qquad \text{(A-40)}$$

The possibility that

$$D_1 - \frac{BE_1 \Gamma_{48}^{1/2} Z_8}{1 - \left(\frac{2\gamma_1}{\gamma_1 + 1} Z_1^2 \right)^{\frac{\gamma_4 - 1}{2\gamma_4}}} = 0 \qquad \text{(A-41)}$$

is excluded because this would imply, by (A-39), that $Z_8 = 0$ or P_{48} becomes infinite. Therefore, (A-40) can be simplified to

$$D_1 - \frac{BE_1 \Gamma_{48}^{1/2} Z_8}{1 - \left(\frac{2\gamma_1}{\gamma_1 + 1} Z_1^2 \right)^{\frac{\gamma_4 - 1}{2\gamma_4}}} =$$

$$\frac{\gamma_4 - 1}{\gamma_1 - 1} \frac{\gamma_1}{\gamma_4} BE_1 \Gamma_{48}^{1/2} Z_8 \cdot \frac{\left(\frac{2\gamma_1}{\gamma_1 + 1} Z_1^2 \right)^{\frac{\gamma_4 - 1}{2\gamma_4}}}{\left[1 - \left(\frac{2\gamma_1}{\gamma_1 + 1} Z_1^2 \right)^{\frac{\gamma_4 - 1}{2\gamma_4}} \right]^2} \qquad \text{(A-42)}$$

or

$$\frac{BE_1 \Gamma_{48}^{1/2} Z_8}{1 - \left(\frac{2\gamma_1}{\gamma_1 + 1} Z_1^2 \right)^{\frac{\gamma_4 - 1}{2\gamma_4}}} = \frac{D_1}{1 + X_1} \qquad \text{(A-43)}$$

where

$$X_1 = \frac{\frac{\gamma_1}{\gamma_4}\frac{\gamma_4-1}{\gamma_1-1}\left(\frac{2\gamma_1}{\gamma_1+1}Z_1^2\right)^{\frac{\gamma_4-1}{2\gamma_4}}}{1-\left(\frac{2\gamma_1}{\gamma_1+1}Z_1^2\right)^{\frac{\gamma_4-1}{2\gamma_4}}} \tag{A-44}$$

The use of (A-43) to eliminate Z_8 from (A-39) leads to

$$\frac{D_1^2\left[1-\left(\frac{2\gamma_1}{\gamma_1+1}Z_1^2\right)^{\frac{\gamma_4-1}{2\gamma_4}}\right]^2}{B^2E_1^2\Gamma_{48}(1+X_1)^2} = C_1Z_1^2\left\{D_1-\frac{D_1}{1+X_1}\right\}^{\frac{2\gamma_1}{\gamma_1-1}} \tag{A-45}$$

This can be solved for Γ_{48} .

$$\Gamma_{48} = \frac{\left[1-\left(\frac{2\gamma_1}{\gamma_1+1}Z_1^2\right)^{\frac{\gamma_4-1}{2\gamma_4}}\right]^2\left(\frac{1+X_1}{X_1}\right)^{\frac{2\gamma_1}{\gamma_1-1}}}{D_1^{2/\gamma_1-1}B^2E_1^2C_1Z_1^2(1+X_1)^2} \tag{A-46}$$

With (A-46) and (A-43) one finds that

$$Z_8 = C_1^{1/2}\left(\frac{D_1X_1}{1+X_1}\right)^{\frac{\gamma_1}{\gamma_1-1}}Z_1 \tag{A-47}$$

The possibility of determining the maximum value of Z_8 from approximation 1 now will be considered. Equation (A-38) can be written symbolically as

$$Z_8 = F_5\left(\gamma_1, \gamma_4, \gamma_8, Z_1, M_{S_1}, \Gamma_{48}\right) \tag{A-48}$$

So, for fixed specific heat ratios and over-all density ratio the conditions for the maximum are

$$\frac{\partial F_5}{\partial Z_1} = 0 \qquad \text{and} \qquad \frac{\partial F_5}{\partial M_{s_1}} = 0 \tag{A-49}$$

Equation (A-38) can be written as

$$Z_8^2 = C_1 Z_1^2 \left\{ 1 + f(M_{s_1}) - \frac{\frac{\gamma_4 - 1}{\gamma_8 + 1}\left(\frac{\gamma_8}{\gamma_4}\right)^{1/2} f(M_{s_1}) \Gamma_{48}^{1/2} Z_8}{1 - \left(\frac{2\gamma_1}{\gamma_1 + 1} Z_1^2\right)^{\frac{\gamma_4 - 1}{2\gamma_4}}} \right\}^{\frac{2\gamma_1}{\gamma_1 - 1}} \tag{A-50}$$

where

$$f(M_{s_1}) = \frac{(\gamma_1 - 1) M_{s_1}}{(2\gamma_1)^{1/2}\left[(\gamma_1 - 1) M_{s_1}^2 + 2\right]^{1/2}}$$

Differentiating (A-50) with respect to Z_1 leads to

$$1 + f(M_{s_1}) = \frac{\frac{\gamma_4 - 1}{\gamma_8 + 1}\left(\frac{\gamma_8}{\gamma_4}\right)^{1/2} f(M_{s_1}) \Gamma_{48}^{1/2} Z_8 (1 + X_1)}{1 - \left(\frac{2\gamma_1}{\gamma_1 + 1} Z_1^2\right)^{\frac{\gamma_4 - 1}{2\gamma_4}}} \tag{A-51}$$

and differentiating with respect to M_{s_1} leads to

$$\frac{\frac{\gamma_4 - 1}{\gamma_8 + 1}\left(\frac{\gamma_8}{\gamma_4}\right)^{1/2} \Gamma_{48}^{1/2} Z_8}{1 - \left(\frac{2\gamma_1}{\gamma_1 + 1} Z_1^2\right)^{\frac{\gamma_4 - 1}{2\gamma_4}}} = 1 \tag{A-52}$$

Equations (A-50), (A-51) and (A-52) can be combined to yield

$$Z_8^2 = C_1 Z_1^2 \tag{A-53}$$

$$\Gamma_{48} = \frac{\left[1 - \left(\frac{2\gamma_1}{\gamma_1+1} \mathcal{Z}_1^2\right)^{\frac{\gamma_4-1}{2\gamma_4}}\right]^2}{C_1 \mathcal{Z}_1^2 \left(\frac{\gamma_4-1}{\gamma_8+1}\right)^2 \frac{\gamma_8}{\gamma_4}} \tag{A-54}$$

and

$$\mathcal{Z}_1^2 = \left[1 + \frac{\gamma_4-1}{\gamma_1-1} \frac{\gamma_1}{\gamma_4} f(M_{s_1})\right]^{-\frac{2\gamma_4}{\gamma_4-1}} \frac{\gamma_1+1}{2\gamma_1} \tag{A-55}$$

When values of M_{s_1} are used to evaluate these expressions, it is found that the only possible values of Γ_{48} are those in the range of about 2 to 17. These are the only values of Γ_{48} for which the expression in brackets in Eq. (A-50) can be equal to one. For larger values of Γ_{48} (which are usually the ones of interest) the maximum value of $\mathcal{Z}_8$ cannot be determined by the above procedure.

A procedure to determine the optimum conditions for approximation 1 curves such as appear in Figs. 10 and 11 will now be considered. These curves were drawn subject to the constraint that the temperatures and molecular weights are specified, and, therefore, $\mathcal{Z}_8$ is no longer a function of two variables. The equation for approximation 1 may be expressed as follows:

$$\mathcal{Z}_8^2 = \frac{\gamma_8+1}{2\gamma_8}\left[1 - B\Gamma_{41}^{1/2}\mathcal{Z}_1\right]^{\frac{2\gamma_4}{\gamma_4-1}} \times \tag{A-56}$$

$$\left\{1 - f(M_{s_1})\left[\frac{\Gamma_{48}^{1/2}\mathcal{Z}_8 \frac{\gamma_1+1}{\gamma_8+1}\left(\frac{\gamma_8}{\gamma_1}\right)^{1/2}}{\Gamma_{41}^{1/2}\mathcal{Z}_1} - 1\right]\right\}^{\frac{2\gamma_1}{\gamma_1-1}}$$

The constraint can be expressed as

$$\frac{\Gamma_{41}}{P_{41}} = \frac{\mu_{41}}{T_{41}} = K^2 \qquad \text{a const.} \tag{A-57}$$

Therefore,

$$\Gamma_{41}^{1/2} Z_1 = \left(\frac{\Gamma_{41}}{P_{41}}\right)^{1/2} M_{s_1} = K M_{s_1} \tag{A-58}$$

and

$$Z_8 = F_6 \left(\gamma_1, \gamma_4, \gamma_8, \Gamma_{48}, M_{s_1}\right) \tag{A-59}$$

The optimum condition can be found from the equation

$$\frac{\partial F_6}{\partial M_{s_1}} = 0 \tag{A-60}$$

The calculation is straightforward but quite involved, so it will not be presented.

The most important result of the above analysis is the following: for given Γ_{48}, Z_8 -maximum increases as K increases (M_{s_1} decreases).

APPENDIX IV

THE BUFFERED SHOCK TUBE WITH AN AREA CONTRACTION AT THE SECOND DIAPHRAGM

The use of an area contraction in conjunction with a buffered shock tube has been considered by several authors.[1,6,8-13,15-18] If the area change is located at the first diaphragm, the flow is that of a simple shock tube with an area change followed by a flow identical to that in a constant-area buffered tube. This case is fully considered in the main body of the report (Sec. 2.2.3).

Suppose that an area contraction exists at the second diaphragm station of a buffered shock tube and that the diaphragm ruptures immediately upon impact of the initial shock (Fig. 16). If the contraction is approximated by a

discontinuous change, the resulting simplified wave diagram will include the incident and transmitted shocks, an interface that separates the two gases, and a reflected wave. The cases of interest will involve supersonic flow behind the initial shock $(M_2 > 1)$, and under this assumption three possible solutions exist. If the contraction is sufficiently small, the reflected wave is an upstream-facing expansion (Q-wave) which is swept downstream (Fig. 16-a). At larger contraction ratios the flow is reduced to the sonic value and a shock wave is required to match conditions at the interface. For a limited range of contraction ratios the shock can be stationary at the area change (Fig. 16-b), but as A_1/A_8 increases a reflected shock is found (Fig. 16-c).

There has been a considerable amount of interest in this problem in recent years.[34, 35] For certain values of incident shock strength and contraction ratio, all three of the above solutions will satisfy the conditions of the problem. This "region of ambiguity" was found to be a direct result of the simplifying assumptions implicit in the wave diagram technique. More exact analyses indicate which solution will hold in any particular case.

For cases of practical interest the area change will be so large that a reflected shock exists, and the flow is adequately represented by Fig. 16-c. The flow from region 4 to region 1 will obviously be represented by the simple shock tube equation. After the passage of the reflected shock the flow will have a small subsonic velocity u_5. In a coordinate system which is stationary with respect to the reflected shock

$$M_{s_r} = \frac{U_{s_r} + u_2}{a_2} \tag{A-61}$$

where U_{s_r} speed of reflected shock

M_{s_r} reflected shock Mach number

The ordinary shock relations hold across the reflected shock.

$$P_{52} = \frac{2\gamma_1 M_{s_r}^2 - (\gamma_1 - 1)}{\gamma_1 + 1} \tag{A-62}$$

$$A_{52} = \frac{\left[2\gamma_1 M_{s_r}^2 - (\gamma_1 - 1)\right]^{1/2} \left[(\gamma_1 - 1) M_{s_r}^2 + 2\right]^{1/2}}{(\gamma_1 + 1) M_{s_r}} \tag{A-63}$$

The flow from region 5 to the beginning of the unsteady expansion 5' is steady. For a monotonic convergence $M_5' = 1$, but if the area change is a converging-diverging section $M_5' > 1$. The usual steady flow relations apply.

$$\left(\frac{a_5}{a_5'}\right)^2 = \frac{1 + \frac{\gamma_1 - 1}{2} M_5'^2}{1 + \frac{\gamma_1 - 1}{2} M_5^2} \tag{A-64}$$

$$\frac{A_1}{A_8} = \frac{M_5'}{M_5} \left[\frac{1 + \frac{\gamma_1 - 1}{2} M_5^2}{1 + \frac{\gamma_1 - 1}{2} M_5'^2} \right]^{\frac{\gamma_1 + 1}{2(\gamma_1 - 1)}} \tag{A-65}$$

From 5' to 6

$$a_5' + \frac{\gamma_1 - 1}{2} u_5' = a_6 + \frac{\gamma_1 - 1}{2} u_7 \tag{A-66}$$

Therefore,

$$\frac{a_6}{a_5} = \left[\frac{1 + \frac{\gamma_1 - 1}{2} M_5^2}{1 + \frac{\gamma_1 - 1}{2} M_5'^2} \right]^{1/2} \frac{1 + \frac{\gamma_1 - 1}{2} M_5'}{1 + \frac{\gamma_1 - 1}{2} \frac{u_7}{a_6}} \tag{A-67}$$

Define G by the expression

$$G \equiv \left[\left(\frac{1 + \frac{\gamma_1 - 1}{2} M_5^2}{1 + \frac{\gamma_1 - 1}{2} M_5'^2} \right)^{1/2} \left(1 + \frac{\gamma_1 - 1}{2} M_5' \right) \right]^{\frac{2\gamma_1}{\gamma_1 - 1}} \tag{A-68}$$

Then

$$\frac{a_6}{a_5} = \frac{G^{\frac{\gamma_1 - 1}{2\gamma_1}}}{1 + \frac{\gamma_1 - 1}{2} \frac{u_7}{a_6}} \tag{A-69}$$

or

$$\frac{a_6}{a_5} = G^{\frac{\gamma_1 - 1}{2\gamma_1}} - \frac{\gamma_1 - 1}{2} \frac{u_7}{a_5} \tag{A-70}$$

Applying the isentropic relation, it is found that

$$P_{56} = \frac{1}{G} \left[1 - \frac{\gamma_1 - 1}{\gamma_8 + 1} \frac{\left(M_{s_8} - \frac{1}{M_{s_8}} \right)}{A_{58} G^{\frac{\gamma_1 - 1}{2\gamma_1}}} \right]^{-\frac{2\gamma_1}{\gamma_1 - 1}} \tag{A-71}$$

Equation (A-71) may be interpreted as meaning that the flow from region 5 to region 8 is equivalent to the flow in a simple shock tube with a pressure ratio GP_{58} and a speed of sound ratio $A_{58} G^{\frac{\gamma_1 - 1}{2\gamma_1}}$. Therefore, G is an equivalence factor for an area change at the second diaphragm. It is important to note that this is not the same as the " q " factor used previously. If equations (A-62), (A-63), and (A-71) are combined, the basic equation for this type of shock tube is obtained.

$$P_{48} = \frac{2\gamma_8 M_{s_8}^2 - (\gamma_8 - 1)}{\gamma_8 + 1} \left[1 - B \left(\frac{\Gamma_{41}}{P_{41}} \right)^{1/2} \left(M_{s_1} - \frac{1}{M_{s_1}} \right) \right]^{-\frac{2\gamma_4}{\gamma_4 - 1}} \times$$

$$\frac{1}{G} \left\{ 1 - \frac{(\gamma_1+1)^2 (\gamma_1 - 1) \left(M_{s_8} - \frac{1}{M_{s_8}} \right) M_{s_1} M_{s_r}}{(\gamma_8 + 1)\, G^{\frac{\gamma_1 - 1}{2\gamma_1}} \left[2\gamma_1 M_{s_r}^2 - (\gamma_1 - 1) \right]^{1/2} \left[(\gamma_1 - 1) M_{s_r}^2 + 2 \right]^{1/2}} \times \right. \tag{A-72}$$

$$\left. \frac{\left(\frac{\gamma_8}{\gamma_1} \right)^{1/2} \left(\frac{\Gamma_{48}}{P_{48}} \right)^{1/2} \left(\frac{P_{41}}{\Gamma_{41}} \right)^{1/2}}{\left[2\gamma_1 M_{s_1}^2 - (\gamma_1 - 1) \right]^{1/2} \left[(\gamma_1 - 1) M_{s_1}^2 + 2 \right]^{1/2}} \right\}^{-\frac{2\gamma_1}{\gamma_1 - 1}} \frac{(\gamma_1 + 1)}{2\gamma_1 M_{s_r}^2 - (\gamma_1 - 1)}$$

However, the equation still involves two unknowns, M_{s_8} and M_{s_r} The equation of continuity across the reflected shock is

$$\rho_2 \left(U_{s_r} + u_2 \right) = \rho_5 \left(U_{s_r} + u_5 \right) \tag{A-73}$$

or

$$u_5 = U_{s_r} \left(\frac{\rho_2}{\rho_5} - 1 \right) + \frac{\rho_2}{\rho_5} u_2 \tag{A-74}$$

By using the relation

$$\frac{\rho_5}{\rho_2} = \frac{(\gamma_1 + 1) M_{s_r}^2}{(\gamma_1 - 1) M_{s_r}^2 + 2} \tag{A-75}$$

in (A-74), it is found that

$$\frac{u_2 - u_5}{a_2} \equiv M_2 - M_5 \frac{a_5}{a_2} = \frac{2}{\gamma_1 + 1} \left(M_{s_r} - \frac{1}{M_{s_r}} \right) \tag{A-76}$$

M_2 is known and M_5 can be calculated from Eq. (A-65), and if (A-65) is used, (A-76) becomes a fourth order algebraic equation for M_{s_r} . In any

practical case Eq. (A-76) can be solved by iteration.

If the area contraction is very large, $u_s \approx 0$ and the shock becomes fully reflected.

$$M_{s_r}^2 = \frac{2\gamma_1 M_{s_1}^2 - (\gamma_1 - 1)}{(\gamma_1 - 1) M_{s_1}^2 + 2} \tag{A-77}$$

This expression may be used to eliminate M_{s_r} from Eq. (A-72).

$$P_{48} = \frac{2\gamma_8 M_{s_8}^2 - (\gamma_8 - 1)}{\gamma_8 + 1} \left[1 - B \left(\frac{\Gamma_{41}}{P_{41}} \right)^{1/2} \times \left(M_{s_1} - \frac{1}{M_{s_1}} \right) \right]^{-\frac{2\gamma_4}{\gamma_4 - 1}} \frac{1}{G_\infty} \frac{(\gamma_1 - 1) M_{s_1}^2 + 2}{(3\gamma_1 - 1) M_{s_1}^2 - 2(\gamma_1 - 1)} \left\{ 1 - \frac{\gamma_1 - 1}{\gamma_8 + 1} \times \frac{(\gamma_1 + 1)}{G_\infty^{\frac{\gamma_1 - 1}{2\gamma_1}}} \frac{\left(M_{s_8} - \frac{1}{M_{s_8}} \right) M_{s_1} \left(\frac{\gamma_8}{\gamma_1} \right)^{1/2} \left(\frac{\Gamma_{48}}{P_{48}} \right)^{1/2} \left(\frac{P_{41}}{\Gamma_{41}} \right)^{1/2}}{\left[2(\gamma_1 - 1) M_{s_1}^2 - (\gamma_1 - 3) \right]^{1/2} \left[(3\gamma_1 - 1) M_{s_1}^2 - 2(\gamma_1 - 1) \right]^{1/2}} \right\}^{-\frac{2\gamma_1}{\gamma_1 - 1}} \tag{A-78}$$

where

$$G_\infty = \left(\frac{\gamma_1 + 1}{2} \right)^{\frac{\gamma_1}{\gamma_1 - 1}}$$

since $M_s = 0$ and $M_s' = 1$ for an infinite monotonic convergence.

APPENDIX V

DERIVATION OF THE DETONATION BUFFER EQUATIONS

Under normal conditions a flame in a tube filled with combustible gas will propagate at the low velocity of a few meters per second. Under certain conditions, however, this slow combustion process is changed into a very

rapid process that propagates at supersonic speeds. This second type of combustion process is known as a detonation. In the following it will be assumed that the chemical reaction occurs instantaneously across a sharply defined front. Then the only difference between a detonation and a pure shock wave is that the chemical nature of the burnt gas differs from that of the unburnt gas and that the reaction influences the energy balance.

In the following three pages the fundamentals of detonation wave theory will be reviewed. Similar developments can be found in standard texts.[25, 28]

Referring to a detonation moving into a quite gas at speed U_D, the Rankine-Hugoniot relations become

$$\rho_1 V_1 = \rho_2 V_2 \tag{A-79}$$

$$p_1 + \rho_1 V_1^2 = p_2 + \rho_2 V_2^2 \tag{A-80}$$

and

$$e_1 + \frac{p_1}{\rho_1} + \frac{1}{2} V_1^2 + \Delta E_c = e_2 + \frac{p_2}{\rho_2} + \frac{1}{2} V_2^2 \tag{A-81}$$

where

$$V_1 = U_D$$

$$V_2 = U_D - u_2$$

ΔE_c is the heat of chemical reaction per unit mass at constant temperature and pressure. From (A-79) and (A-80) the relation

$$\frac{p_2 - p_1}{v_1 - v_2} = \rho_1^2 V_1^2 = \rho_2^2 V_2^2 > 0 \tag{A-82}$$

follows, just as in the case of pure shock waves. Here $v = 1/\rho$ is specific volume. Equation (A-82) implies that there are two different types of processes

compatible with the conservation laws: those in which both pressure and density increase and those in which both pressure and density decrease. Processes of the first kind are detonations while processes of the second kind are slow combustions or deflagrations. By considering pure shock waves $(\Delta E_c = 0)$, it is found that deflagration-type processes $(p_2 \leq p_1)$ are excluded because they would involve a decrease in entropy. However, this argument does not apply to the case where a chemical reaction occurs.

By proper manipulation of (A-79) and (A-80) the relation

$$V_2^2 - V_1^2 = (p_1 - p_2)(v_1 + v_2) \tag{A-83}$$

is found, which when used in Eq. (A-81) yields

$$e_2 - e_1 = \frac{1}{2}(p_2 + p_1)(v_1 - v_2) + \Delta E_c \tag{A-84}$$

This relation involves only thermodynamic variables and is commonly called the Hugoniot relation. The internal energy can be considered a function of the pressure and specific volume; in particular for an ideal gas with constant specific heats

$$e = \frac{pv}{\gamma - 1} \tag{A-85}$$

Therefore, knowing ΔE_c, e, p_1 and v_1, the Hugoniot relation can be plotted in a p-v plane. This plot of (A-84) subject to the restriction of Eq. (A-82) is called a Hugoniot curve (Fig. 29). The curve has a detonation branch $(v \leq v_1)$ and a deflagration branch $(p \leq p_1)$. The present study will just consider the detonation branch; most phenomena to be considered for this branch will have an analogue in the deflagration branch.

A straight line through the point (p_1, v_1) will in general intersect the Hugoniot curve in two points. By increasing the slope of this line (decreasing

the angle ϕ) the two points of intersection eventually come together at point C which is known as the Chapman-Jouguet point. Detonations represented by points below C will be called weak detonations; those represented by points above C will be called strong or over-driven detonations.

The Chapman-Jouguet process has certain peculiar properties that can be derived from thermodynamic considerations. Among these are the following: of all detonation processes the detonation velocity U_D and the entropy of the burnt gas s_2 are minima for a Chapman-Jouguet process, and a Chapman-Jouguet front when observed from the burnt gas moves with the sound speed.

$$V_2 = U_D - u_2 = a_2 \tag{A-86}$$

Also, by thermodynamic arguments, certain general statements can be derived which are called Jouguet's Rules. These can be stated as: the gas flow relative to the reaction front is supersonic ahead of any detonation, supersonic behind a weak detonation, and subsonic behind a strong detonation. If a more detailed analysis is made of the reaction process, taking heat conduction and viscosity into account, it can be shown that weak detonations are possible only under extreme and rare circumstances.

Consider a detonation front which is being followed by a piston moving with constant velocity u_p . This problem is quite similar to the problem of a detonation in a shock tube where the condition of constant pressure and velocity at the contact surface replaces the piston. Suppose that $u_p > U_D - a_2$. Then the velocity of the gas behind the front is greater than that which exists at the Chapman-Jouguet point, and the detonation is over-driven. If $u_p = U_D - a_2$, a pure Chapman-Jouguet detonation is sustained. If $u_p < U_D - a_2$, a Chapman-Jouguet detonation will occur, but is will be immediately followed

by a centered expansion wave. The front of the expansion will just coincide with the detonation front since

$$U_D = u_2 + a_2 \tag{A-87}$$

If the piston is not moved at all, $u_p = 0$, and a Chapman-Jouguet detonation is still possible. In this case the expansion will decelerate the flow to zero velocity. That this detonation is the one that actually occurs, is the Chapman-Jouguet hypothesis.

During the use of a detonation in a shock tube it is desirable to eliminate the expansion fan which follows the front. Therefore, only driver pressures which are great enough to support or overdrive a pure Chapman-Jouguet detonation will be considered. From (A-79)

$$u_2 = U_D \left(1 - \Gamma_{12}\right) \tag{A-88}$$

and from (A-80)

$$u_2 = \frac{p_2 - p_1}{\rho_1 U_D} \tag{A-89}$$

After multiplying these two relations together and dividing by a_1^2,

$$\left(\frac{u_2}{a_1}\right)^2 = \frac{\left(1-\Gamma_{12}\right)\left(P_{21}-1\right) p_1}{\rho_1 a_1^2} \tag{A-90}$$

or

$$\frac{u_2}{a_1} = \frac{\left(P_{21}-1\right)^{1/2}\left(1-\Gamma_{12}\right)^{1/2}}{\gamma_1^{1/2}} \tag{A-91}$$

Assume that both the burnt and unburnt gases are ideal gases with constant specific heats.

$$e_1 + \frac{p_1}{\rho_1} = c_{p_1} T_1 = \frac{a_1^2}{\gamma_1 - 1} \tag{A-92}$$

When (A-92) is used in Eq. (A-81),

$$\frac{\gamma_1 - 1}{2} M_{s_1}^2 + 1 = \frac{V_2^2}{a_1^2} \frac{\gamma_1 - 1}{2} + \left(\frac{a_2}{a_1}\right)^2 \frac{\gamma_1 - 1}{\gamma_2 - 1} - \varphi \tag{A-93}$$

where

$$\varphi = \frac{\Delta E_c}{c_{p_1} T_1}$$

From Eqs. (A-79), (A-88), (A-93), and the definition of the speed of sound

$$M_{s_1}^2 = \frac{\left(\frac{u_2}{a_1}\right)^2}{\left[1 - \Gamma_{12}\right]^2} = \frac{2}{\gamma_1 - 1} \frac{\frac{\gamma_2}{\gamma_1} \frac{\gamma_1 - 1}{\gamma_2 - 1} P_{21} \Gamma_{12} - \varphi - 1}{\left[1 - \Gamma_{12}^2\right]} \tag{A-94}$$

If this expression is combined with (A-89),

$$\Gamma_{21} = \frac{\frac{\gamma_2 + 1}{\gamma_2 - 1} P_{21} + 1}{P_{21} + \frac{\gamma_1 + 1}{\gamma_1 - 1} + \frac{2\gamma_1}{\gamma_1 - 1} \varphi} \tag{A-95}$$

This can be used in (A-94) to obtain M_{s_1} as a function of P_{21}, but the corresponding expression is quite complex. Consequently, we shall use P_{21} as a measure of shock strength rather than M_{s_1}.

Consider a constant-area buffered tube similar to that shown in Fig. 1 with the exception that the buffer gas is a detonable mixture. Assume that the driver and driven gases are perfect gases. The equations which hold across the detonation front have been derived above. The burnt gas will not behave as a perfect gas in the expansion from region 2 to region 6, and the flow through the fan should properly be evaluated by numerically integrating the equations of characteristics. For the purpose of our simplified analysis assume that the isentropic relation can be written as

$$\frac{p_2}{p_6} = \left(\frac{a_2}{a_6}\right)^{\frac{2\gamma_{av}}{\gamma_{av}-1}} \tag{A-96}$$

where γ_{av} is the average specific ratio between region 2 and region 6, and the nonsteady expansion relations can be adequately represented by

$$a_6 = a_2 - \frac{\gamma_{av}-1}{2}\left(u_7 - u_2\right)\Big\} \tag{A-97}$$

Then the basic equation for this shock tube is

$$P_{48} = P_{78}\left\{1 - \frac{\gamma_4-1}{2}\,\frac{u_2}{a_1}\,\frac{a_1}{a_4}\right\}^{-\frac{2\gamma_4}{\gamma_4-1}} \quad X \tag{A-98}$$

$$\left\{1 - \frac{\gamma_{av}-1}{2a_2}\left(u_7 - u_2\right)\right\}^{-\frac{2\gamma_{av}}{\gamma_{av}-1}}$$

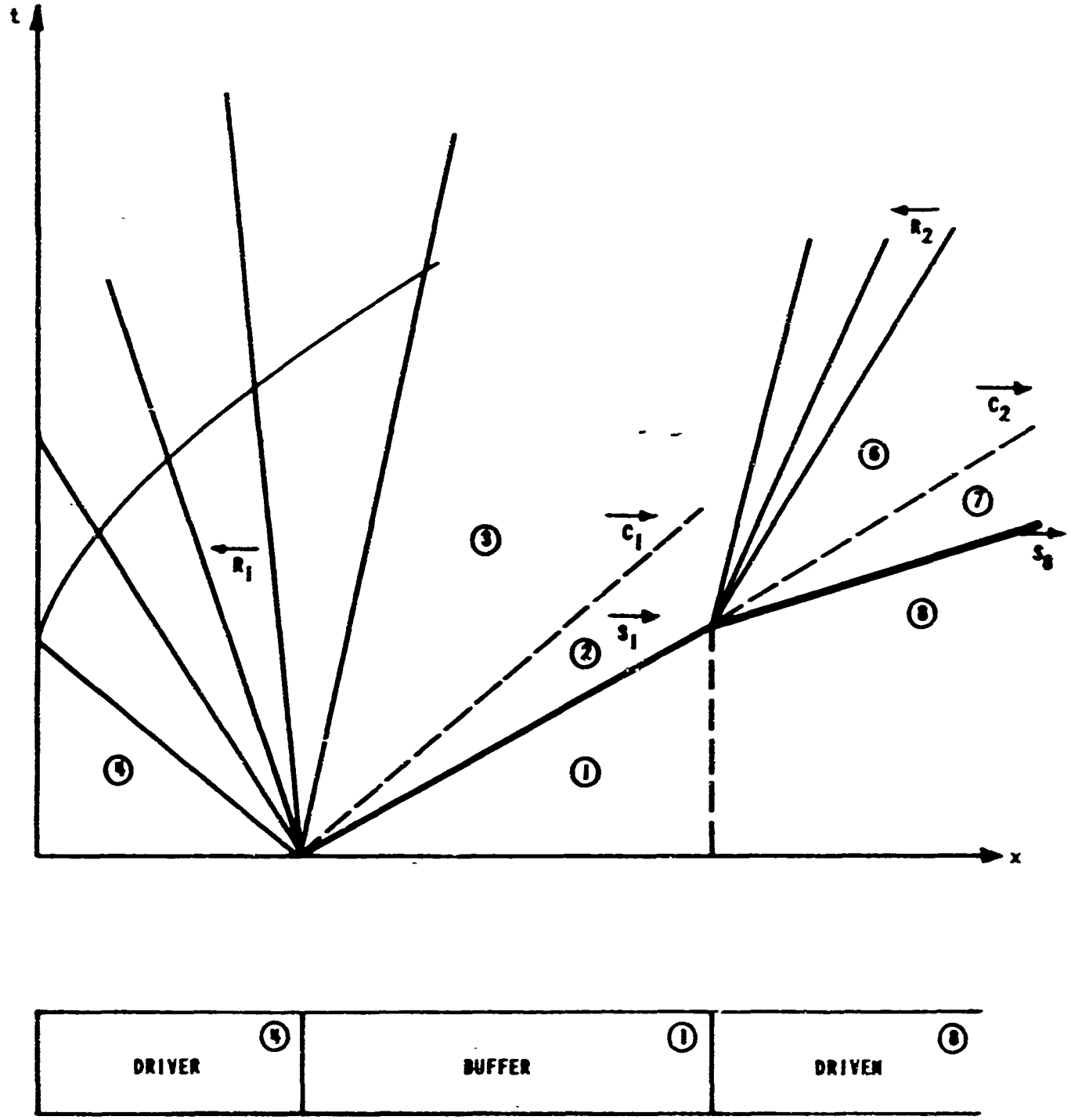

Figure 1 INITIAL FLOW IN CONSTANT-AREA BUFFERED SHOCK TUBE - UNSTEADY-EXPANSION TYPE

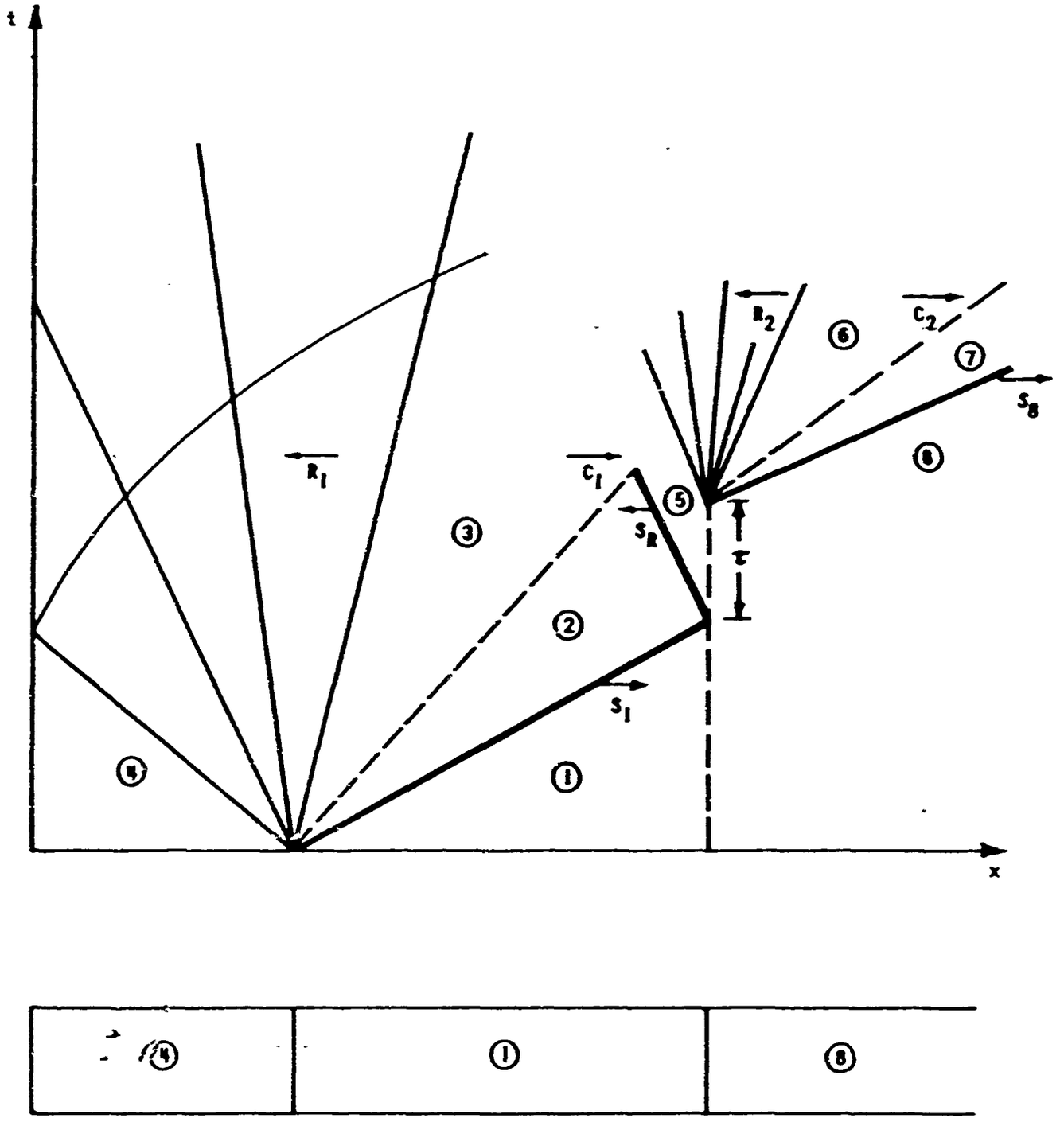

Figure 2 INITIAL FLOW IN CONSTANT-AREA BUFFERED SHOCK TUBE - REFLECTED-SHOCK TYPE

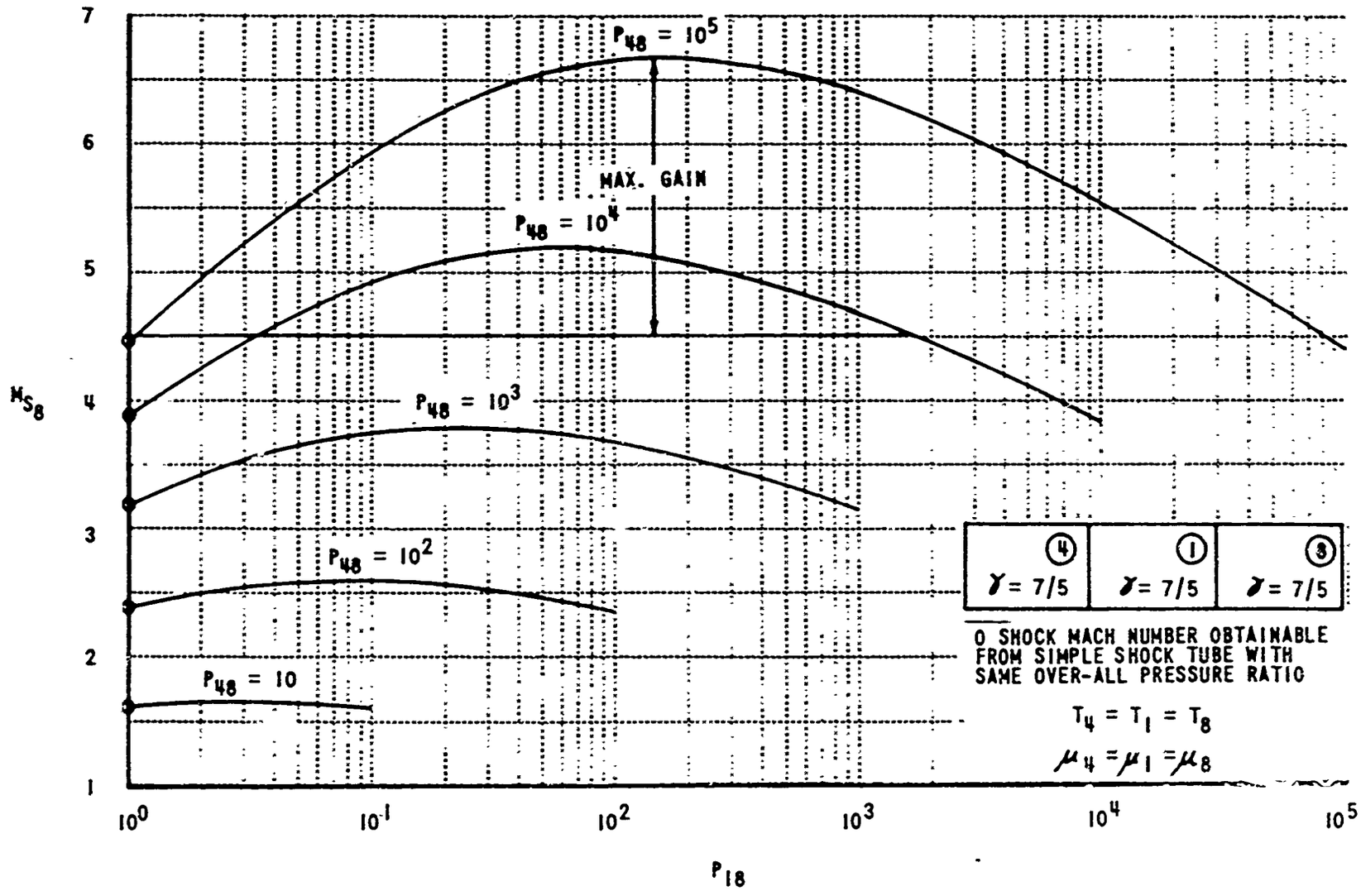

Figure 3 PERFORMANCE OF CONSTANT-AREA BUFFERED TUBE - UNSTEADY-EXPANSION TYPE - WITH THE SAME DIATOMIC GAS USED THROUGHOUT (Ref. 9)

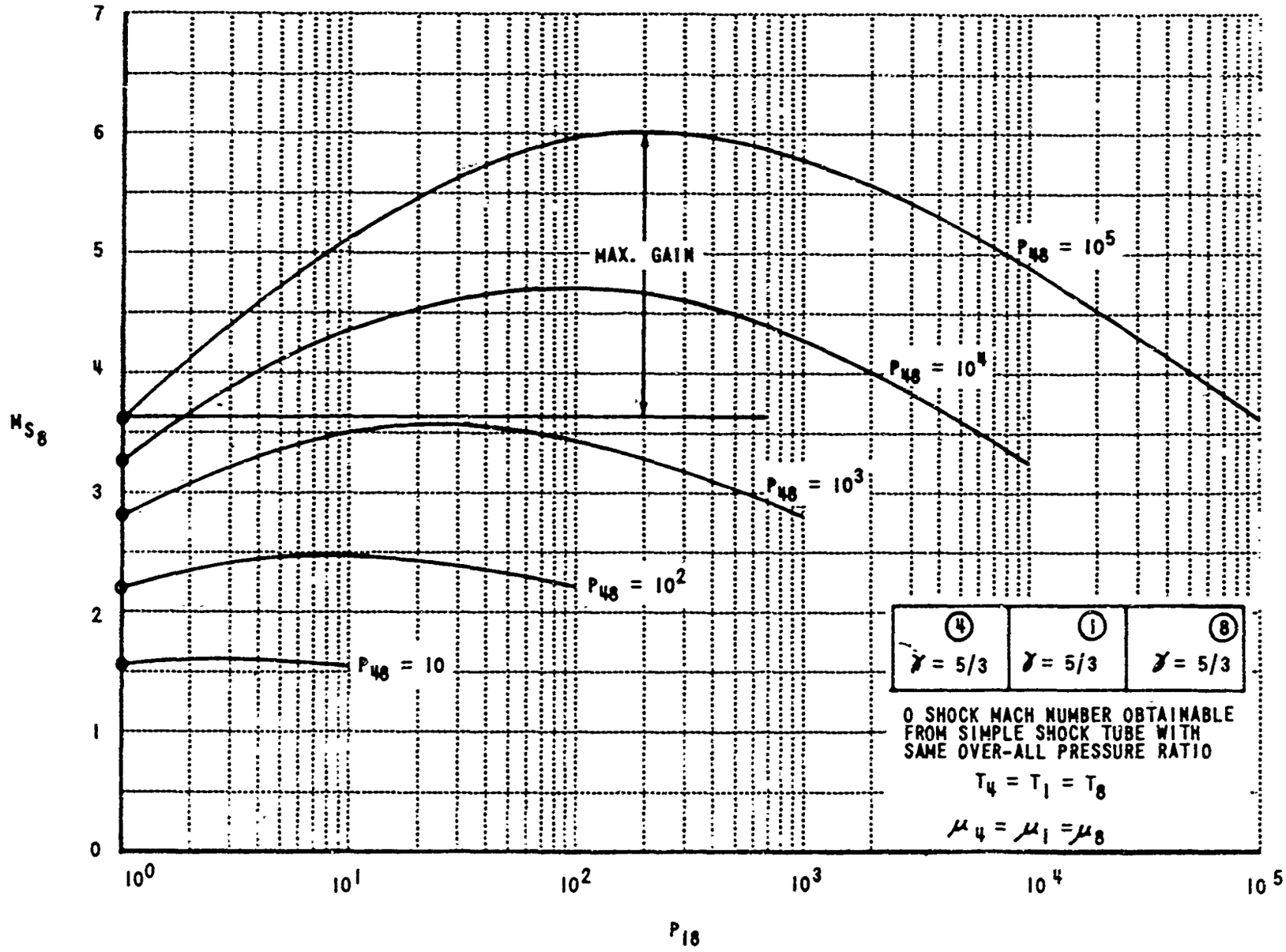

Figure 4 PERFORMANCE OF CONSTANT-AREA BUFFERED TUBE - UNSTEADY-EXPANSION TYPE - WITH THE SAME MONATOMIC GAS USED THROUGHOUT

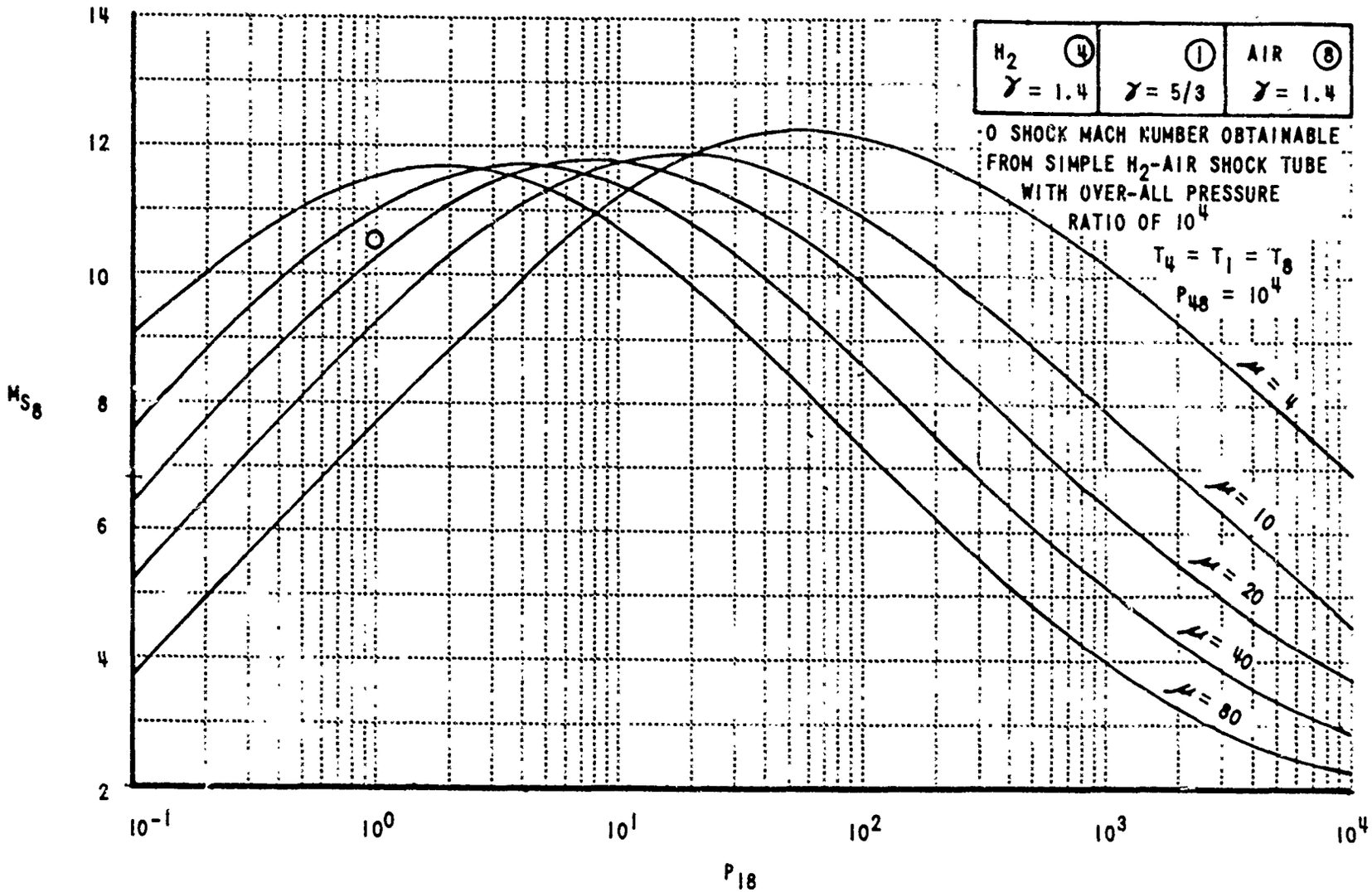

Figure 5 EFFECT OF PRESSURE RATIO DISTRIBUTION AND BUFFER GAS MOLECULAR WEIGHT UPON STRENGTH OF FINAL SHOCK

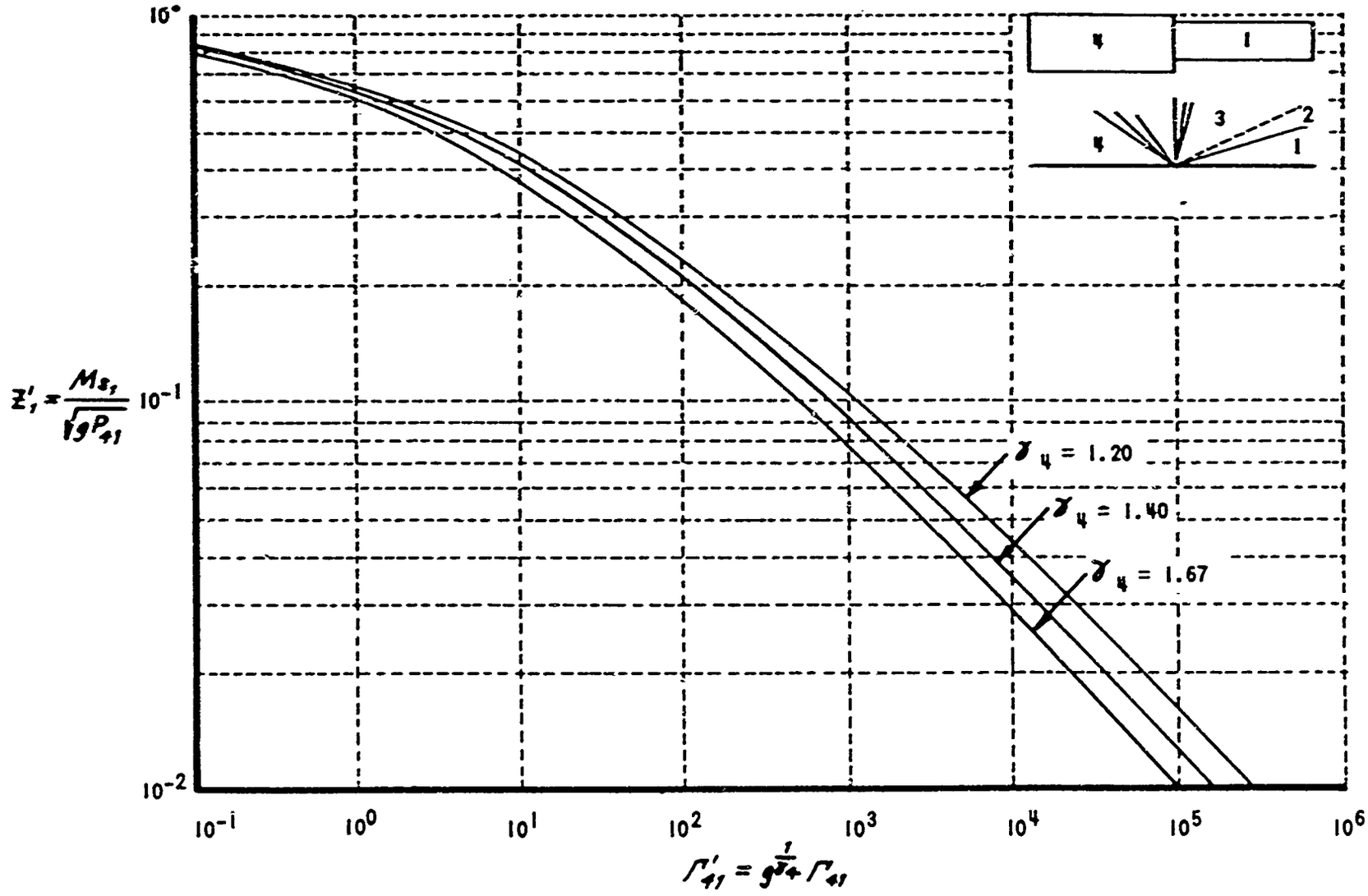

Figure 6 PERFORMANCE OF SIMPLE SHOCK TUBE WITH AREA CHANGE APPLICABLE FOR $M_{s_1} > 3$ AND ARBITRARY γ_1 (Ref. 19)

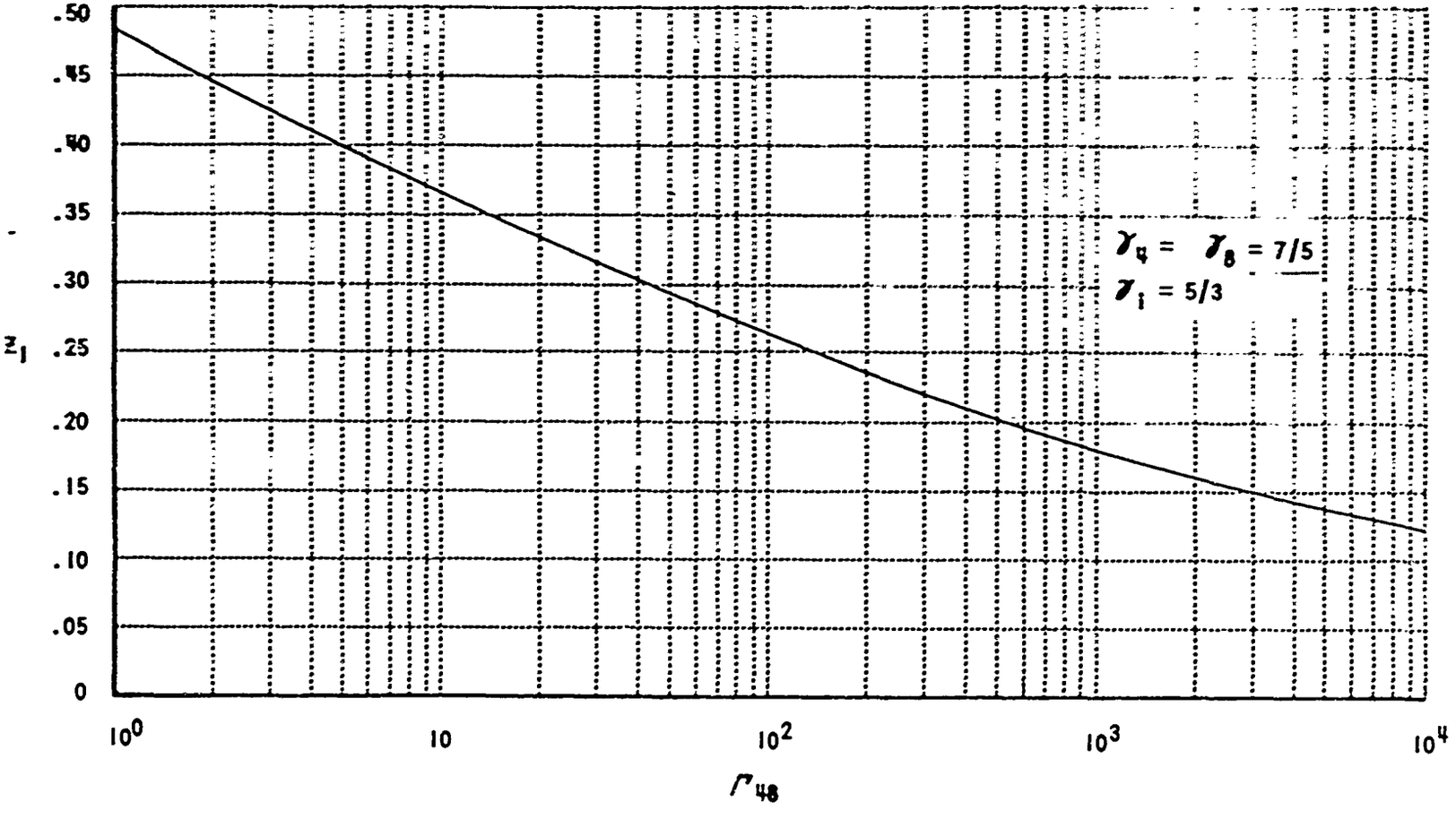

Figure 7 OPTIMUM VALUES OF INITIAL SHOCK STRENGTH FOR GIVEN OVER-ALL DENSITY RATIO WITH CONSTANT-AREA BUFFERED TUBE

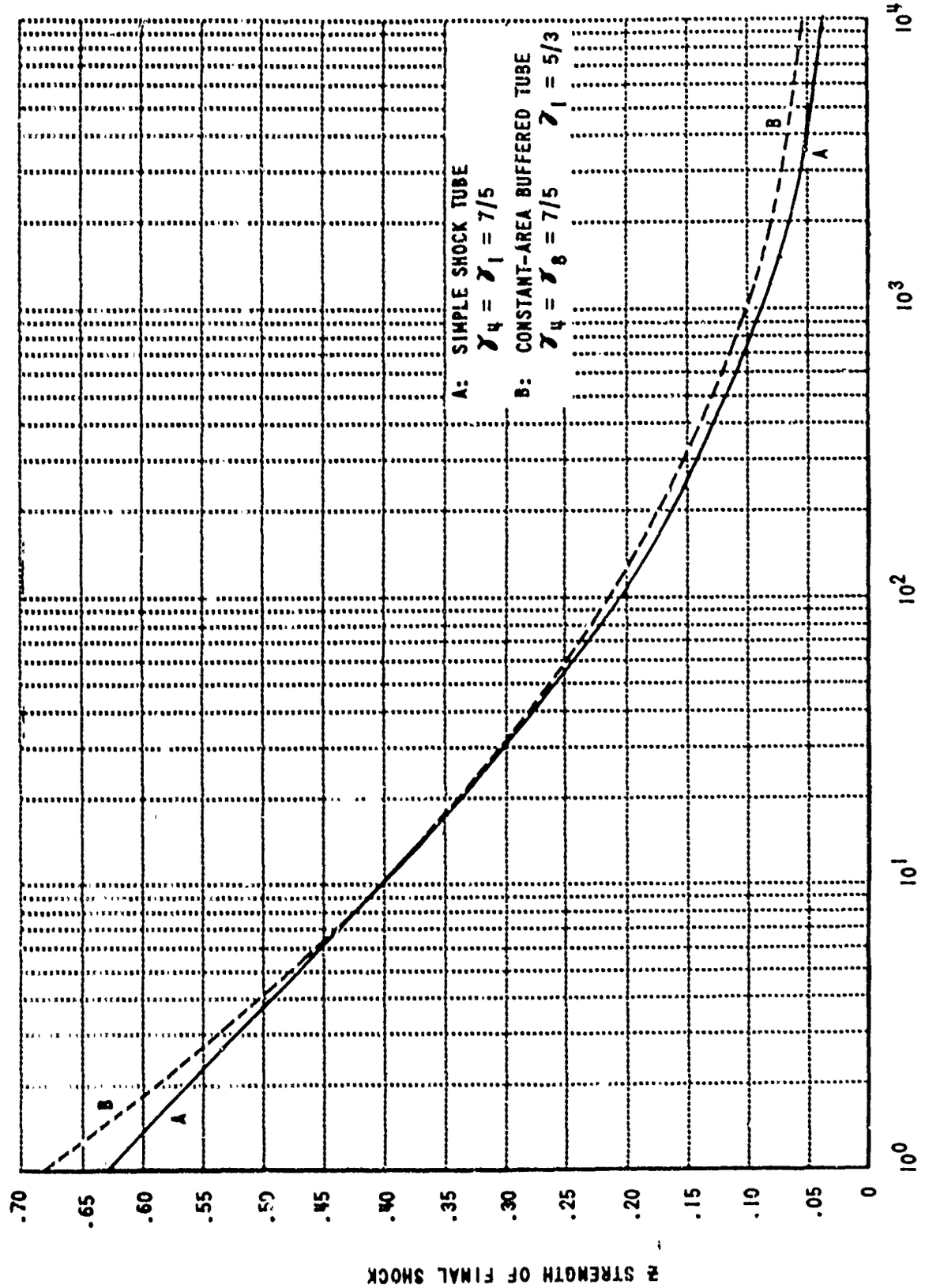

Figure 8 OPTIMUM PERFORMANCE OF A CONSTANT-AREA BUFFERED SHOCK TUBE COMPARED WITH THE PERFORMANCE OF A SIMPLE SHOCK TUBE

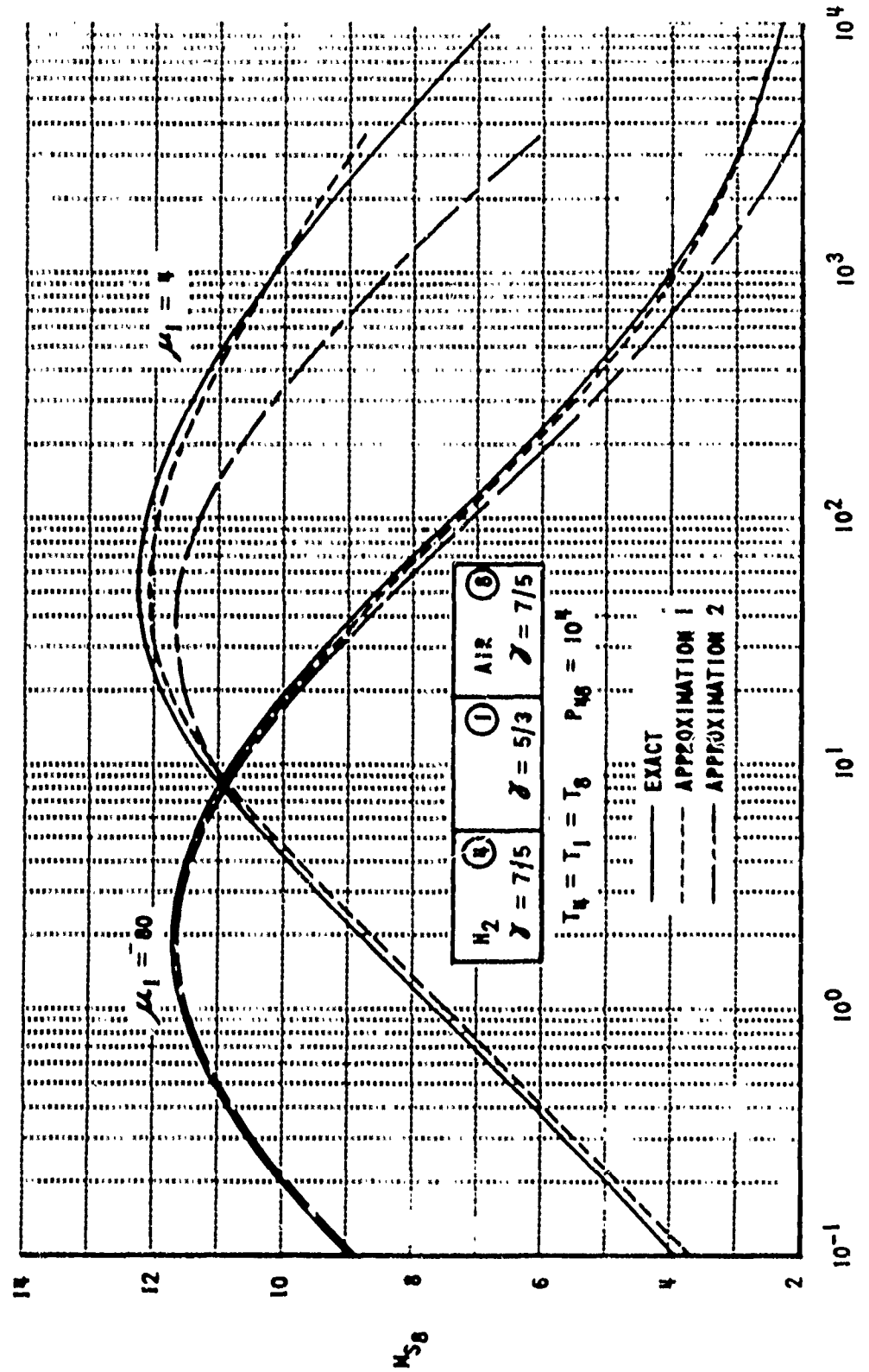

Figure 9 COMPARISON OF THE EXACT EQUATION WITH APPROXIMATIONS ONE AND TWO FOR THE CONSTANT-AREA BUFFERED TUBE

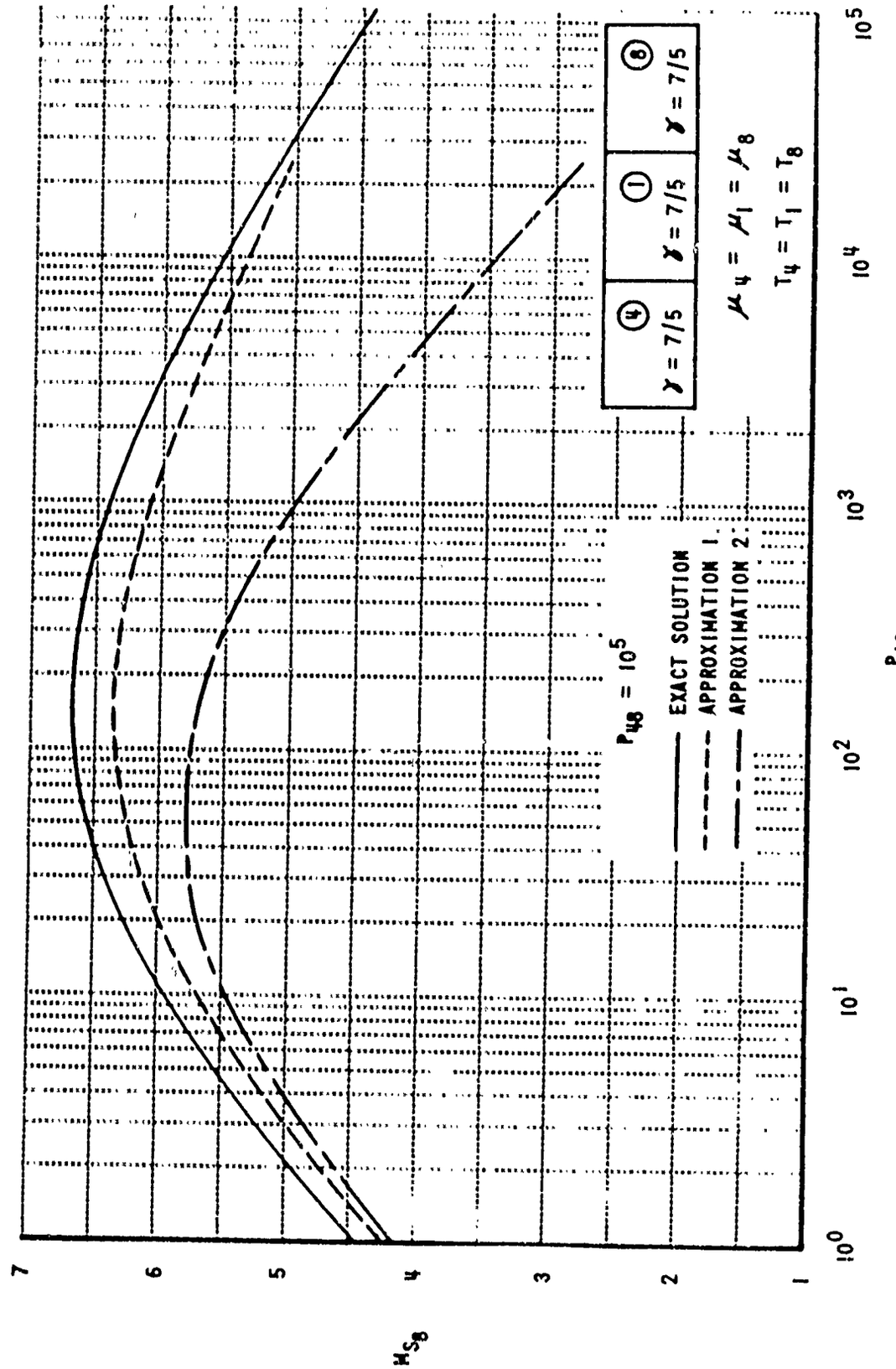

Figure 10 COMPARISON OF THE EXACT EQUATION WITH APPROXIMATIONS ONE AND TWO FOR THE CONSTANT-AREA RUFFERED TUBE

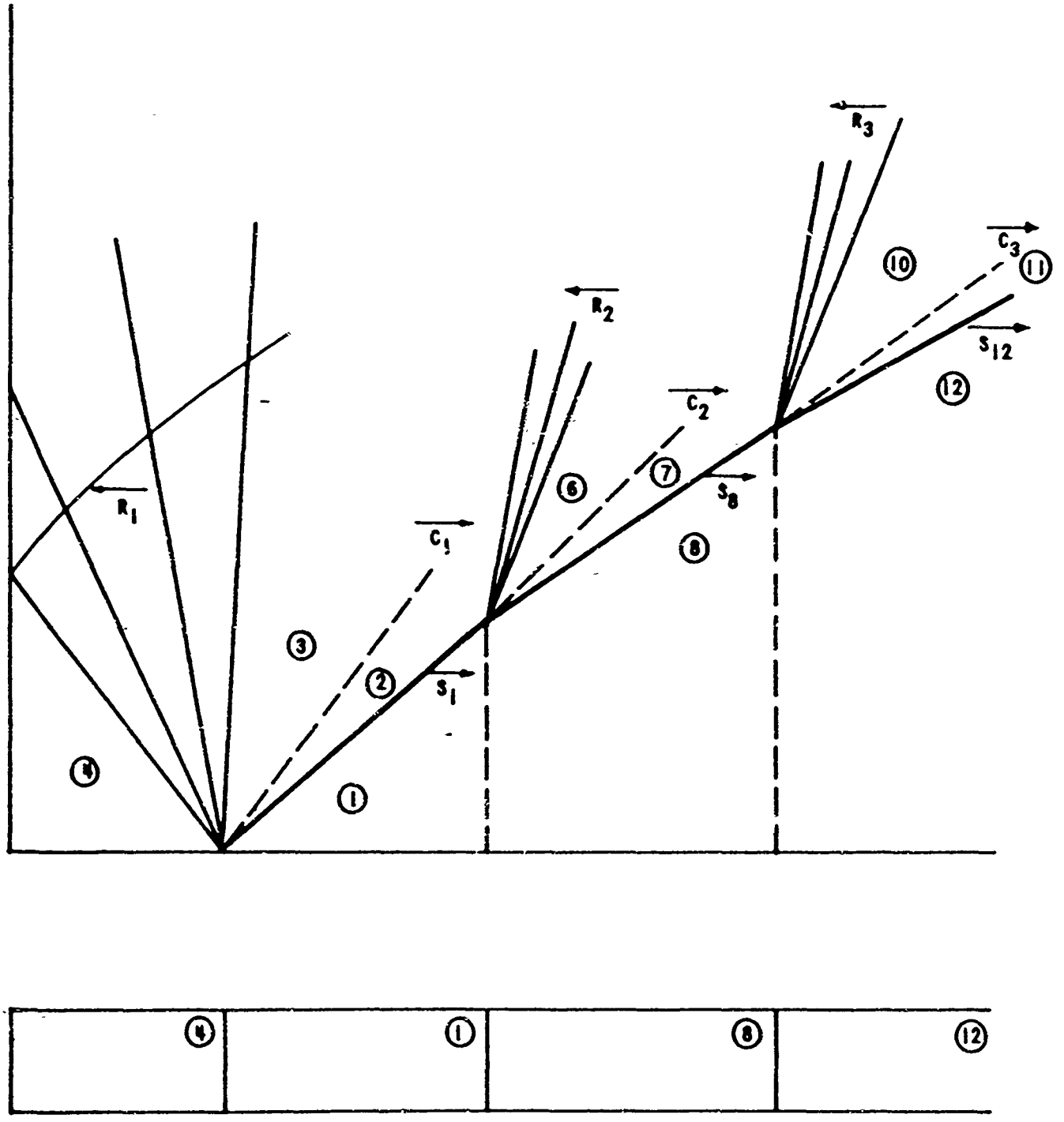

Figure 11 WAVE DIAGRAM FOR THE CONSTANT-AREA, DOUBLE-BUFFERED SHOCK TUBE

BLANK PAGE

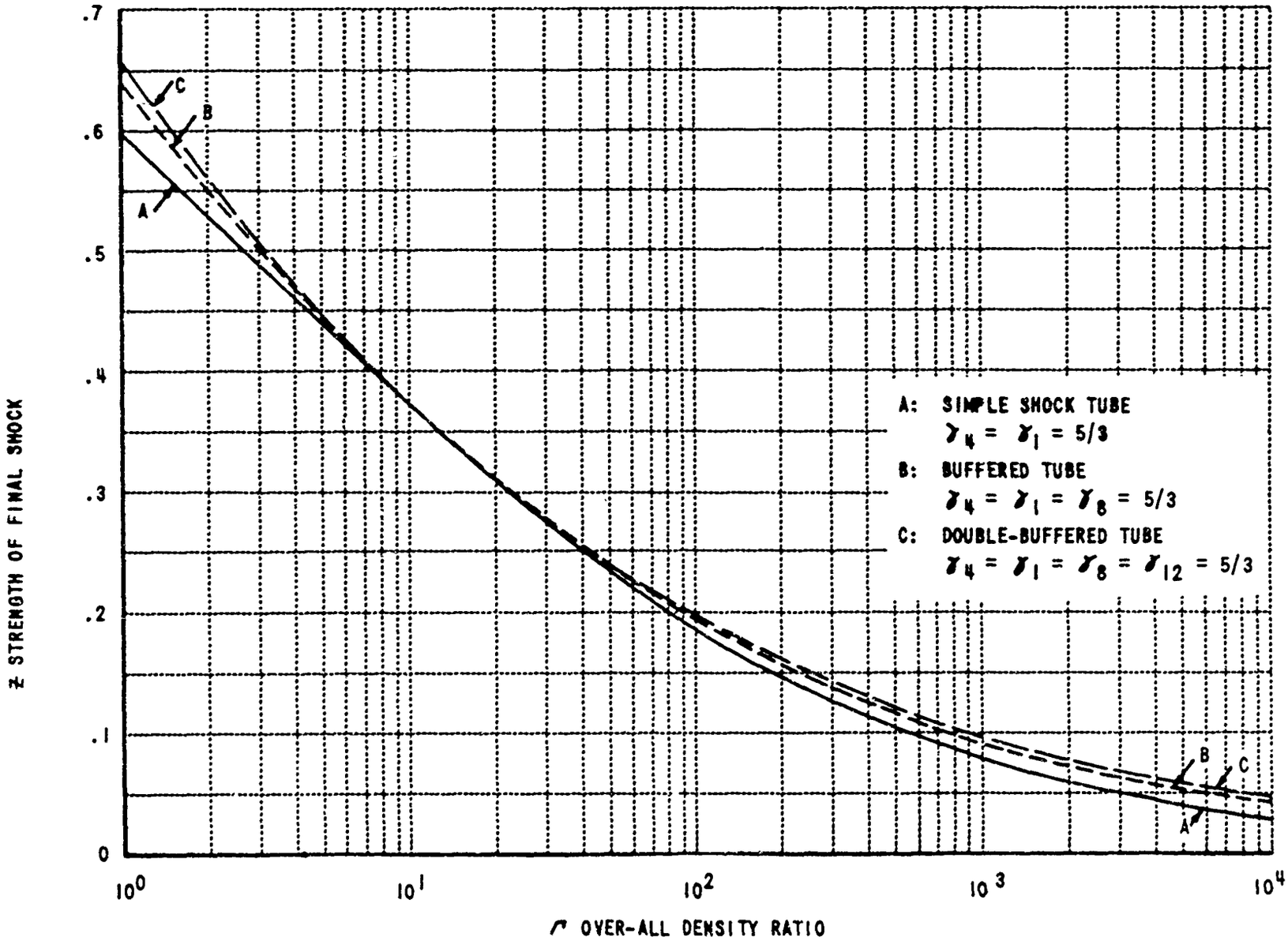

Figure 12 OPTIMUM PERFORMANCE OF BUFFERED SHOCK TUBE WITH ONE OR TWO BUFFERS COMPARED WITH SIMPLE SHOCK TUBE

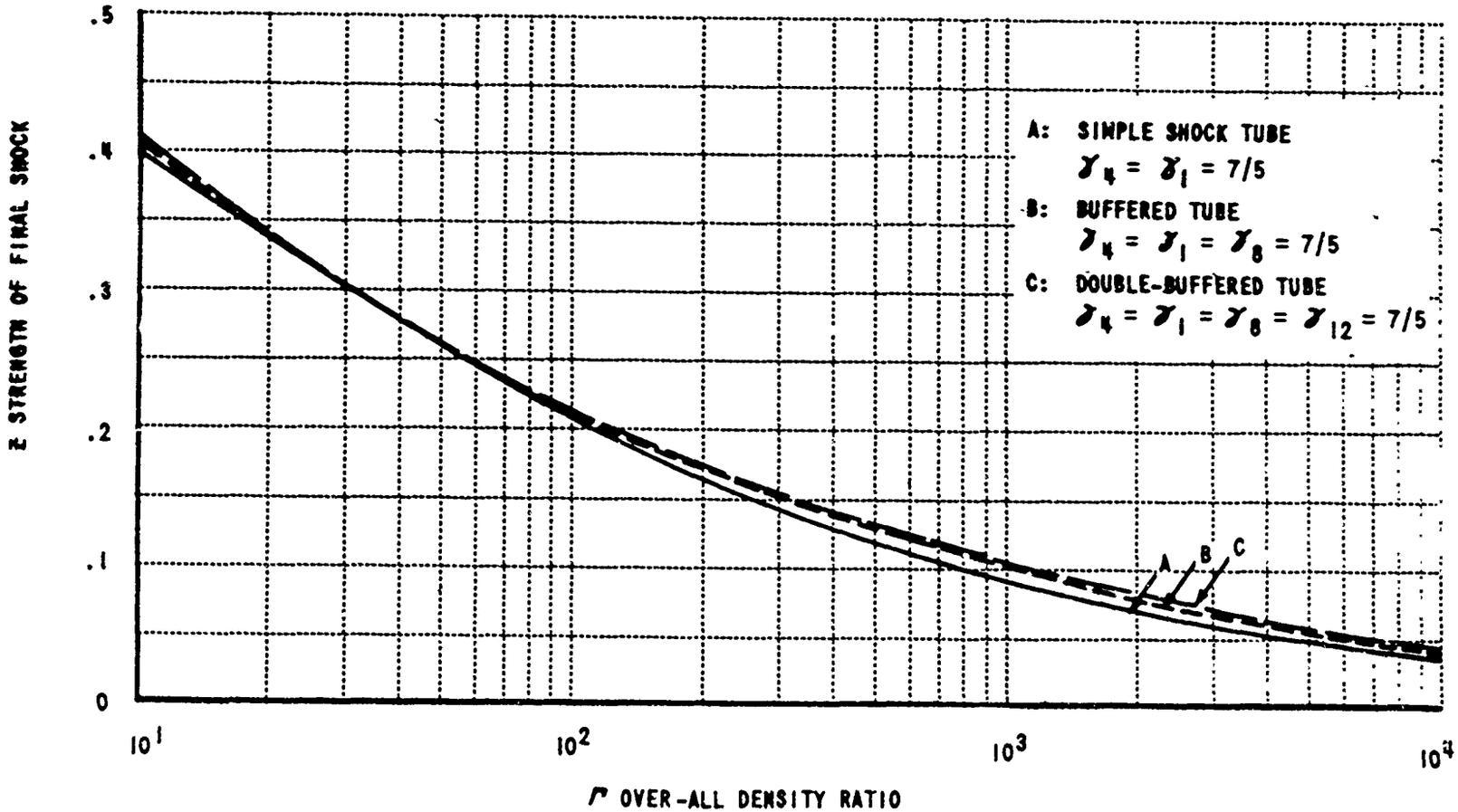

Figure 13 OPTIMUM PERFORMANCE OF BUFFERED SHOCK TUBE WITH ONE OR TWO BUFFERS COMPARED WITH SIMPLE SHOCK TUBE

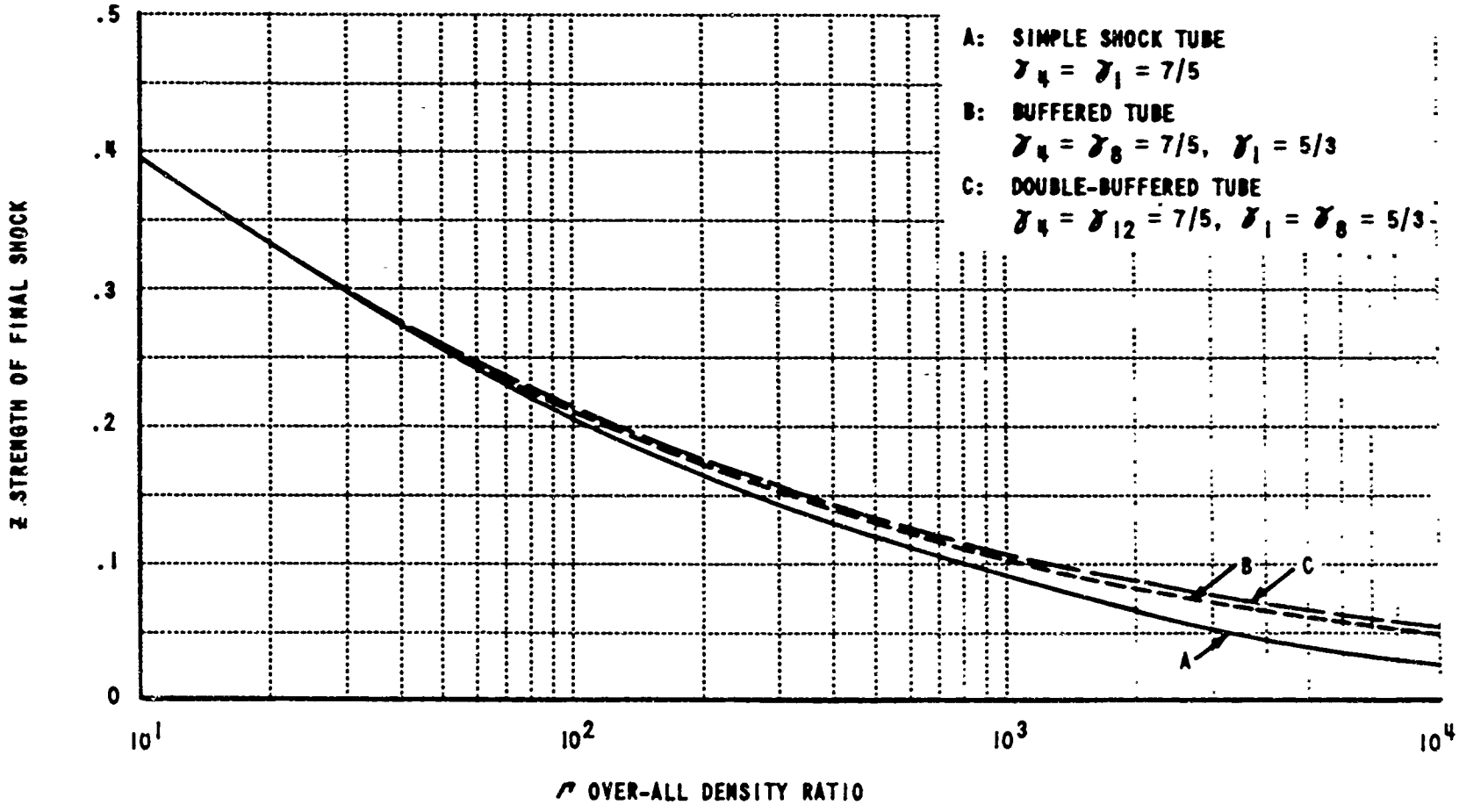

Figure 14 OPTIMUM PERFORMANCE OF BUFFERED SHOCK TUBE WITH ONE OR TWO BUFFERS COMPARED WITH SIMPLE SHOCK TUBE

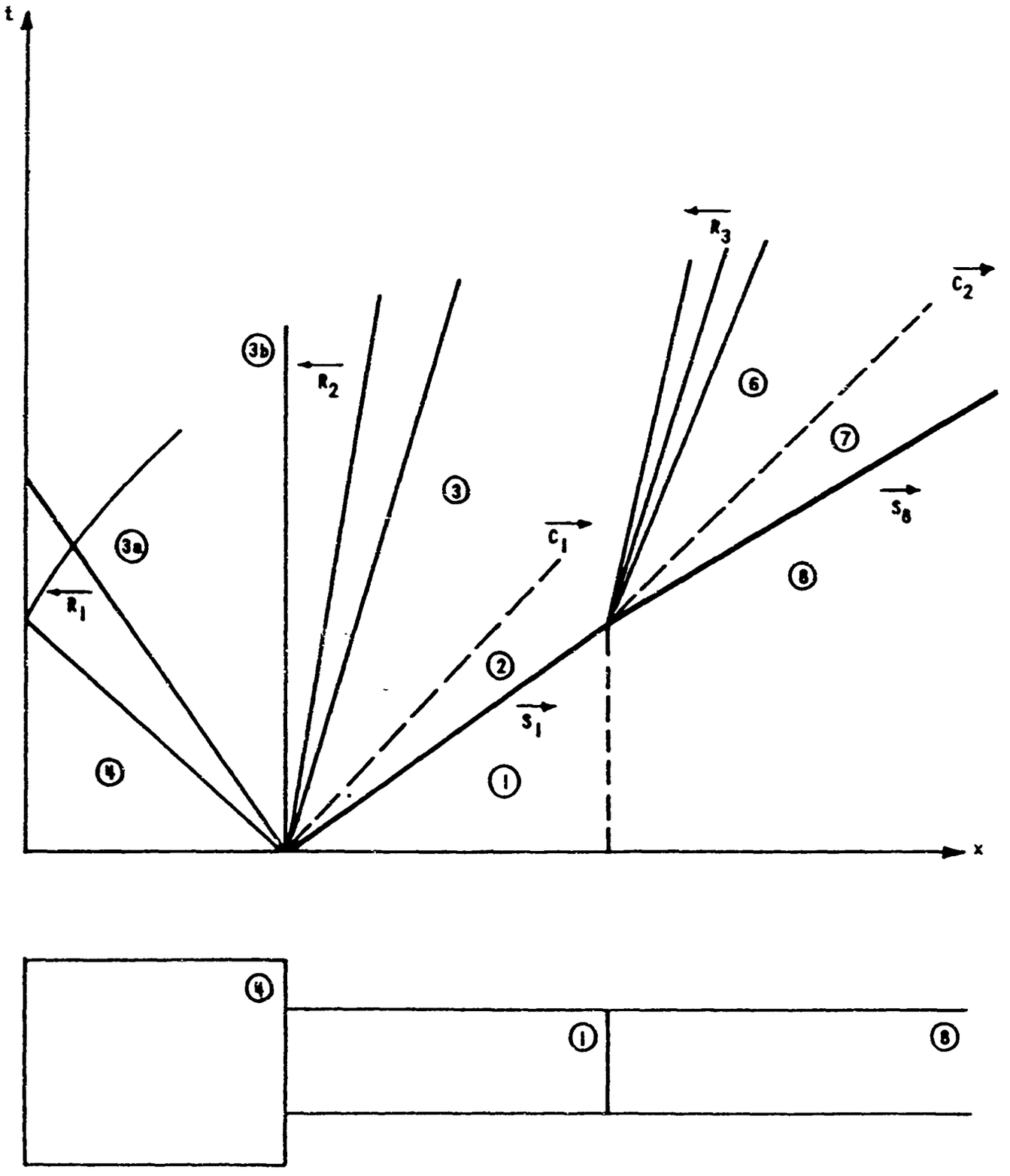

Figure 15 WAVE DIAGRAM FOR BUFFERED SHOCK TUBE WITH AREA CONTRACTION AT FIRST DIAPHRAGM STATION

BLANK PAGE

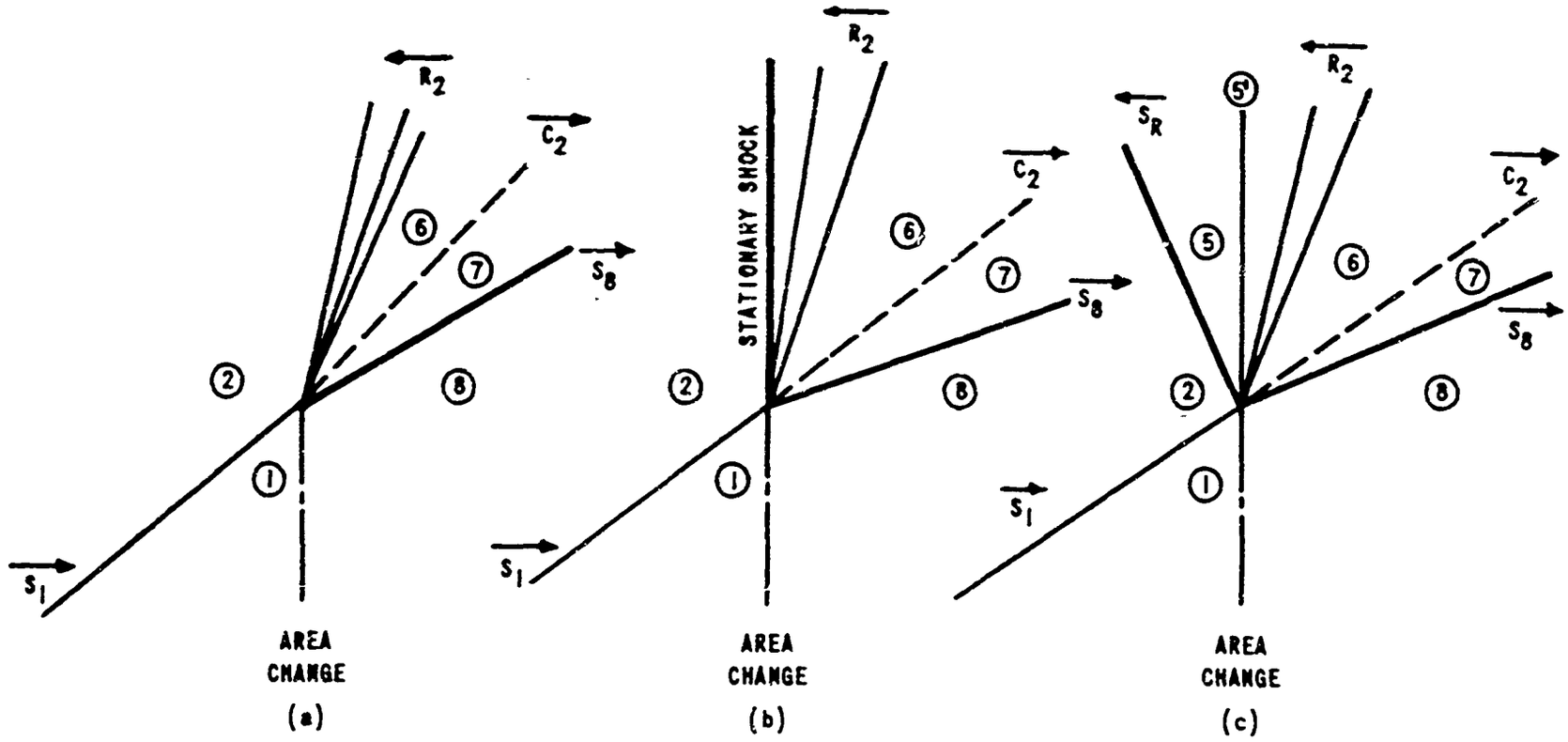

Figure 16 POSSIBLE WAVE PATTERNS AT A MONOTONIC CONVERGENCE AT THE SECOND DIAPHRAGM IN A BUFFERED SHOCK TUBE WITH $M_2 > 1$

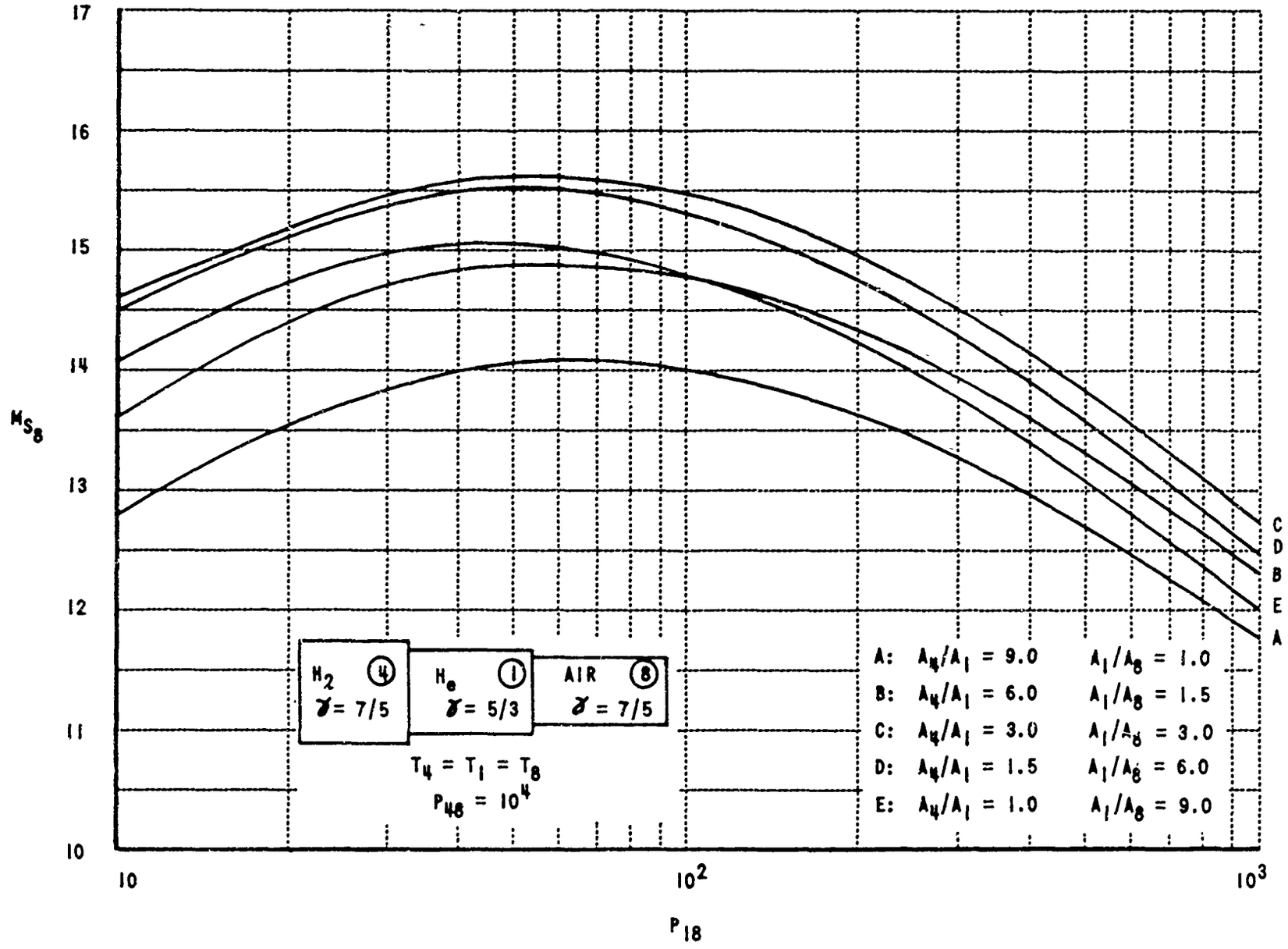

Figure 17 PERFORMANCE OF VARIOUS BUFFERED SHOCK TUBE CONFIGURATIONS WITH AN OVER-ALL AREA CONTRACTION OF 9.0

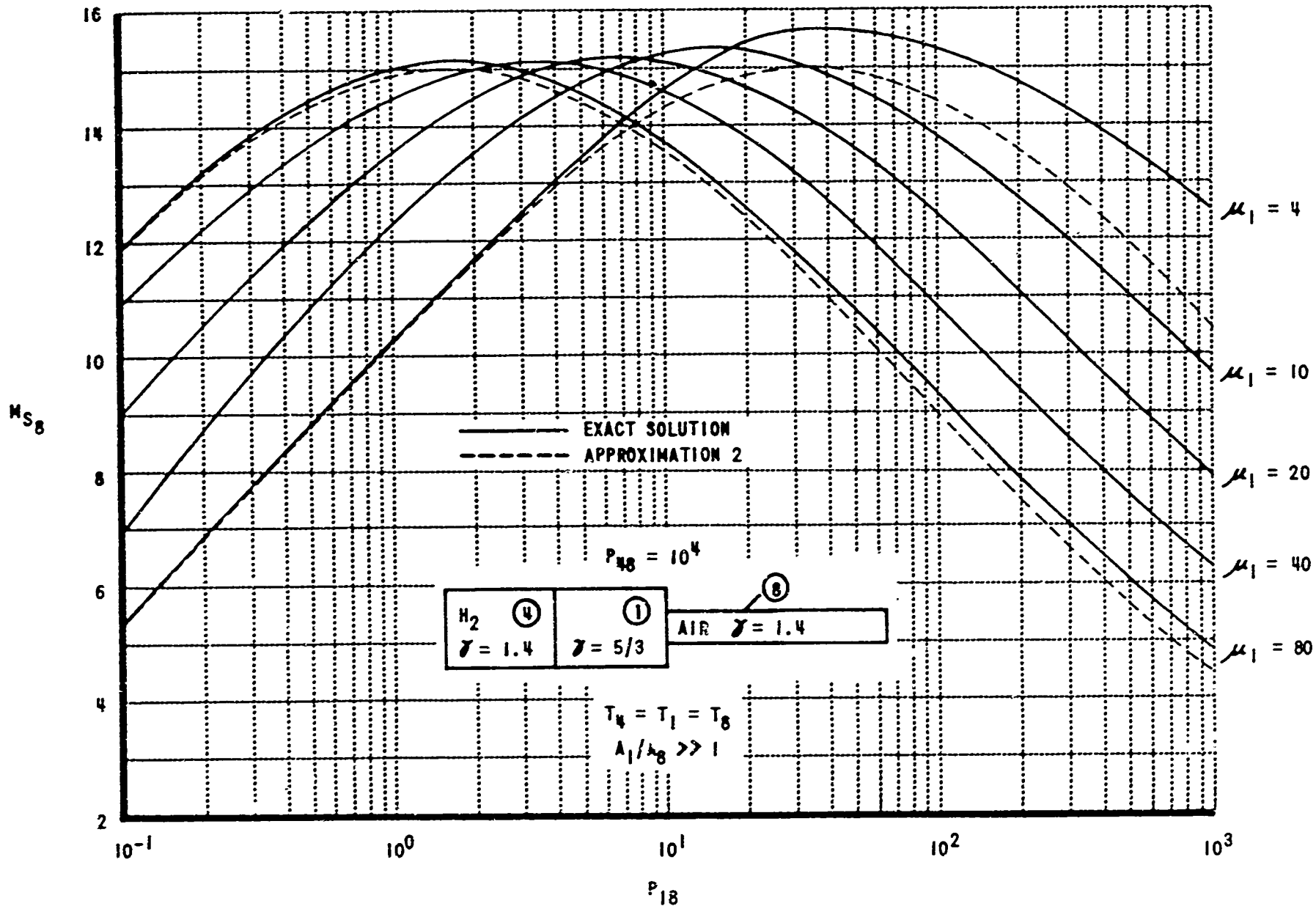

Figure 18 COMPARISON OF THE EXACT AND APPROXIMATE EQUATIONS FOR THE BUFFERED SHOCK TUBE WITH A LARGE AREA CONTRACTION AT THE SECOND DIAPHRAGM

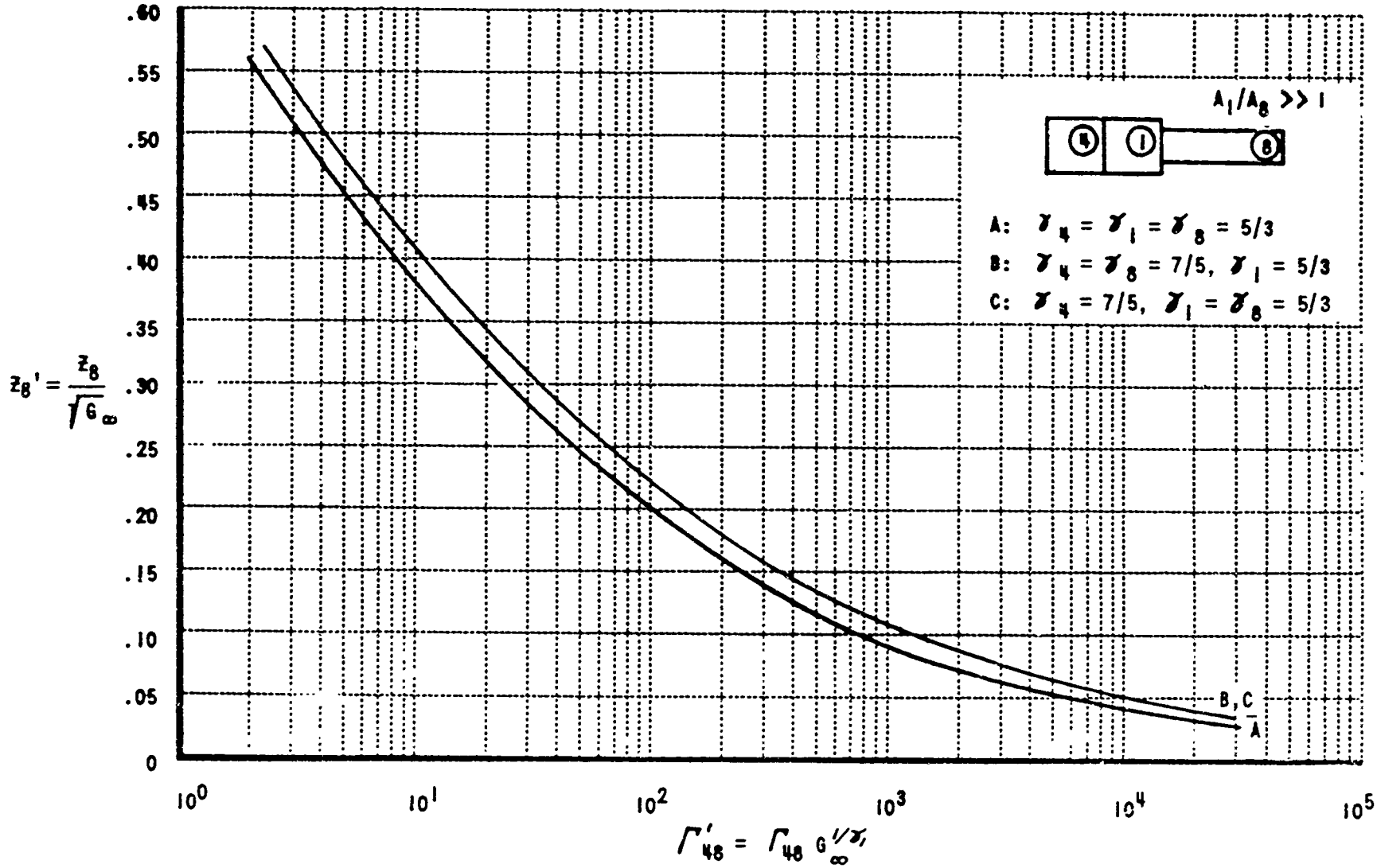

Figure 19 OPTIMUM PERFORMANCE OF A BUFFERED SHOCK TUBE WITH A LARGE AREA CHANGE AT THE SECOND DIAPHRAGM

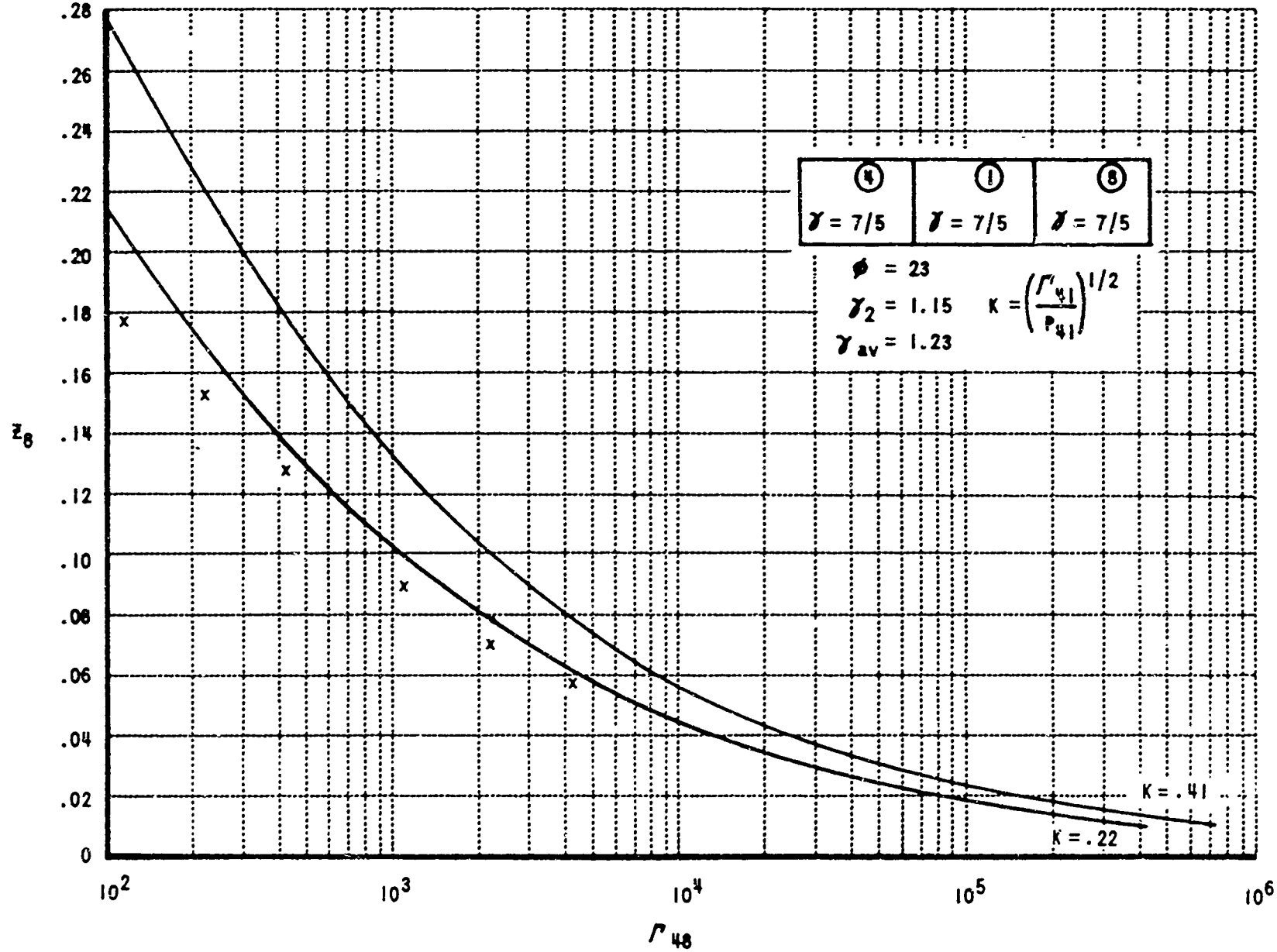

Figure 20 PERFORMANCE OF A DETONATION BUFFER WITH TWO DIFFERENT VALUES OF K

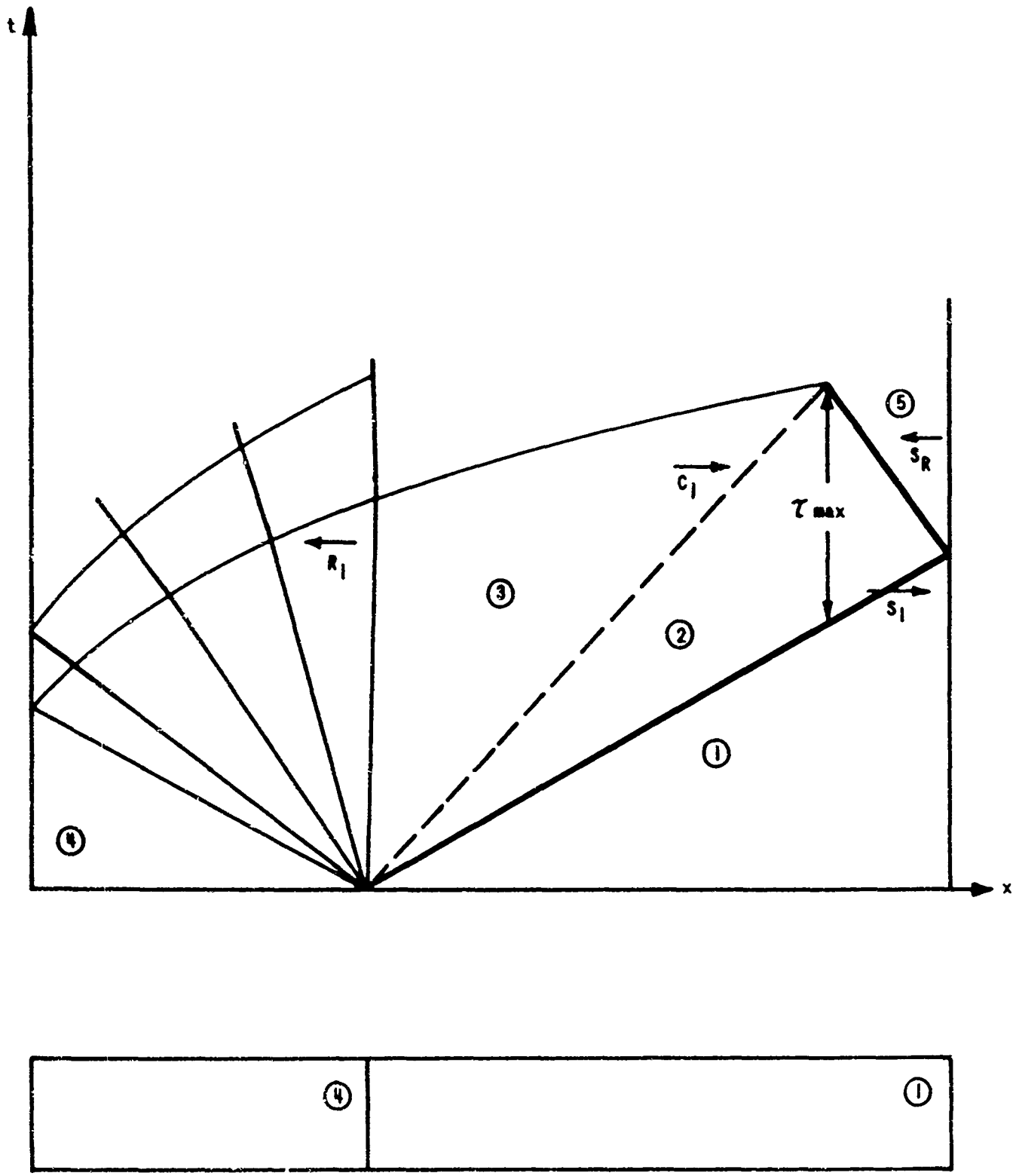

Figure 2: WAVE PATTERN IN A SIMPLE SHOCK TUBE OF FINITE LENGTH FOR THE PRODUCTION OF MAXIMUM TESTING TIME

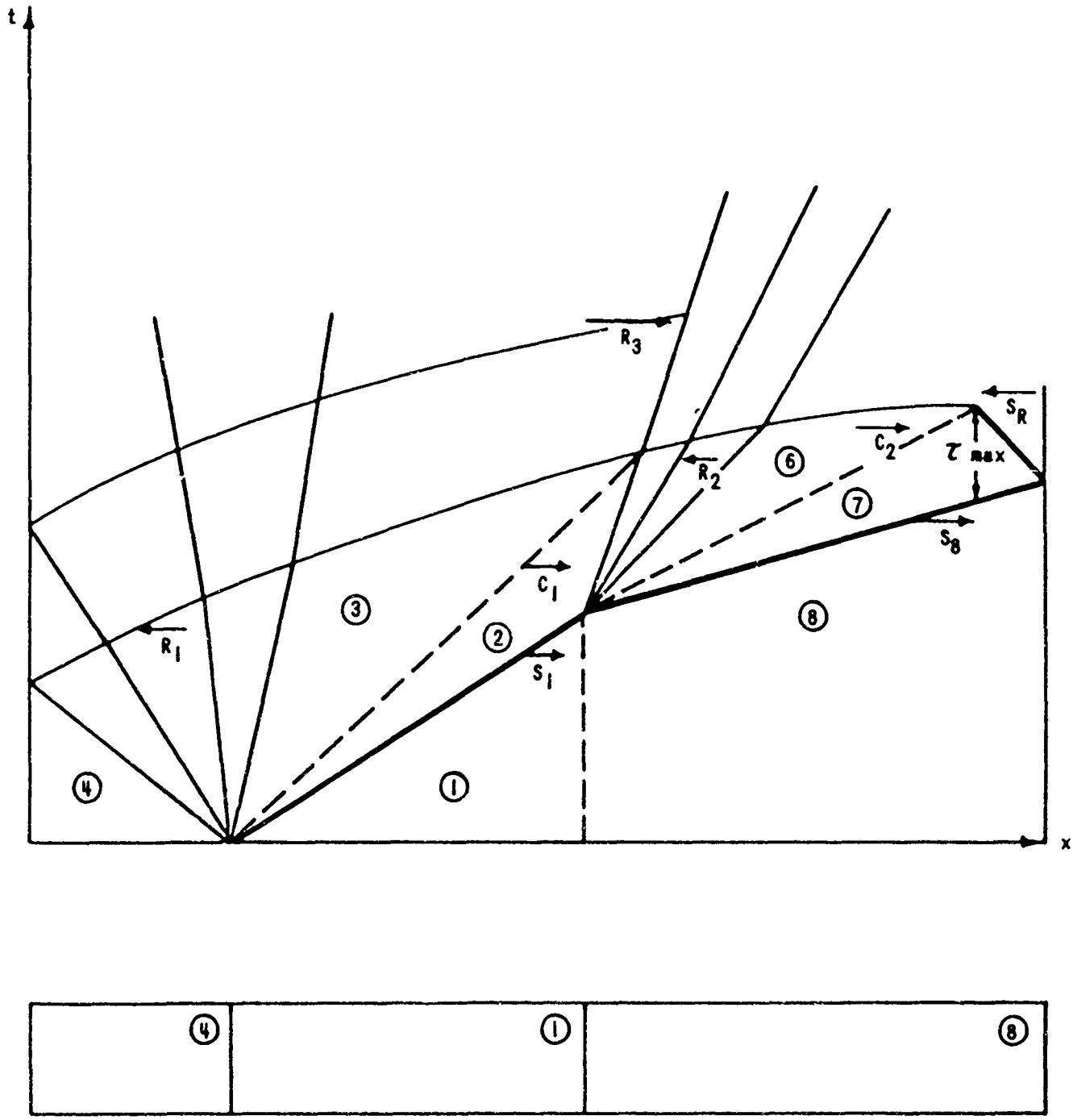

Figure 22 WAVE DIAGRAM FOR A BUFFERED SHOCK TUBE OF FINITE LENGTH

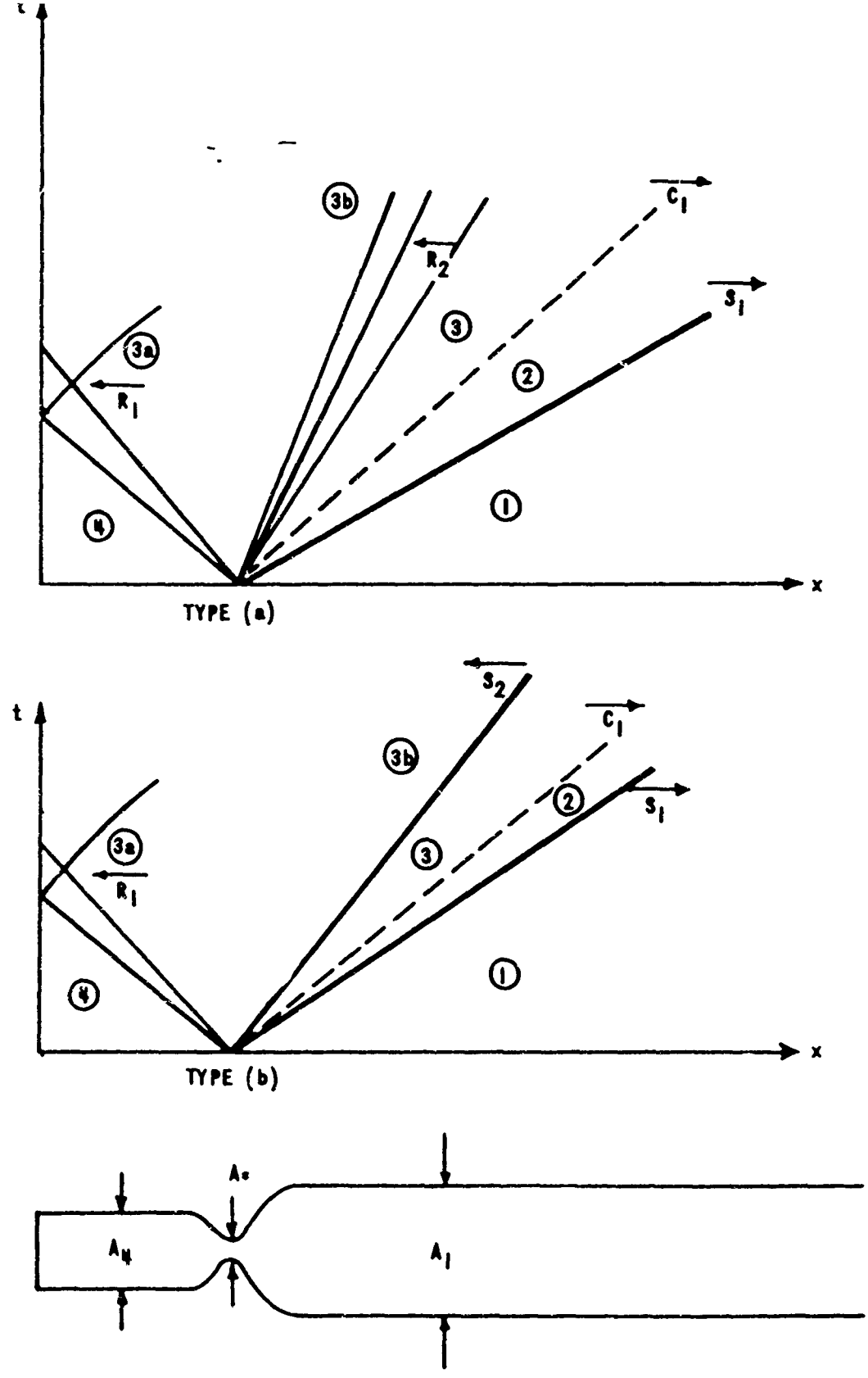

Figure 23 POSSIBLE WAVE PATTERNS RESULTING IN A SHOCK TUBE WITH AN AREA CHANGE NEAR THE DIAPHRAGM

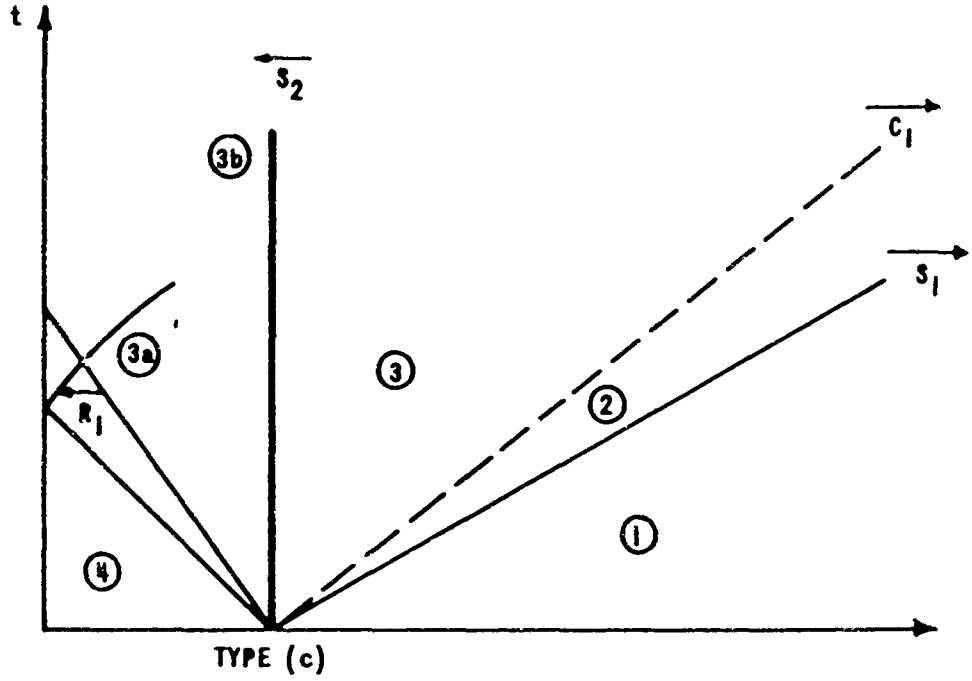

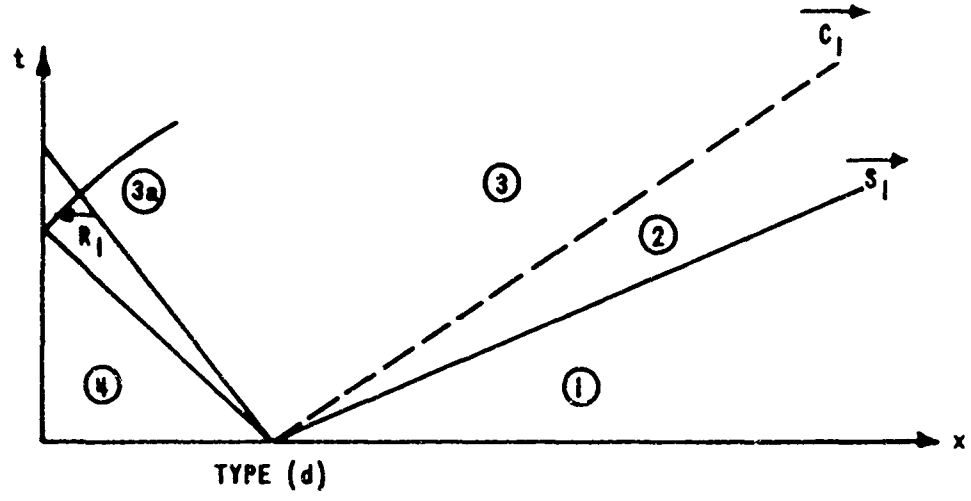

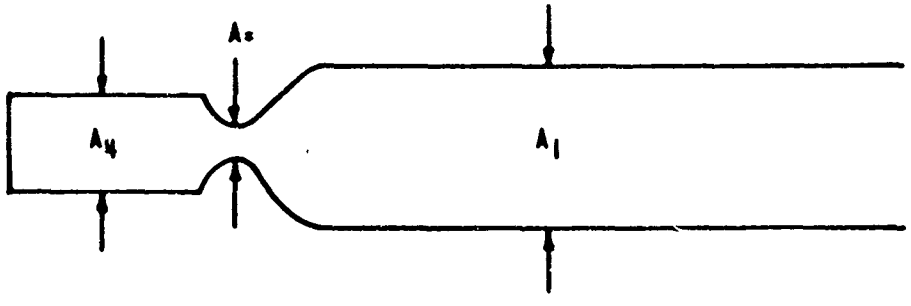

Figure 23 continued

CONT.

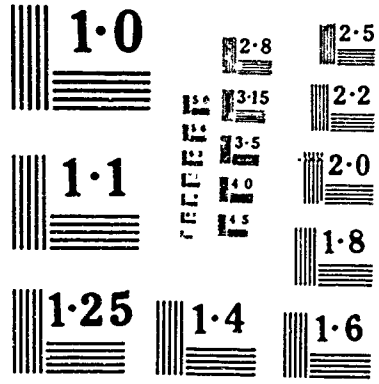
1·0
1·1
1·25
1·4
1·6
1·8
2·0
2·2
2·5
2·8
3·15
3·5
4·0
4·5

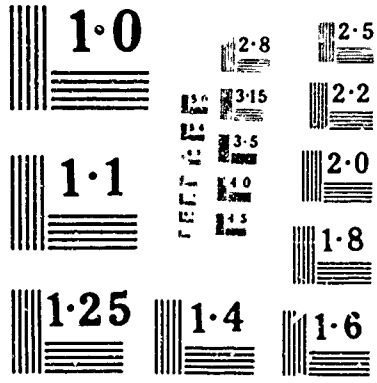
1·0
1·1
1·25
1·4
1·6
1·8
2·0
2·2
2·5
2·8
3·15
3·5
4·0
4·5

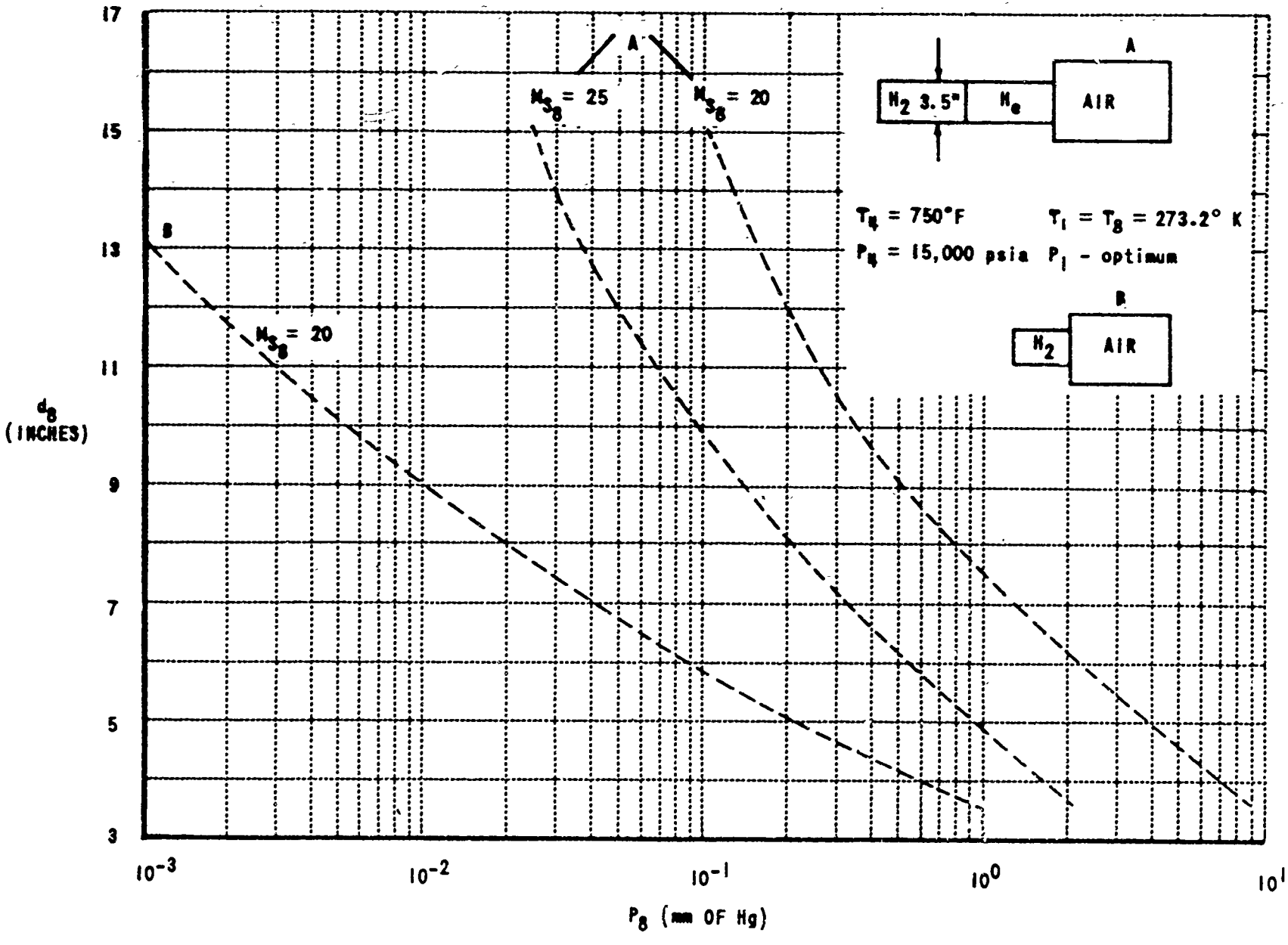

Figure 24 PRESSURE REQUIRED IN DRIVEN SECTION TO MAINTAIN A GIVEN SHOCK MACH NUMBER AS DRIVEN SECTION DIAMETER IS INCREASED

BLANK PAGE

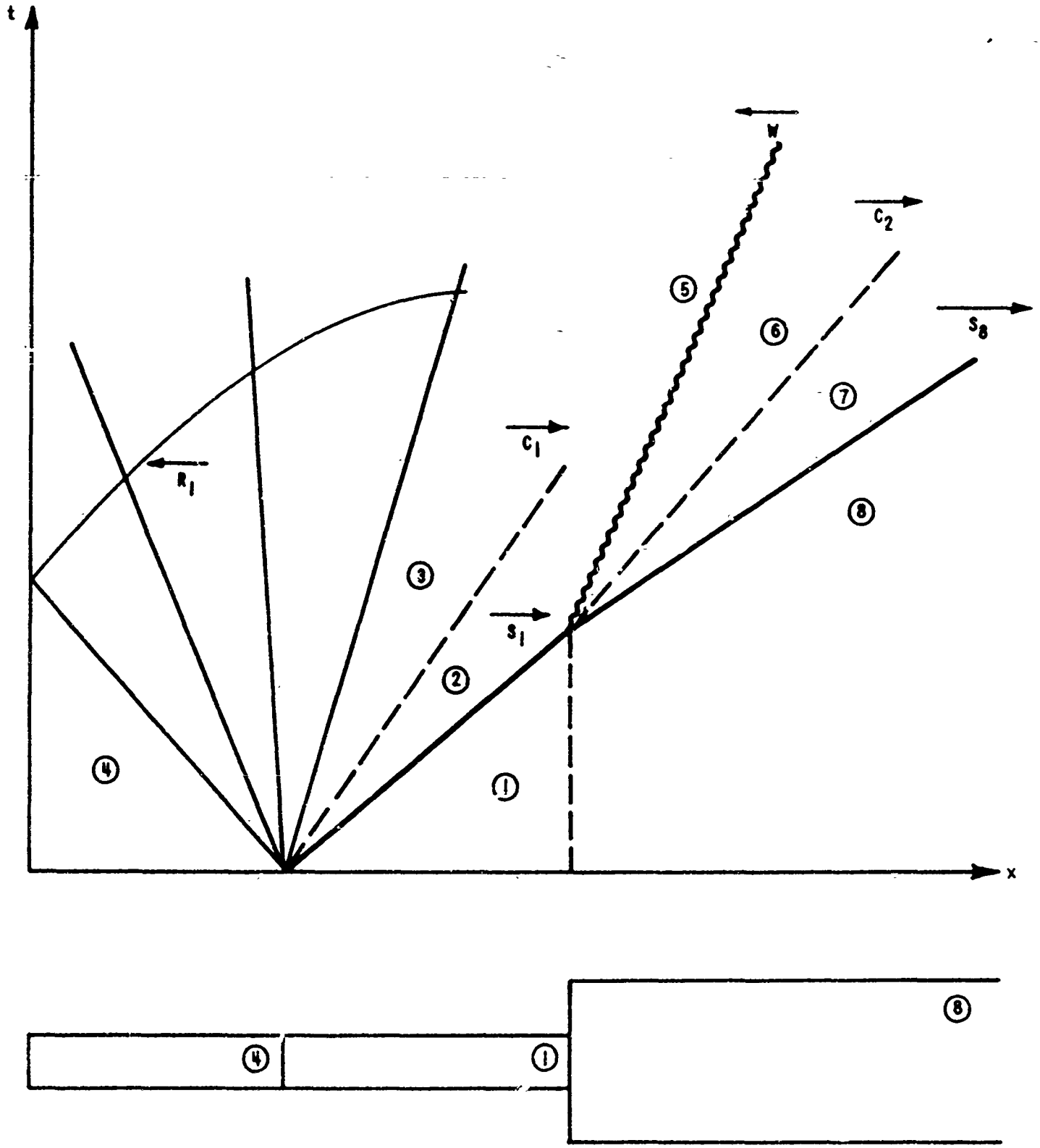

Figure 25 WAVE DIAGRAM OF SHOCK TUBE WITH AREA EXPANSION AT SECOND DIAPHRAGM

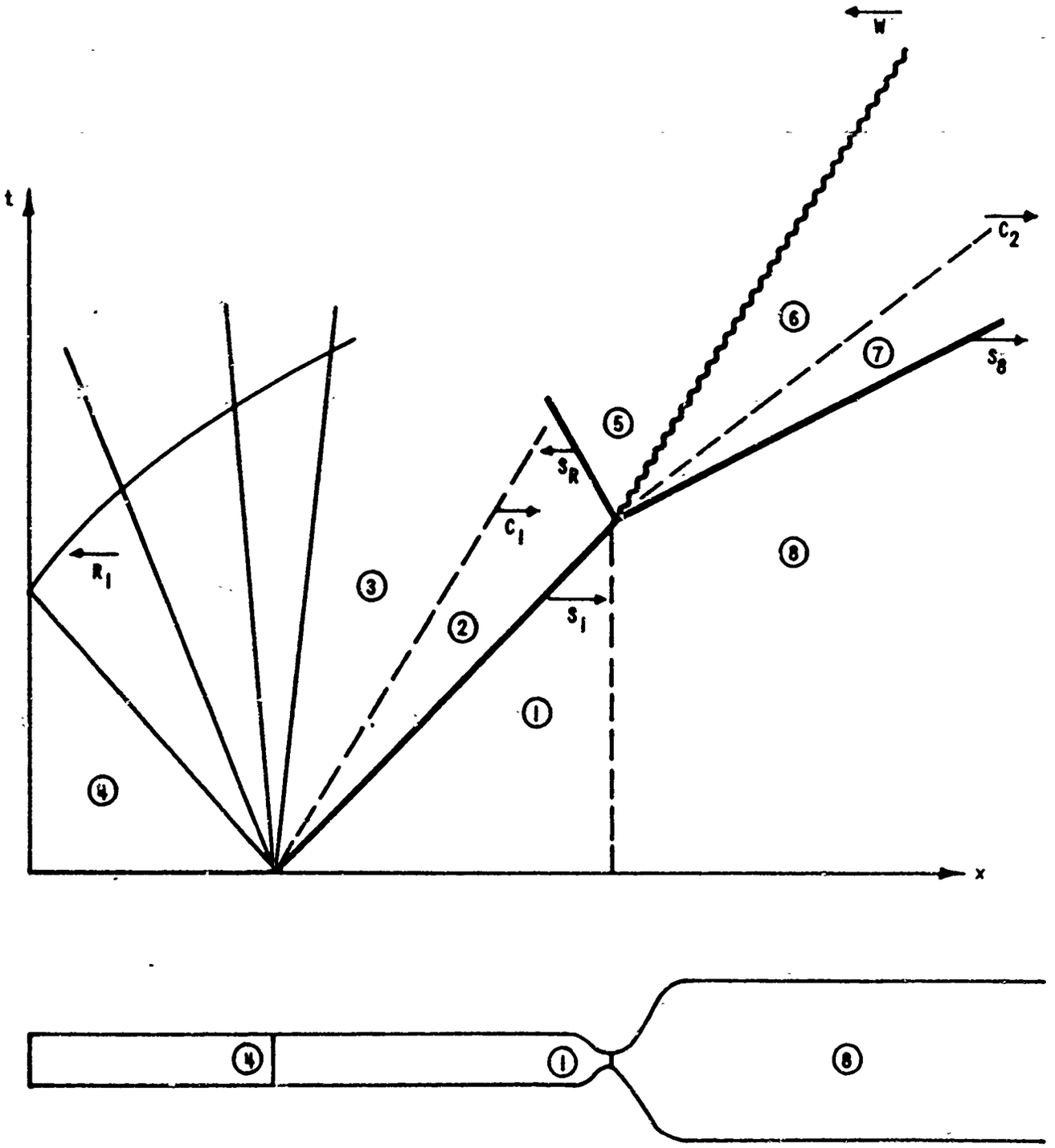

Figure 26 WAVE DIAGRAM FOR A BUFFERED SHOCK TUBE WITH A CONVERGING-DIVERGING SECTION AT THE SECOND DIAPHRAGM

BLANK PAGE

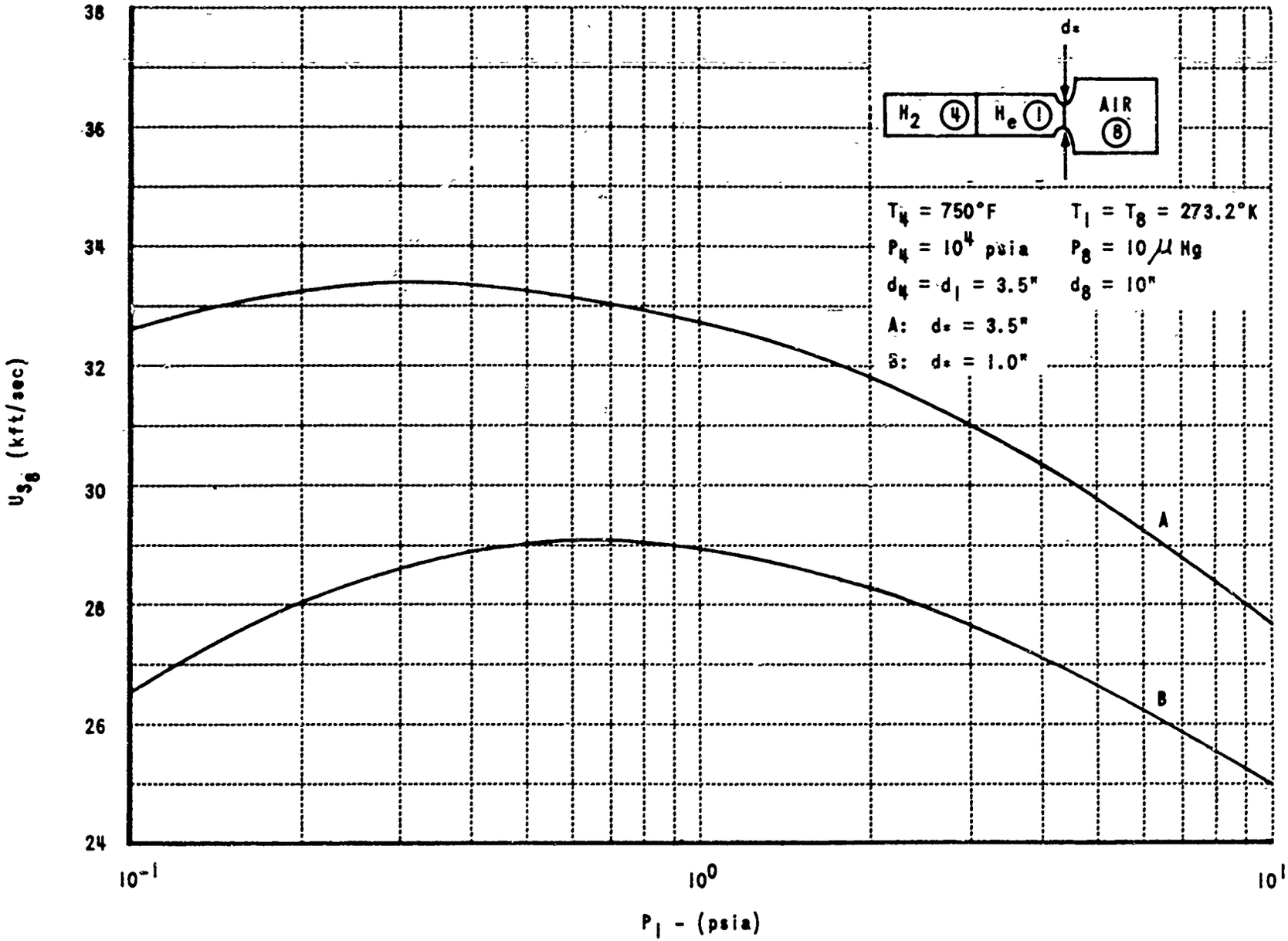

Figure 27 EFFECT OF A THROAT AT THE SECOND DIAPHRAGM ON THE PERFORMANCE OF A BUFFERED TUBE WITH LARGER DRIVEN SECTION THAN DRIVER

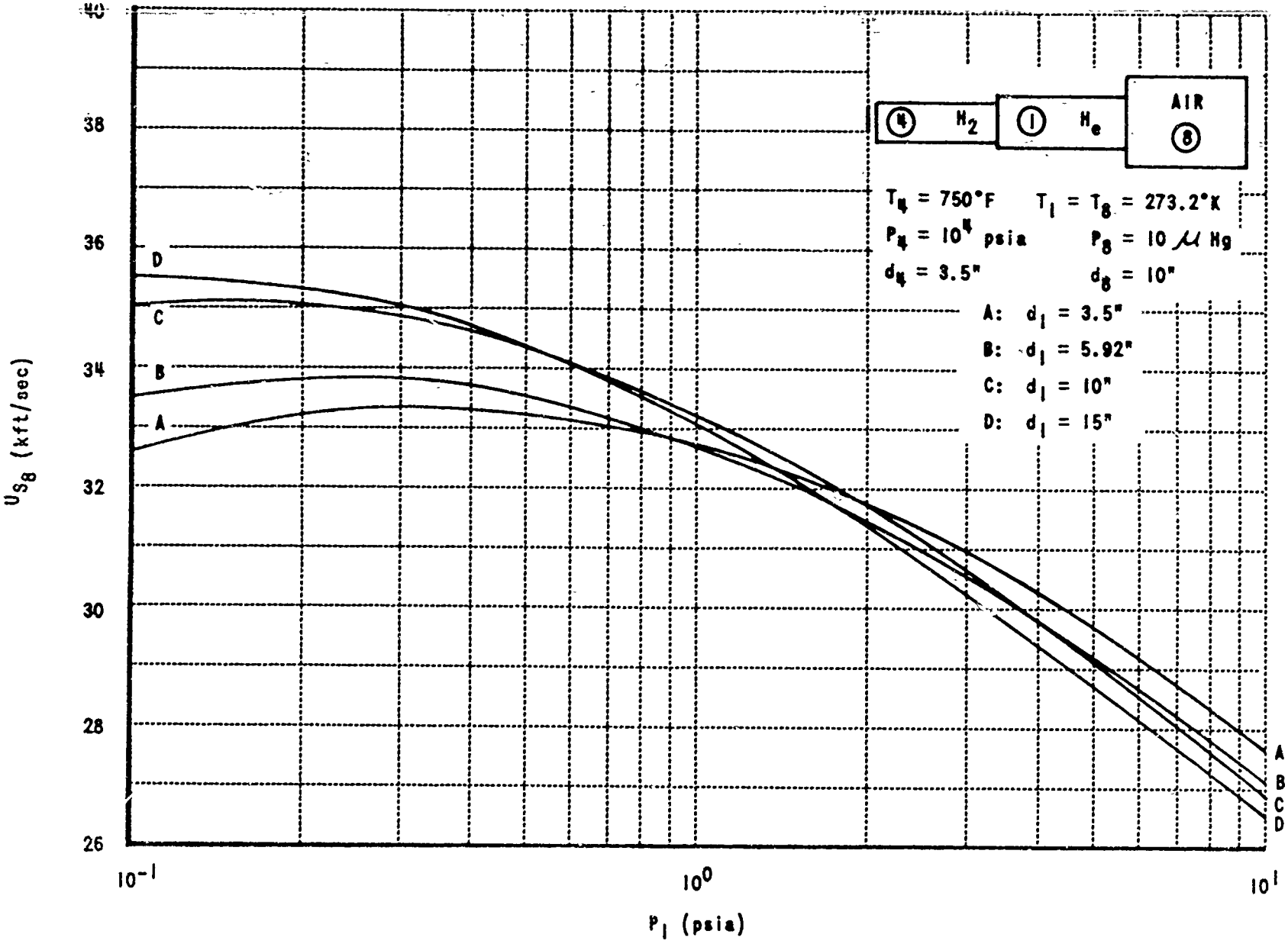

Figure 28 EFFECT OF VARYING BUFFER DIAMETER ON THE PERFORMANCE OF A BUFFERED SHOCK TUBE WITH A LARGER DRIVEN SECTION THAN DRIVER

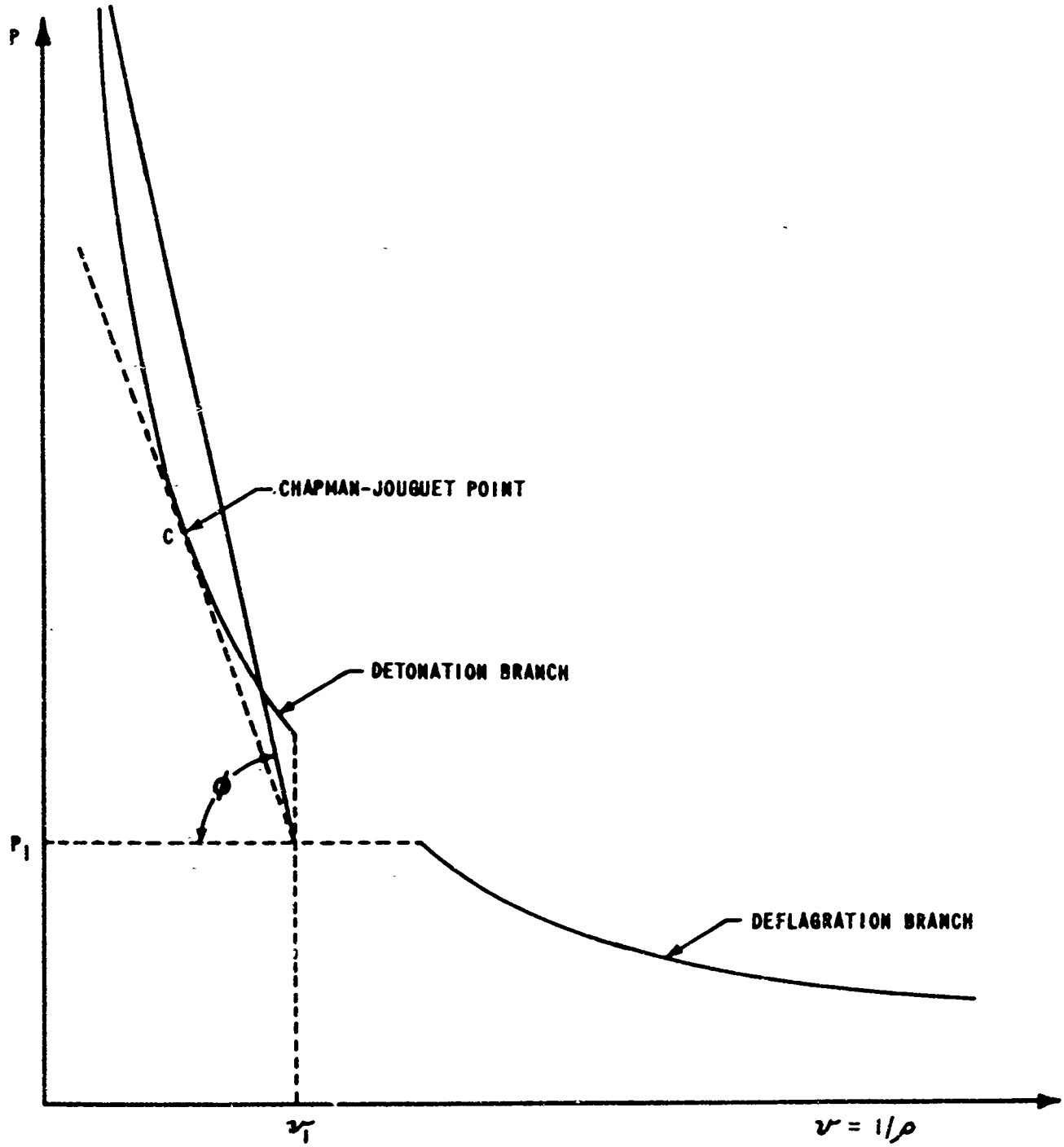

Figure 29 HUGONIOT CURVE FOR DETONATIONS AND DEFLAGRATIONS